DEVELOPMENT OF A MICROGRAVITY UAS TEST BED

By

JACOB HATHAWAY

BACHELORS OF SCIENCE IN MECHANICAL
ENGINEERING
Oklahoma State University
Stillwater, Ok
2014

BACHELORS OF SCIENCE IN AEROSPACE
ENGINEERING
Oklahoma State University
Stillwater, Ok
2014

Submitted to the Faculty of the
Graduate College of
Oklahoma State University
in partial fulfillment of
the requirements for
the Degree of
MASTER OF SCIENCE
July, 2016

DEVELOPMENT OF A MICROGRAVITY UAS TEST BED

Thesis Approved:

Dr. Jamey Jacob

Thesis Advisor

Dr. James Kidd

Dr. Joe Conner

ACKNOWLEDGMENTS

The author would like to acknowledge all his, research colleges, peers and professors alike for the the support, advice and guidance through out the 6 years combined in undergraduate and graduate studies at Oklahoma State University. A personal acknowledgment to Dr. Jamey Jacob for sharing his knowledge and time throughout the duration of this thesis project. Dane Johnson, Sri Vuppala and Rakshit Allamraju proved to be very helpful with integration of the Stabilis autopilot system and the author would like to thank them for their hard work and dedication.

[1] Acknowledgements reflect the views of the author and are not endorsed by committee members or Oklahoma State University.

Name: Name Date of Degree: July, 2016

Institution: Oklahoma State University Location: Stillwater, Oklahoma

Title of Study: DEVELOPMENT OF A MICROGRAVITY UAS TEST BED

Pages in Study: 114 Candidate for the Degree of Degree

Major Field: Mechanical and Aerospace Engineering

The ultimate goal is to develop a vehicle that can produce a microgravity environment for space system research within a small to medium sized UAV. This weight class of vehicle provides a platform that is more available and less expensive than other methods of generating microgravity which ultimately makes it a better choice for underfunded researchers. It is possible to achieve weightlessness with manual flight but due to the nature of smaller aircraft, pilot input must be more responsive to counteract the larger effects of atmospheric conditions on the airframe. Alternatively, an on board computer can control the vehicle with enough responsiveness to mitigate these effects. The first step in creating an autonomous microgravity UAS is the development of the flight control logic. Multiple concepts for controlling the vehicle are discussed and ultimately a flight path and throttle controller are selected. Aerodynamic models were developed and validated in digital Datcom and X-Plane so that simulation results were more realistic. A Simple 3 DOF simulator was created to show that the proposed controller can generate a microgravity environment with high repeatability. The next step is to then integrate the flight model and controller into a higher fidelity 6DOF X-Plane simulation. Here, HIL tests can be conducted using X-Plane software which shows the ability of the system to create microgravity. A HIL test plan has been developed to determine the systems ability to respond to to simulated gust effects. The microgravity system is ultimately judged on duration and quality of the weightlessness during HIL. Finally, the flight computer was integrated into a COTS vehicle and a flight test plan was developed.

ADVISOR’S APPROVAL: Dr. Jamey Jacob

TABLE OF CONTENTS

Chapter Page

LIST OF FIGURES

Figure Page

NOMENCLATURE

t	Time, s
g	Earth's gravitational acceleration (earth frame)
h	Altitude (earth frame), m
υ	Velocity along x body axis, m/s
ν	Velocity along y body axis, m/s
ω	Velocity along z body axis, m/s
n	Aircraft load factor
F	Force, N
T	Thrust, N
L	Lift force, N
D	Drag force, N
V	True airspeed, m/s
q	Dynamic pressure, Pa
m	Mass, kg
W	Weight (1 g), N
b	Wing span
c	Wing chord
S	Wing area
e	Oswald efficiency factor
$\mathbf{AR}$	Wing aspect ratio
$\bar{c}$	Mean aerodynamic chord
LE	Wing leading edge

TE	Wing trailing edge
$\mathbf{t}$	Thickness
ϕ	bank angle
α	Angle of attack, degrees
β	Side slip angle, degrees
θ	Pitch angle, degree
δ	Control deflection angle
ROC	Rate of climb
$\mathbf{M}$	Local Mach number
P, Q, R	Angular Velocity Components, degrees/s
$\hat{P}, \hat{Q}, \hat{R}$	Non dimensional angular velocity components
I_x, I_y, I_z, I_{xz}	Moment of inertia and inertia product
L	Roll moment
M	Pitch moment
N	Yaw moment
C_D	Drag coefficient
C_L	Lift coefficient
C_M	Pitching-moment coefficient
C_{M_0}	Constant non-dimensional pitching-moment coefficient
C_A	Axial force coefficient
C_N	Normal force coefficient
C_t	Propeller thrust coefficient
Lift curve stability derivatives	
C_{l_α}	Change in lift due to angle of attack
$C_{l_{\hat{Q}}}$	Change in lift due to pitch velocity
$C_{l_{\delta e}}$	Change in lift elevator deflection
Pitching moment derivatives	

C_{m_α}	Pitch moment due to angle of attack
$C_{m_{\dot{\alpha}}}$	Pitch moment due to the rate of change in angle of attack
C_{m_q}	Pitching moment due to pitch velocity
$C_{m_{\delta e}}$	Pitching moment due to elevator deflection
Rolling moment derivatives	
C_{l_β}	Rolling moment due to sideslip angle
$C_{l_{\hat{P}}}$	Rolling moment due to rolling velocity
$C_{l_{\hat{R}}}$	Rolling moment due to yawing velocity
$C_{l_{\delta a}}$	Rolling moment due to aileron deflection
$C_{l_{\delta r}}$	Rolling moment due to rudder deflection
Yawing moment derivatives	
C_{n_β}	Yawing moment due to sideslip angle
$C_{n_{\hat{P}}}$	Yawing moment due to rolling velocity
$C_{n_{\hat{R}}}$	Yawing moment due to yawing velocity
$C_{n_{\delta a}}$	Yawing moment due to aileron deflection
$C_{n_{\delta r}}$	Yawing moment due to rudder deflection
Side force derivatives	
C_{y_β}	Side force due to sideslip angle
$C_{y_{\hat{P}}}$	Side force due to rolling velocity
$C_{y_{\hat{R}}}$	Side force due to yawing velocity
$C_{y_{\delta r}}$	Side force due to rudder deflection
Subscripts	
x	Body frame in the x direction
y	Body frame in the y direction
z	Body frame in the z direction
X	Earth frame in the x direction
Y	Earth frame in the y direction

Z	Earth frame in the z direction
max	Maximum
cg	About the center of gravity
ac	About the aerodynamic center
ne	never exceed
a	Aileron
e	Elevator
r	Rudder
B	denotes body frame system
L	denotes lift
D	denotes drag
f	denotes force

CHAPTER 1

Introduction

1.1 Motivation

It is possible to create a free fall environment within Earths atmosphere using vehicles that accelerate with gravity. This condition has many titles including free fall, weightlessness or microgravity but they all define the same state of motion. This is the state where all local accelerations, forces (excluding pressure and atmospheric drag) and moments are very close to zero. In fact, the word “microgravity” is a compound word for small-gravity. Any object that does not experience a change in acceleration will satisfy this condition. This includes any objects in orbit which are essentially in constant free fall around the Earth. Microgravity research was originally conducted to overcome certain challenges that would be encountered by spacecraft in the low gravity conditions associated with orbital flight [1]. Although the physics of space flight is much further understood today, the need for new technologies to be tested in reduced gravity has not diminished. For example, additive printing is a relatively new technology that has high potential. It can reduce the weight and volume for tools and other items which is vital to prolonged space flight. The nature of additive printing requires a force that adheres the successive layers of material together while they harden. The adhering force on earth is usually due to gravity accelerating the mass of the print material, but new methods must be implemented in weightlessness. Made In Space is a additive manufacturing company that was selected by NASA (National Aeronautics and Space Agency) in November of 2015 to fly the first 3D printer aboard the ISS (International Space Station). The Made In Space printer

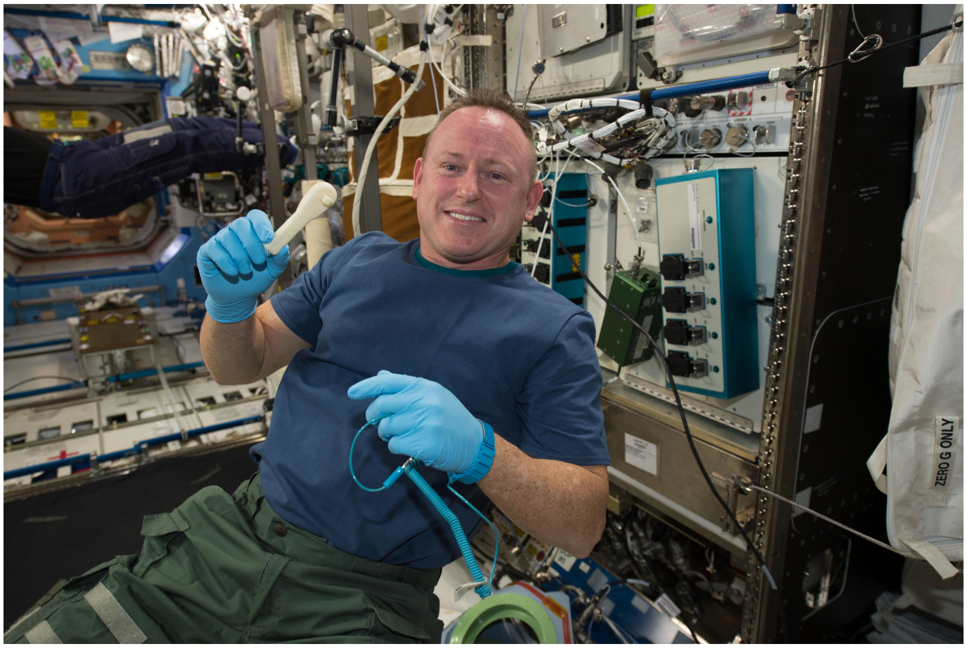

Figure 1.1: Astronaut Barry Wilmore with the first 3D printed part in space [2]

went through many preliminary microgravity flights to ensure that the system would work properly and now sits aboard the ISS. A part printed by the first ever 3D printer is held by astronaut Barry E. Wilmore in figure 1.1 and would not have been possible without preliminary microgravity research.

Fluid mechanics is extremely hard to simulate analytically. Even with the advancements in super computers, turbulent fluid interaction remains difficult to predict and still has a high value of uncertainty during testing. It can take weeks and even months for complex CFD analysis to converge on the highest performance computers. It can also be more expensive to build high accuracy simulations than to conduct experiments. This down time, increased cost and uncertainty forces the researchers to also take an experimental approach on almost all complex fluids problems. It is much more simple for the research to put the fluid in a similar environment and observe. Fluid mechanics is unavoidable in the space industry and today aerodynamics use a combination of analytical and experimental research to test new designs. For example, fluid slosh is still a major concern for rockets and satellites systems. Slosh can cause instabilities in spacecraft dynamics and lower the amount of usable fuel in spin stabilized rockets. Microgravity experimental testing remains the best way to ensure the effectiveness of new technologies and biologies in space.

National space agencies like NASA, RFSA (Russian Federal Space Agency) and more recently the ESA (European Space Agency) have been the major contributors to microgravity experiments. The American microgravity research program began in the 1960s with the C-131 Samaritan aircraft. This aircraft paved the way for reduced gravity research and was used to train people, develop procedures and test hardware in a weightlessness environment. Over the years NASA and the US. Air Force switched aircraft eight times of which the most notable are the KC-135 and C-9 aircraft. These vehicles were not limited to government personnel, they also used these platforms to get university students involved with microgravity research. The Reduced Gravity Education Flight Program provided a unique academic experience for undergraduate students to successfully propose, design, fabricate, fly and evaluate a reduced gravity experiment of their choice over the course of four-six months (reference microgravity website). Unfortunately this program was canceled in 2014 due to the high cost and logistical strain on the relatively small funding. Today NASA still uses microgravity research for new biological and technological studies but these opportunities are not available to low budget researchers. It is important that microgravity laboratories are available to universities and entry level researchers because it will bring new innovative technologies to the space industry and excite the next generation of researchers.

UAS (Unmanned aerial systems) provide a safe, inexpensive and effective way for researchers to conduct repeatable short term microgravity experiments. UAS also eliminate the concerns of pilot fatigue caused by increased g-loadings during long duration missions. The only drawbacks to using small to medium sized UAVs is the short free fall duration and the atmospheric effects to a smaller aircraft with less mass. However, improvements to autopilots in recent years have allowed much smaller IMUs (Inertial measurement units) more computational power to be included on small UAVs (Unmanned aerial vehicles). These autopilots can be powerful enough to correct for small gusts or perturbations in the local atmosphere which can cause a variation in local accelerations. Autopilots have become less expensive and more powerful, allowing most UAVs to be controlled for microgravity flight.

1.2 Goals

The main goal of this project is to develop a small UAS that is able to complete a weightless maneuver. The system is comprised of multiple subsystems that all need to interact together in achieving the goal. Intermediary goals include selection of vehicle, development of a useful model and simulator, development of microgravity controller and flight logic, showing that the system works HIL (Hardware in the loop) testing and finally flight testing the vehicle with the integrated controller. HIL and flight tests will concluded that UAVs in general are a viable platform for experimental microgravity testing. In particular, the developed system must produce reduction in local accelerations down to $\pm 0.01g$ for a duration of at least 5 seconds in order to be experimentally viable. It's also of high priority to conduct an effective overall experiment and submit meaningful research for future engineers to build on.

1.3 Objectives

The project must investigate the effectiveness of different types of UAS as a microgravity test bed and find a suitable platform. This will be done by implementing the equations of motion for a microgravity vehicle and calculating the performance characteristics of each option. Performance characteristics determine the maximum duration of free fall achievable and quality of the hold. Another variable that is taken into account for vehicle selection is the size of the payload bay and vehicle MTOW. Once a platform is selected, development of aerodynamic models for the aircraft must be completed so that control logic can be tested in simulation. This is done with the tools of the digital Datcom, MATLAB and X-Plane. Once complete, the autopilot will need to be implemented into an existing autopilot and integrated with X-Plane for HIL testing. HIL testing verifies the controllers ability and tests different vehicles performance. The controllers PID (Proportional Integral Derivative) gains will then be optimized and set for flight testing. Initial flight testing will be done with a payload bay accelerometer on board to measure the local accelerations where the experiment would reside.

CHAPTER 2

Background

2.1 Microgravity platforms

Drop towers, aircraft and sounding rockets each provide its own set of unique capabilities in terms of purity of gravity level, duration of reduced gravity time, weight of the potential experiment and interaction with the researcher [1]. Table 2.1 below includes a list of the different options for generating weightlessness. The Zero Gravity Research Facility at NASA Glenn Research Center is shown in figure 2.1. The facility includes two ground based, drop towers that allow microgravity research. The drop tower is essentially a 132 m tall pressure vessel that can reduce pressure to 0.01 Torr. Creating a close to vacuum environment mitigates the effects of aerodynamic drag and allows a reduction in gravity down to 0.00001 g [3]. For reference, drop towers produce a quality even closer to zero gravity than what is experience aboard the ISS. The international may be orbiting at 250 miles above the earth but it is still being effected by earths atmosphere gradually decelerating it, causing a residual acceleration. Drop towers can simulate an environment even closer to deep space missions. The two drop towers as NASA Glenn can produce a repeatable 5.18 second free fall for a 1.26 m^2 payload volume with a maximum weight of 455 kg [3]. The drop towers at the Glenn Research Center is shown in figure 2.1. The major advantage of using a drop tower is the quality of weightlessness which is not available by any other microgravity platform within earths atmosphere. Drop towers in general are also not as expensive compared to aircraft and sounding rockets, although the duration of weightlessness is very short. This is an important parameter because some experiments require a

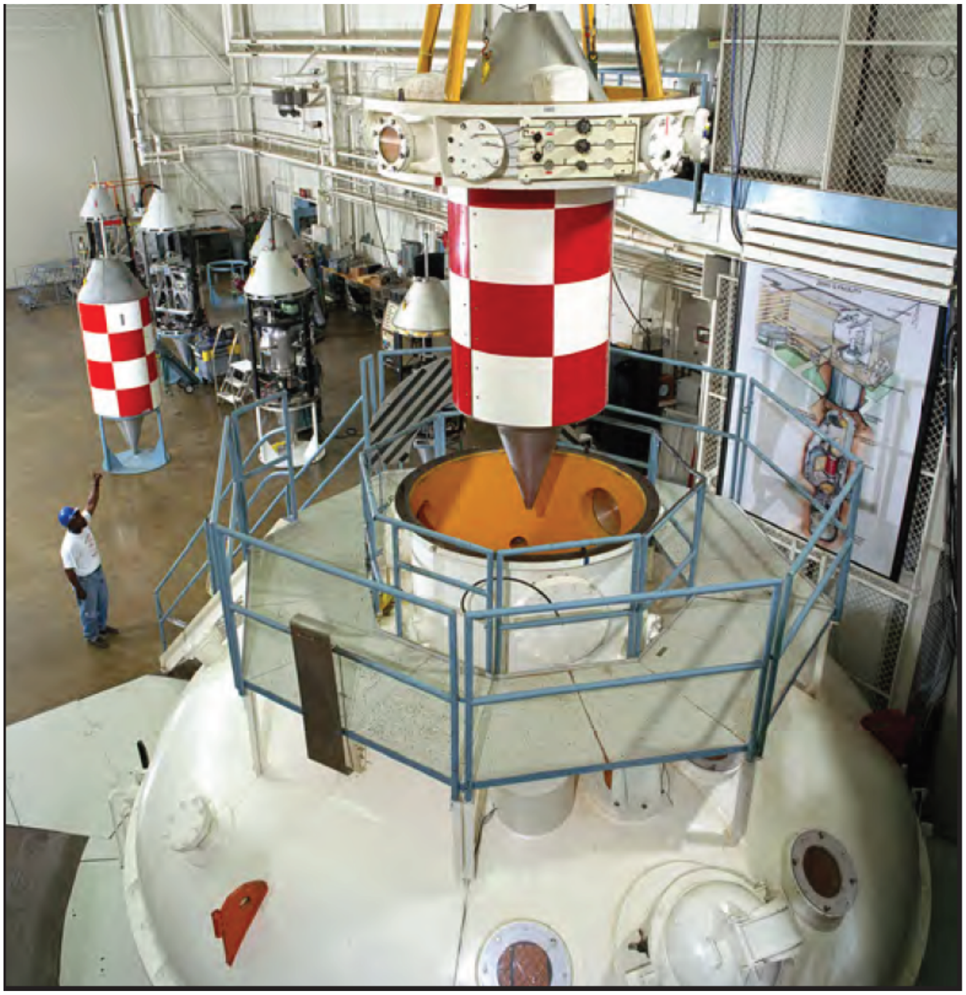

Figure 2.1: NASA's drop tower facility at Glenn Research Center[3]

warm up time that can not be accommodated by the 5.18 second duration. A test duration of 10 seconds or greater is highly desired. Experimenters are also not able to interact with the experiment during drop tower operation due to the small space and rapid deceleration. The maximum deceleration of experiments can reach 65 g which also means that the experiment itself must be more robust and battle hardened to prevent damage. All of these drawbacks that were mentioned severely limit the types of experiments that can be tested at ground based drop tower facilities.

Another microgravity vehicle option is the sounding rocket. Rockets are generally used to put satellites and other spacecraft into orbit but they can also be used to place an experiment into a sub-orbital trajectory. Sub-orbital trajectories happens when

Figure 2.2: NASA's "Weightless Wonder" C-9 flying laboratory [2]

one full orbit of the Earth is not completed and object falls back into the atmosphere. These types of orbits usually allow reduced gravity times of an estimated 15 minutes. Rockets can also deliver large payloads although the cost increases exponentially with weight and volume. Even very small payloads are quite expensive. The issue here is that both weight and volume of the experiment must be optimized to reduce the vehicle cost. Optimizing the weight and volume draws attention away from the experiment and greatly increases overall cost. This issue is similar to any experiment that is tested on the ISS. Another major drawback to both orbital and sub orbital platforms is that the platform can not provide variability in weightlessness. Variability in acceleration is important for testing experiments in Martian or Lunar conditions and can be induced by both the drop tower and aircraft platforms. Martian research is becoming more common with increasing possibility of manned missions to Mars. Sub-orbital rockets obviously do not allow experimenter interaction during testing and the time in between experiments quite long due to recovery re-launching.

Flying laboratories can maintain a free fall for up to 30 seconds which is a good amount of time to run a short experiment. Generally, flying laboratories are heavily modified, medium sized aircraft that fly a series of parabolic arcs to create a weightless environment. Figure 2.2 shows the “weightless wonder” which has been conducting microgravity experiments for years this has proven to be an effective way to test a number of large experiments. The author has experienced a microgravity maneuver first hand aboard this aircraft. The pilots use the aircraft control computer to help follow a parabolic flight path. The process needs the pilot for elevator control, the co-pilot for throttle control and an aircraft computer to control rudder/ailerons deflections. In this scenario, the pilot follows a pitch attitude that the computer has calculated to be optimal while the co-pilot does the same for engine thrust. The method allows each pilot to concentrate on each respective job and ultimately achieve a steady microgravity environment for the on board experiments. Although this platform allows multiple experiments and researchers to test at 30 second increments, the price of the operation is very high. For example, the Zero-g cooperation, which uses a modified 727, charges 165,000 per flight with 36 participants and 5-8 experiments [4]. Without significant funding, researchers can not afford to test experiments aboard these aircraft.

Table 2.1: The properties of different microgravity platforms

Method	Duration [s]	Acceleration accuracy [g_0]	Payload Volume [m^3]	Payload mass [kg]
Drop towers	5.18	10^{-5}...10^{-6}	1.2	455
UAS	15	10^{-1}	.25	5
Flying labs	30	10^{-2}	20	500
Sub-orbital	900	10^{-3}...10^{-6}	1	200
Orbital	indefinitely	10^{-3}...10^{-6}	5	300

2.2 UAS role

The major drawbacks for most microgravity vehicles is the extreme cost. UAS are much less expensive but they can not provide the duration, quality, the interaction with the researcher or the payload size that other methods provide. At the university level, cost is more significant than experimental duration, quality or size. This builds on the idea that a more cheap experiment/project still provides an equal research/learning experience. A UAV would allow small components and experiments around 0.25-0.5m^2 volume and 5-20kg payload to be tested for research and teaching projects. Due to the unmanned nature of UAVs, the operator is able to fly more aggressively. For a microgravity maneuver this means that the duration of weightlessness could be increased beyond estimation. Also, pilot fatigue is no longer an issue so repeatability and endurance are both increased. Additionally, a lower turn around time would allow more experiments to be tested in a shorter amount of time. SUAS and TUAS can be launched from small runways, grass and even catapult launched which eliminates the need for a large maintained runway or airport clearance for testing to take place. Using a UAS, the test operator can oblige any experimental requests regarding test conditions, magnitudes of reduced gravity and residual acceleration.

UAS in the 1-90kg range often have the payload capability and performance for microgravity mission profile. The SUAS (Small UAS) or STUAS (Small Tactical UAS) is the sizing range of the vehicle. A SUAS is defined by Jay Gundlach in “Designing UAS” of a UAV with a 1-25kg gross weight and a STUAS to be classified as the 25-90kg weight class[5]. Size of the UAS ultimately determines the maximum size of the experimental payload. Mass of the aircraft is closely related to effect of gusts and atmospheric unsteadiness on the airframe which ultimately determines how closely the vehicle can maintain zero acceleration. A SUAS airframe will be affected significantly more than a Boeing-727 sized aircraft. The test operator may choose to fly in only ideal conditions depending on the requested experimental conditions.

Some aerodynamic parameters can increase the atmospheric effect as well. Some of the major contributors are, overall C_D, C_L, and b.

Engine parameters are vital to increasing the free fall duration of the maneuver. The dynamics of microgravity will be explained with more depth in the following chapter but generally, a higher thrust to weight ratio is related to an increase in duration. SUAS can be integrated with two different types of propulsion including an electric or internal combustion engine (ICE). Electric engines will provide greater thrust to weight ratio depending on the amount of batteries included but have a relatively short endurance. Aircraft with shorter endurance will need to land to switch out batteries often which will extend the overall experimentation time. Electric engines also generate less vibrations than an ICE which can cause issues with accelerometer data. ICEs on the other hand, will proved a longer endurance and also a slightly less thrust to weight ratio due to the additional equipment needed for the fuel system. Most SUAS and STUAS ICEs do not standardly include a fuel pump and are gravity fed instead. This is obviously an issue during microgravity flight where the acceleration is negligible. The solution to the problem is simple, add a fuel pump, but the issue needs to be addressed if an ICE is used. Neither engine has significant advantages or disadvantages over the other so both are still viable options.

2.3 Previous Work

Due to Moores law, the past 5 years has revealed UAVs as useful platforms for more than just military missions. Avionics are getting smaller, more powerful and less expensive which makes UAS available to a variety of new applications. A study conducted by the ESA in 1995 provided useful recommendations and concluded that improved autopilots and powerplants, particularly a gas turbine, would best suited for this type of mission, but were not readily available and/or cost-effective at that time. Fast forward 16 years and the range of sensor and powerplants to test the

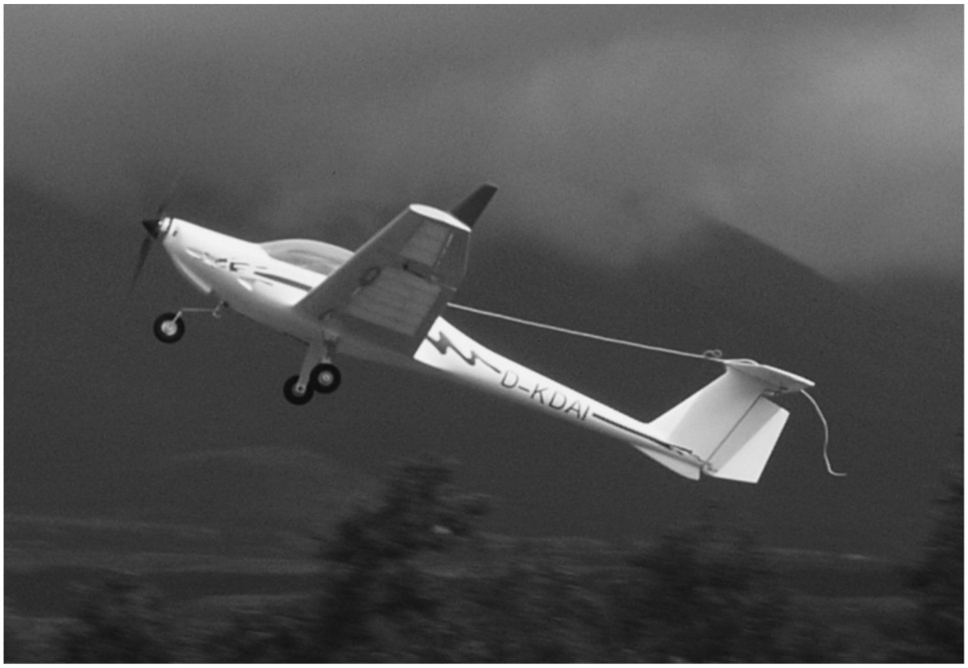

Figure 2.3: Test-Bed Vehicle for Higashino and Kozai [7]

feasibility have surfaced [6].

2.3.1 Kyushu University

Higashino and Kozai show that a low performance aircraft can be used to obtain a $0.15g$. They also examine the feasibility of small single engine aircraft in microgravity flight by developing a model and simulation of the system. The model and simulation is created with the USAF (United States Air Force) digital Datcom along with 6 degree of freedom (DOF) equations of motion (EOM). The simulation compares the developed acceleration feedback control system in the wind and body axis. The researchers then determine which of the two control methods would be ideal. The selected control is implemented it into the vehicle shown in figure 2.3 for flight testing. The test-bed vehicle is a low wing, light weight, COTS, T-tail aircraft. The wing span is $2.4m$ with an area of $0.4m^2$ and an aircraft gross weight of $2.5kg$ [7].

Accelerations in X_B were controlled with a PID using feedback from the throttle input. Accelerations in Z_B were controlled with a secondary PID using elevator

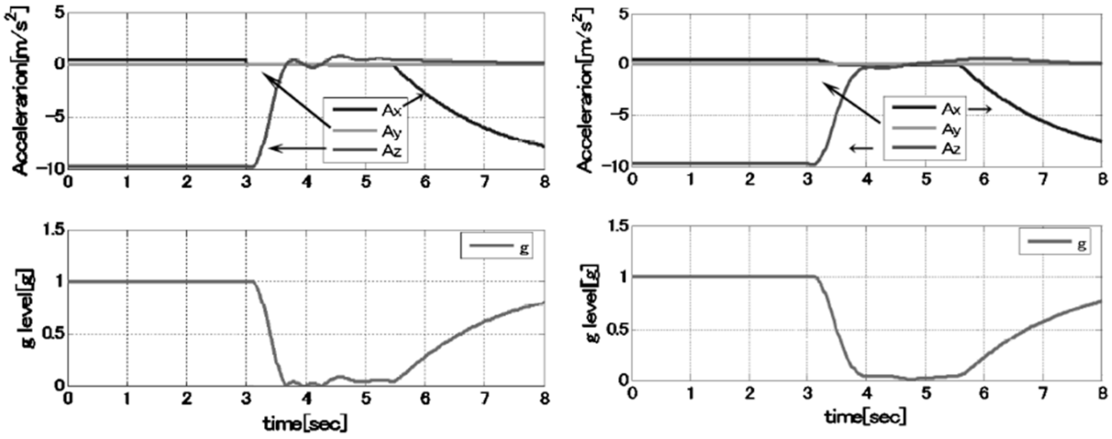

Results from using body axis controller

Results from using wind axis controller

Figure 2.4: Simulation comparison between two feedback controllers [7]

feedback. The researchers explain that the PID gains were determined by considering stability of the feedback system response time and damping characteristics. The same control system is implemented for the wind axis acceleration feedback controller and results were compared in simulation. The wind axis is generally better suited for implementing the aerodynamic forces like lift, drag, etc. The simulation results showed strong advantages to using a wind body axis controller and can be referenced in figure 2.4. The advantages include longer and more stable reduced gravity hold for the wind axis controller. A repeatability study was not mentioned by the researchers for review of results–although, the simulation that was developed for testing did not model air turbulence or sensor error as far as the author is aware of.

In any case, the promising wind axis controller that was tested in simulation was not able to be flight tested due to the lack of an α (or angle of attack) sensor on the aircraft. Sensors that can measure this angle include, multi hole Pitot probes or wind vanes mounted on the side of the aircraft. The normal body axis acceleration feedback controller was flight tested on board a SUAS with two different mission profiles. One mission was a steady dive maneuver and secondary mission was to start the maneuver in a climbing attitude. The flight test included an on board control system as well as a data communication system that would relay information to the ground control station (GCS). The control algorithm was generated into C language and imported to the aircraft CPU which controlled six servo actuators for the control surfaces and the motor. A breakout sensor board was included that communicated accelerometer, rate gyro and barometer information to the CPU. The overall systems is referenced in figure 2.5 Flight tests results reveal sampling time issues with the barometric sensor which cause larger errors in the altitudes sensed data. Altitude data is not critical to the control of the dive so the maneuver continues successfully. However, the results show that the quality and duration of the free fall is not ideal. Although the Higashino and Kozai do not accomplish a complete zero acceleration with the test-bed vehicle, it is close enough to conduct scientific experiments at Lunar and Martian gravities which are 16.5 and 37.5 percent earths gravitation respectively. This is still a viable option because the discovery of liquid water on Mars is increasing the need for new technologies to be tested in similar environments. Not only does the aircraft not achieve a zero acceleration, the maximum duration of free fall was 3.5 seconds. This is hardy enough time to conduct any sort of meaning full research. Additionally, the g-level is unsteady for the duration. The researchers do recommend improvements to the design which, a more resolute altitude sensor, including an angle of attack sensor, replacing the powerplant with higher performance engine and optimizing control gains. The control gains were difficult to tune because of the short duration of the flight.

The major contribution of this research is the proof of concept for acceleration feedback control. Although the results are not ideal, the control system in both wind and body axis can be considered as acceptable methods to create microgravity in a SUAS. The comparison between wind and body axis has also proven that the wind frame of reference should be used when possible. Higashino and Kozai have also proved that it is possible to model microgravity flights in simulation using the USAF

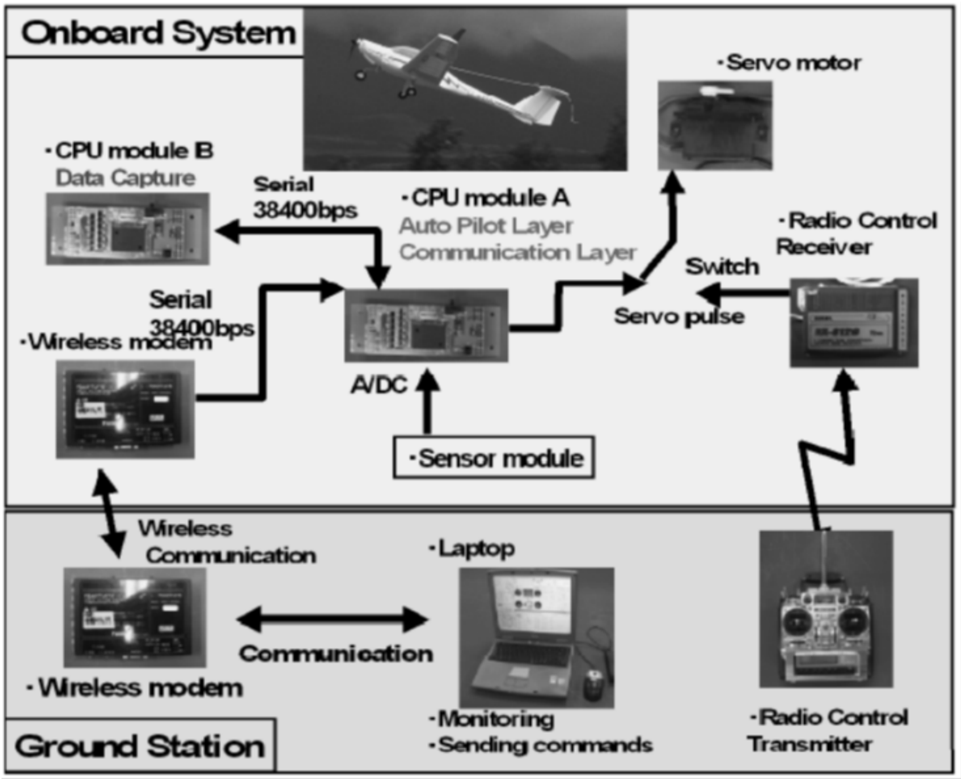

Figure 2.5: The flight testing system for Higashino and Kozai [7]

digital Datcom and 6 DOF EOMs. This research has demonstrated the importance of aircraft performance and quality avionics for long duration, high quality microgravity flight. Acceleration feedback in the body axis will be considered in control of the current microgravity vehicle among other concepts.

2.3.2 University of Braunshweig

Hofmeister and Blum reported similar research to Higashino and Kozai a month later in November of the year 2010. The test bed vehicle they used was a "UR-Modellbau" aircraft that was able to sustain a free fall for up to 16 second duration. The aircraft was also able to achieve Lunar and Martian like reduced gravity holds for 17 and 21 seconds respectively. First the researchers flight tested a much smaller vehicle with a mass of $2kg$ which was remotely piloted and able to achieve zero gravity for 4 seconds with only $0.1g$ residual accelerations. Figure 2.6 reveals that the quality and duration

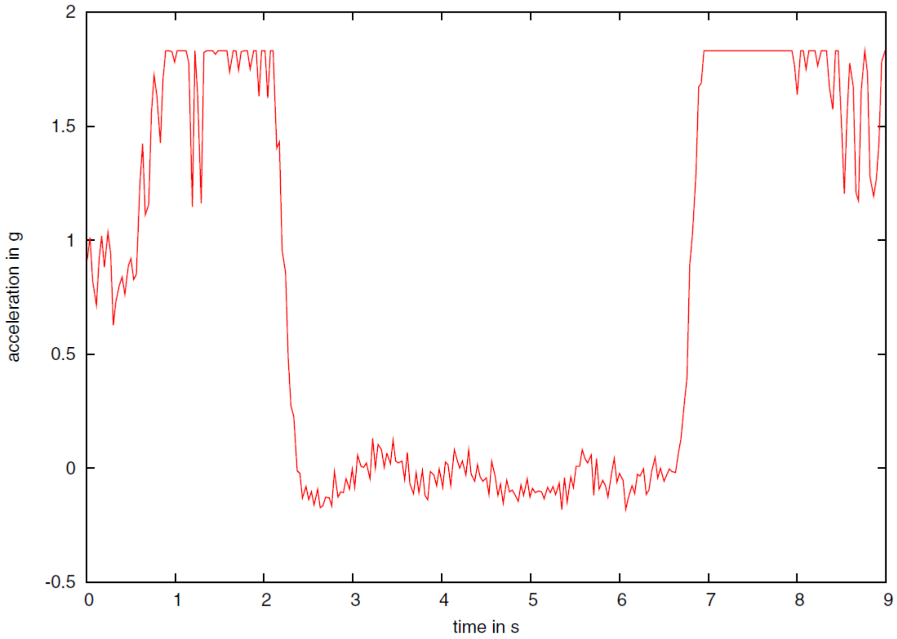

Figure 2.6: The residual accelerations during a preliminary flight test [8]

is quite good for such a small UAS although accelerometers get saturated during pull up maneuvers. The researchers do not explain how the pilot was manually able to achieve such good results from the small aircraft but one can assume there was visual acceleration magnitude feedback during the flight. Hofmeister et al. do explain that this was a preliminary flight test that motivated the following test of a larger vehicle.

The test-bed vehicle used by Hofmeister and Blum is shown in figure 2.7. It is a jet engine powered delta wing aircraft with a canard surface for control. The aircraft is quite sporty with a maximum velocity or V_NE of $100m/s$. It has a MTOW (maximum takeoff weight) of $25kg$ and a wingspan of $2m$. The airframe can also handle a positive $5g$ loading for pitch up maneuvers. The engines provide $180N$ of thrust and has fuel tanks that are prevented from running dry in low gravity flight [8].

Hofmeister and Blum also created a simulation to conclude that the larger flight test vehicle could perform adequately. The simulation tool was able to vary the

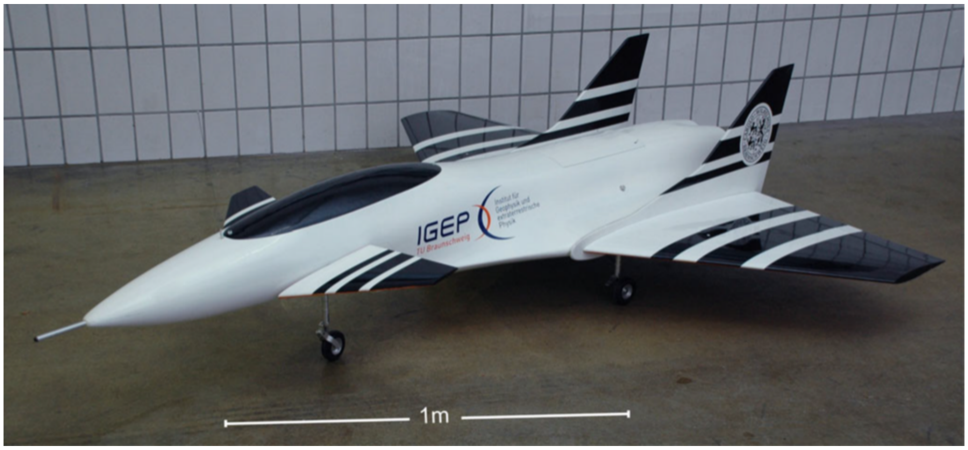

Figure 2.7: The test platform UAV for Hofmeister and Blum [8]

initial speed of the aircraft, the acceleration during pull-up, the targeted reduced gravity magnitude and the duration of the pull op phase. So the target flight path is a full parabolic arc that starts with a pull up maneuver, continues through the zero-g portion and then ends with the successive pull op maneuver. A full parabolic flight is ideal for maximum duration and decreasing the down time between successive weightless portions. A fault of this simulation is that the aerodynamic drag in not simulated and instead, is assumed to always be equal to the thrust. The simulator is essentially a simple projectile motion calculation for different flight conditions. This can be used to determine the maximum velocity and altitude that the aircraft needs to sustain and maximum angular rate. Determining the maximum velocity that the vehicle will achieve given a duration and initial velocity is important to compare to the vehicles V_{NE}. Every aircraft has a never exceed velocity or V_{NE} determined by the aircrafts structural build and aerodynamic coefficients. If the velocity ever approaches V_{NE} then the maneuver must be canceled by leveling out to avoid damage or loss of the aircraft. The condition at which maximum velocity from the simulator equals the V_{NE} is the maximum duration of microgravity that the vehicle can withstand. It is also important to determine a maximum altitude so that the pilot knows what height to start the maneuver from. Maximum angular rate needs to be determined

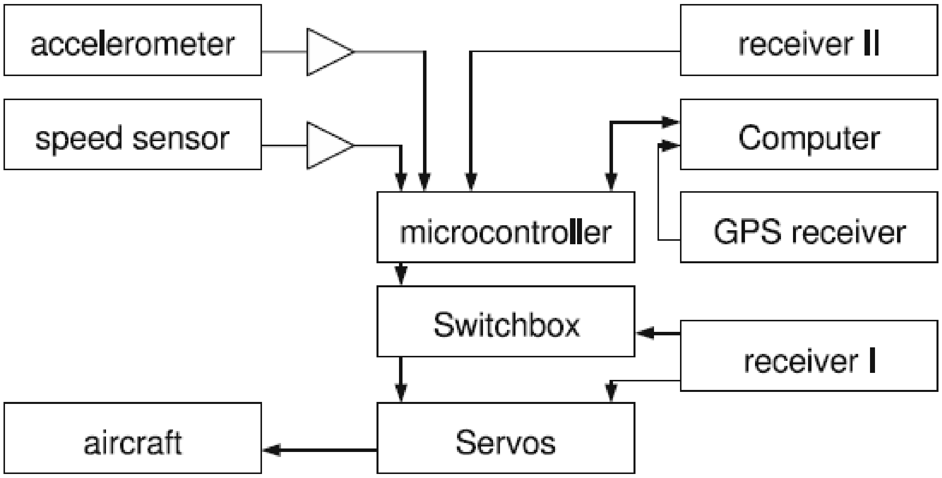

Figure 2.8: The electrical system for Hofmeister and Blum [8]

to estimate the centrifugal forces that will be caused by the pitching of the aircraft.

Hofmeister and Blum used a pre-determined path planning control method. The control algorithm is not documented by the researchers but the other can assume that It uses the current attitude and heading of the aircraft, calculates the optimal path to follow and executes waypoint navigation or path following. The researchers mention a method of predicting the aerodynamic drag of the aircraft by calculating wind speed from a Pitot while knowing the C_D of the airframe. With this information the idea was to control the throttle to around for accelerations in the X-axis. However, this seems like a problematic control theory because both the drag of the aircraft and output thrust of the engine is very hard to predict. The autopilot control was implemented onto a Linux microcomputer and interfaced with the other avionics as shown in figure 2.8.

The results from the flight test were not ideal. The pre-determined path planing and control method that was implemented did not respond well to windy conditions and the adaptive control was not able to tune the gains in a quick enough amount of time. They concluded that the control surface effectiveness was not large enough and the moment of inertia to great to correct for disturbances caused by wind. Issues in the x-axis control theory prevented the vehicle from achieving even a remotely close to zero acceleration free fall and ultimately led to a re-designing of the controller. The researchers quote sensor drift and un-tuned gains as the reasons for an unsuccessful flight test but also state the fundamental issues in the control theory.

The research shows that microgravity can be achieved by a radio control (RC) piloted UAV without feedback control as long as the aircraft is small and has a high responsiveness to control inputs. Preliminary flight test for the SUAS will follow this method and include a manual attempt at microgravity. Manual testing not only allows the pilot to become more confident with the maneuver but also creates a caparison to auto controlled maneuvers. Comparisons to an estimated trajectory should help with tuning PID control gains due to the general knowledge of how the flight path should look. The simulation method used for calculating maximum velocity, maximum angular rate and altitude will not be used because there is more simple methods to do so. Determining these parameters of the aircraft can be done with the methods explained in more detail within the next chapter. A comment that will contribute to flight testing, a forward CG helps to damp out any oscillation in the roll and yaw axis which is favorable during parabolic flight [8].

2.3.3 NASA

The NASA UMFP (Unmanned Microgravity Flight Program) is an ongoing project created by a team of engineers at JSC (Johnson Space Center) in Houston Texas. The project has three phases of operation including phase 1 which consist of manual control of the aircraft with autopilot system logging data continuously through flight testing. The pilot will fly the aircraft using FPV (first person view) cameras and an array of screens that have HUDs (heads up displays) in which provide visual feedback of acceleration magnitudes. Phase 2 implements the autopilot to maintain stability in roll and yaw axis using feedback control. The pilot will then only need to control

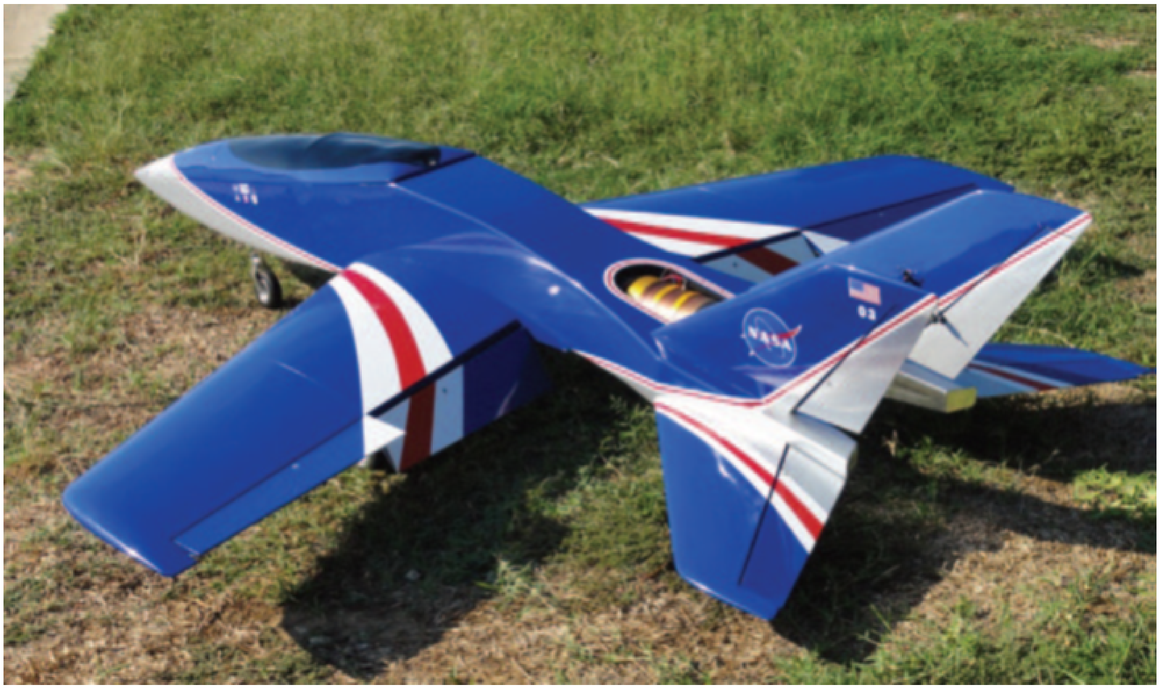

Figure 2.9: NASA's DV8R platform for the Unmanned Microgravity Program [9]

throttle and pitch angle of the aircraft which will ultimately produce less residual acceleration during the maneuvers. This procedure is similar to what is used in the historical C-9 aircraft flown by NASA test pilots. The third phase turns over all control to the autopilot while the pilot monitors, and can take control at any time [6]. The control system is not explained in detail but will be used to increase the steadiness or quality of the reduced gravity maneuver. It seems like the idea for each phase of the program is to progressively minimize residual accelerations.

The test bed vehicle is a modified TroyBuilt DVR8 aircraft shown in figure 2.9. The airframe has a wing span of $2.10m$, length of $2.21m$ and a dry weight of 10 kg. The small turbine engine weighs $1.6kg$ and produces $178N$ of thrust at 123,000rpm. A fuel pump was added for complete flow rate in reduced gravity. For 15 seconds of microgravity, projectile motion equations determine that he aircraft must be able to achieve a $305km/h$ velocity. In general a higher swept wing is better for high speed flight. This is due to the fact that the air flow around the wing encounters a more

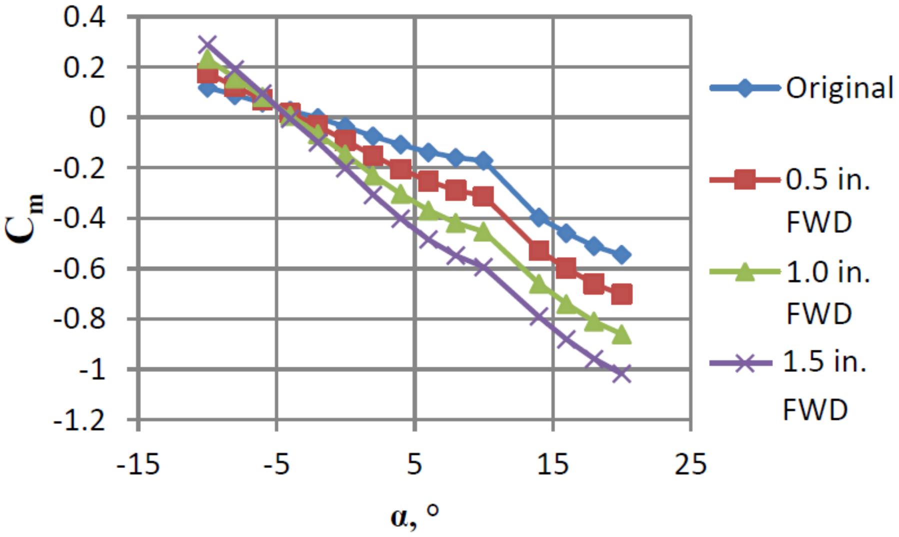

Figure 2.10: Moment reference center shift analysis of the DVR8 [9]

thin airfoil, allowing the flow to stay attached at higher speeds. This also increases effects aileron effectiveness at high speeds and leads to a more responsive aircraft.

A full aerodynamic study was conducted by Joshua Castagnetta nd Robbert Larson who are researchers of the USAF Academy [9]. The goal here was to obtain baseline aerodynamic and stability characteristics of the DVR8 by conducting a wind tunnel experiment. Once the aerodynamic coefficients are determined, they can be used in 6 DOF simulations that can be used in generating a flight envelope. Control power and cross-control derivatives were also defined. The V_{ne} is usually not calculated for most COTS UAVs like the DVR8. Since this is such an important parameter duration, the researchers plan on placing strain gages on key components of the airframe during a normal flight conditions or in wind tunnel testing. The strain data can be compared with a "failure tested" wing or fuselage to determine the definitive flight limits for airspeed and g-loading. Adding on to the envelope study, the effect of longitudinal stability and controllability due to the CG travel was researched. The results concluded that a CG shift forward increases the longitudinal static stability seen by increasing the slope shown in figure 2.10.

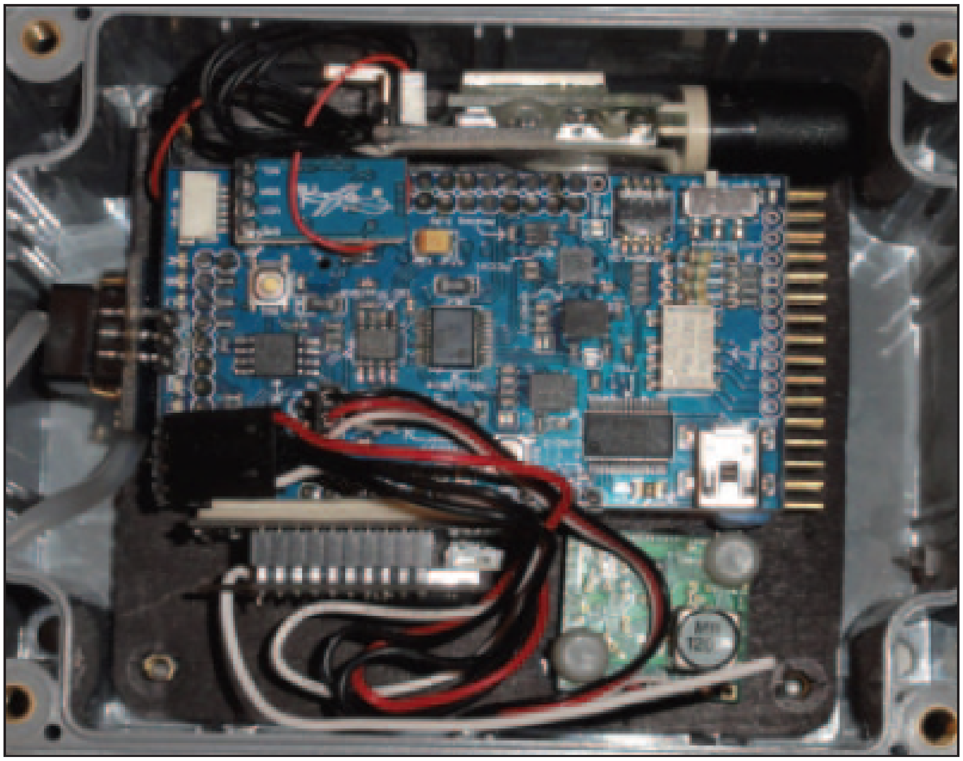

Figure 2.11: NASA's autopilot sensor suite [6]

An open source COTS autopilot will be used for first two phases of the UMFP. The selected autopilot is shown in figure 2.11 and communicates with barometric pressure, accelerometer, rate gyro, magnetometer, airspeed and GPS sensors. The final phase of the program will either need to modify the firmware of the COTS autopilot or integrate completely new control algorithm into an on board micro controller. This program did not contribute to the authors knowledge or methodology in the topic of controls systems due to the lack of detail provided by the researchers.

The program is still in the early phases but the team is currently working on getting the DVR8 clearance to move forward with the initial flight test. At angles of attack of greater than 10°, major drop offs in control authority of aileron, ruder and elevator control were observed. Therefore the aircraft maximum angle of attack must be 10° during the parabolic maneuver in order to ensure controllability. Uncertainty analysis of the aerodynamic coefficients show relatively good results ranging from

3.19% to 16.9% on $C_{L_{\delta a}}$ and $C_{L_{\delta e}}$ respectively. A maneuverability envelop study resulted in defining a maximum load factor for the airframe with different CG locations ranging from to be from $2.5g$ to $12.5g$.

The NASA research reveals many possibilities for using COTS autopilots for initial microgravity HIL and flight testing. Using the Autopilot to maintain the status in both roll and yaw axis allows the pilot to concentrate on pitch and throttle inputs and very similar to the method NASA pilots use on the C-9 aircraft. This method is cheap, available and can determine if the aircraft has the required performance prior to flight testing with acceleration feedback control. Conducting an entire maneuverability envelope analysis based on CG travel and maximum load is beyond the scope of this thesis due to the extensive wind tunnel testing that is required. Determining maximum structural loads using strain gages is a good approach but is considered to be unimportant if the failure flights conditions are avoided. A conservative estimate of the airframes V_{ne} can be made based on the type of material, build, and wing span. With that being said, most o A full wind tunnel analysis can be avoided as well by estimating aerodynamic characteristics with the digital Datcom.

CHAPTER 3

Theory

This chapter discusses the theory that will be used to develop the different controllers of microgravity vehicles as well as the metrics that will be used to evaluate both the vehicle and the control logic. The basic governing equations for aircraft flight are described as well as basic control theory and the different concepts used for microgravity control. The equations of motion will serve as mathematical models of the aircraft and ultimately are used in the development of a MATLAB simulation. A discussion of what creates weightlessness is also included so that control methods may build upon free fall dynamics. An understanding of microgravity dynamics also allows for a discussion of what parameters most effect quality and duration of the free fall. Later in the chapter, the author describes the different methods of control that are available and the ones that will be further evaluated.

3.1 Equations of motion

An understanding of the static and dynamic characteristics of an airplane is important in assessing its handling or flying qualities as well as for designing autopilots [10]. Having a mathematical model of the aircraft also aids in aerodynamic modeling and simulation. Microgravity flight is considered to be nonlinear from the point of view of the vehicle motion however, the aerodynamic forces and moments acting on the vehicle during the parabola can be considered to be linear as long as the aircraft does not approach stall [7]. These governing equations mathematically describe how the aircraft moves in 6 DOF (degrees of freedom) and are known as the EOMs (equations

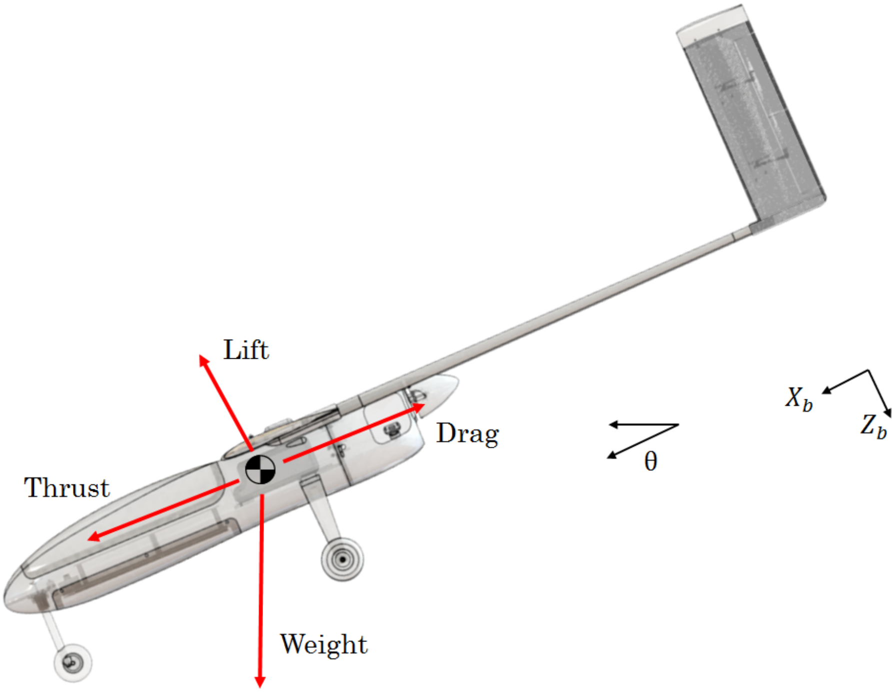

Figure 3.1: Forces on a reduced gravity aircraft

of motion) [10]. The six degrees of freedom include the aircraft velocity in X_B, Y_B and Z_B directions as well as the rotation in roll, pitch, yaw. Equations 3.1, 3.2 and 3.3 are the body axis force equations. Assuming a correct CG and aircraft symmetry the EOM can be simplified. With this assumption, I_{yz} and I_{xy} are equal zero and the moments can be reduced to the equations 3.4, 3.5 and 3.6 [10].

$$X - mg\sin\theta = m(\dot{u} + Qw - Rv) \tag{3.1}$$

$$Y + mg\cos\theta\sin\phi = m(\dot{v} + Ru - Pw) \tag{3.2}$$

$$Z + mg\cos\theta\cos\phi = m(\dot{w} + Pv - Qu) \tag{3.3}$$

$$L = I_x\dot{P} - I_{xz}\dot{r} + QR(I_z - I_y) - I_{xz}PQ \tag{3.4}$$

$$M = I_y\dot{Q} + RP(I_x - I_z) + I_{xz}(P^2 - R^2) \tag{3.5}$$

$$N = -I_{xz}\dot{P} + I_z\dot{R} + PQ(I_z - I_x) + I_{xz}QR \tag{3.6}$$

The 6 DOF (degree of freedom) non-linear equations are not useful for some simulations in the current form of equations 3.1-3.6. They have been been converted into the more convenient form of equations 3.7 through 3.12. In this form, the aerodynamic coefficients instead of may be used. There are many ways to estimate the aerodynamic characteristics of various aircraft and these will be discussed in later chapters. These EOMS are vital to modeling aircraft flight and are implemented in the simulators described in later chapters. Equation 3.7, 3.7 and 3.7 describe the forces in the X_B, Y_B and Z_B axis respectively. Equations 3.10, 3.11 and 3.12 describe the roll, pitch and yaw moments respectively. It is important to note, that these EOMS only describe the motion of the aircraft according to a body frame of reference and further steps must be taken for reference to earth frame. Also, depending on the objective of the simulator, all six degrees of freedom may not be needed to define the important dynamics.

$$X = qS((C_{L_\alpha}\alpha + C_{L_{\hat{Q}}}\hat{Q} + C_{L_{\delta e}}\delta_e)\sin\alpha - (C_{D_0} + \frac{C_L^2}{\pi\mathbf{AR}e})\cos\alpha + C_t) \tag{3.7}$$

$$Y = qS((C_{y_\beta}\beta + C_{y_{\hat{P}}}\hat{P} + C_{y_{\hat{R}}}\hat{R} + C_{y_{\delta r}}\delta_r) \tag{3.8}$$

$$Z = -qS((C_{L_\alpha}\alpha + C_{L_{\hat{Q}}}\hat{Q} + C_{L_{\delta e}}\delta e)\cos\alpha + (C_{D_0} + \frac{C_L^2}{\pi\mathbf{AR}e})\sin\alpha) \tag{3.9}$$

$$L = qSb(C_{l_\beta}\beta + C_{L_{\hat{P}}}\hat{P} + C_{l_{\hat{R}}}\hat{R} + C_{l_{\delta a}}\delta_a + C_{l_{\delta r}}\delta_r) \tag{3.10}$$

$$M = qS\bar{c}(C_{m_0} + C_{m_\alpha}\alpha + C_{m_{\dot{\alpha}}}\dot{\alpha} + C_{m_{\hat{Q}}}\hat{Q} + C_{m_{\delta e}}\delta_e) \tag{3.11}$$

$$N = qSb(C_{n_\beta}\beta + C_{n_{\hat{P}}}\hat{P} + C_{n_{\hat{R}}}\hat{R} + C_{n_{\delta a}}\delta_a + C_{n_{\delta r}}\delta_r) \tag{3.12}$$

3.1.1 Projectile motion

A ballistic trajectory is described as the path a lunched object takes when gravity is the only force acting on it (i.e. drag force is negated). This trajectory is described by the projectile motion equations 3.13, 3.14 and 3.15 that follow [11]. Equation 3.13 and 3.14 describe the objects velocity components with respect to an initial condition υ_0 and time t. Its important to note here that the x component of velocity υ_x is independent of time and will remain constant when drag is not present. Equation 3.15 describes the altitude of the object dependent of time. Any object or aircraft following this path will be in free fall and will have a local net acceleration of zero. If the goal is to have the vehicle sustain microgravity for objects within, these equations directly describe the objective path. Given an initial condition, these equations are used to command the optimal path of the aircraft to maintain for reduced gravity flight. The gravity term can easily be reduced in the equations to describe the path required to maintain Martian and lunar gravity environments.

$$\upsilon_x = \upsilon_0 \cos\theta \tag{3.13}$$

$$\upsilon_y = \upsilon_0 \sin\theta - gt \tag{3.14}$$

$$h = \upsilon_y t + \frac{1}{2}at^2 \tag{3.15}$$

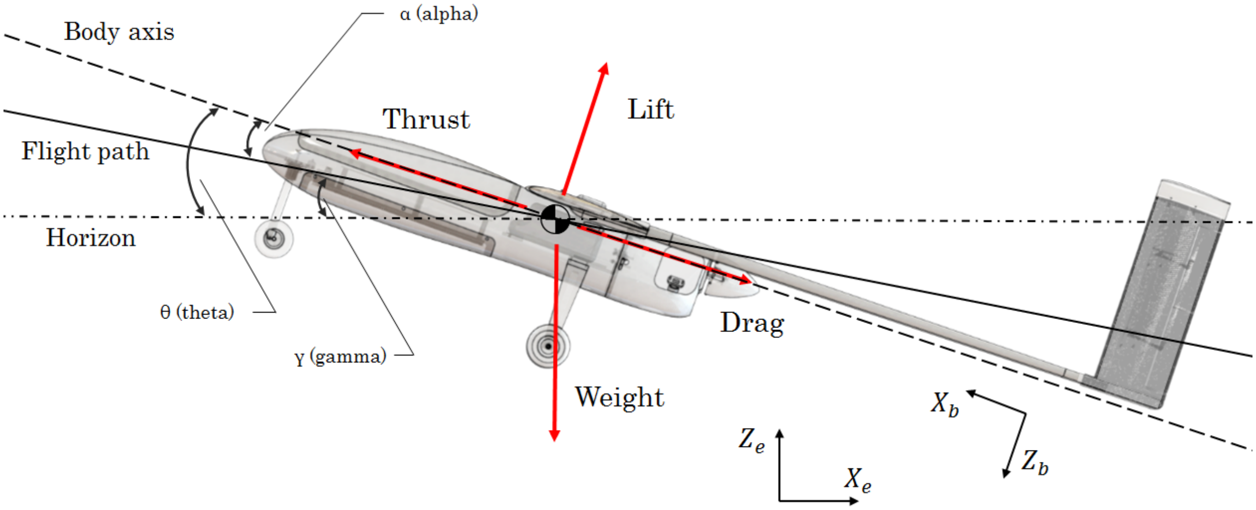

Figure 3.2: Earth to Body frame of reference

3.1.2 Longitudinal Motion EOMs

The three DOF(degree of freedom) forces acting on a microgravity aircraft are shown in figure 3.2. Here, the body frame of an aircraft consists of only the x and z-axis–excluding the y-axis. This pure longitudinal study is an acceptable approach for both a dynamic model of an aircraft in free with the assumption that the motion in the yaw and roll direction is negligible. This assumption is valid due to the fact that heading hold and stabilized roll autopilot control is common and robust. A longitudinal approach simplifies and reduces the number of equations used to estimate the dynamics of the system thus increasing the reliability of simulations [12]

$$F_X = T\cos\theta - D\cos\gamma - L\sin\gamma \tag{3.16}$$

$$F_Z = -mg + T\sin\theta - D\sin\gamma + L\cos\gamma \tag{3.17}$$

Thrust and drag are assumed to be acting in only the aircraft positive and negative body frame x-axis respectively. Aligning thrust and drag further simplifies the equations of motion and is good estimated assumption for simulation purposes. As mentioned in previous section, the original EOMs described the motion of the aircraft in the body frame of reference. Equation 3.16 states the forces in the earth frame of reference in the x direction and equation 3.17 includes the force reactions in the vertical direction derived from figure 3.2. These equations are used in the simple MatLab simulator created for initial controller design and verification of concepts.

3.1.3 Maximizing duration and quality

Based on projectile motion the desired altitude, velocity and attitude across the duration is determined. The duration of the reduced gravity period will be determined by how long the vehicle can follow this path. Maximum duration is a function of aircraft performance and is impacted less by controller robustness. Although, some parameters of the flight path can impact the duration like launch velocity and starting altitude. For reference, a vehicle with zero upward velocity V_y will fall 4,500m in 30 seconds. The initial launch angle is optimally 45 degrees because it splits up velocity into X and Y components evenly but V_y is more important for reducing maximum speed. Velocity is a function of gravitational acceleration so flight speeds become unobtainable within 30 seconds depending on the upward velocity. One method of increasing V_y is by carrying the aircraft's energy through to the next microgravity period shown in figure 3.3. Momentum allows the vehicle to achieve a greater V_y than before. This is yet another parameter influenced by aircraft performance characteristics as a low drag, high thrust vehicle is optimal. Increasing vehicle weight increases momentum but also reduces climb rate so it is better just to increase thrust to weight ratio and reduce drag. Quality is determined by how closely the ballistic motion path is followed so it is ideal to minimize offsets with high speed controllers. The aircraft geometry also plays a part in quality of the due to larger aspect ratio wings being more affected by drag. Gusts can push the aircraft away from the desired path.

Equation 3.18 is called the speed damping derivative and is important in determining the maximum duration. The speed damping derivative notes that the forces

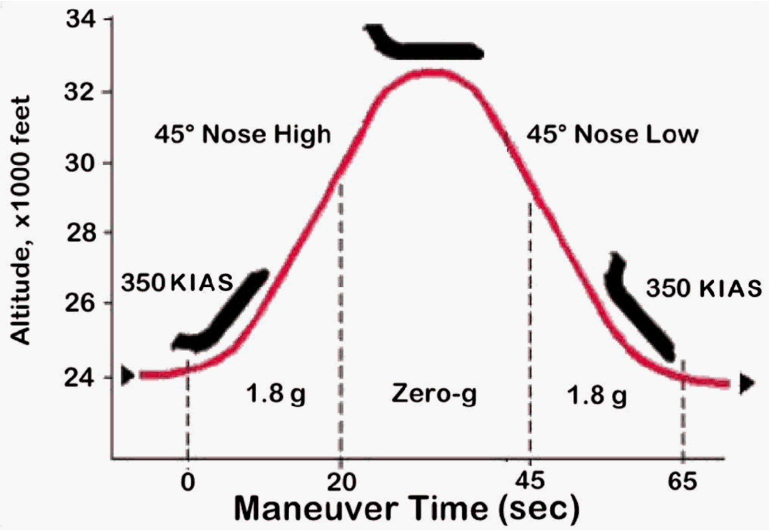

Figure 3.3: Flight path of a microgravity vehicle **??**

in the X_B direction change with velocity due to the fact that drag and thrust increase with speed. The throttle controller must create a thrust equal to the current drag in order to maintain zero gravity. This concept is important to understand because it is potentially limiting the duration if the engine can no longer produce the thrust required to accelerate through drag. C_L also changes with velocity and is described in equation 3.19 where $\mathbf{M}$ is the local Mach number. It has also been observed that aircraft during the microgravity maneuver are also producing zero lift in order to fly like a projectile. Lift is varied with angle of attack but at higher speeds, obtaining zero lift becomes more difficult.

$$\frac{\partial X}{\partial v} = -\frac{\partial D_f}{\partial v} + \frac{\partial T}{\partial v} \tag{3.18}$$

$$\frac{\partial C_L}{\partial \mathbf{M}} = \frac{\mathbf{M}}{1 - \mathbf{M}^2} C_L \tag{3.19}$$

The performance of the aircraft will limit the maximum free fall period as stated above. The equations that quantify the important performance characteristics are in the following. Climb rate of an aircraft is limited by the thrust to weight ratio described in equation 3.20. The pitch angle θ is shown in equation 3.21 which can be re-organized algebraically to calculated the climb rate at a 45 degree angle. This estimates the ROC based on the current velocity.V_{ne} the never exceed velocity and is determined by the aircrafts maximum structural stress due to dynamic pressure with increased speed. The location of probable failure during high speed flight is at the wing root. A large bending moment is applied to this location from wing drag and span length. The V_{ne} is not usually made available by manufacturers of COTS aircraft but estimates can be made with wing drag coefficient and maximum spar strength. Additionally, a failure case can be tested with load cells on a similar wing and the flight envelope can be shifted accordingly.

$$ROC_{max} = \frac{T_{max} - D_f}{W} \times V \tag{3.20}$$

$$\theta = sin(\frac{ROC}{V}) \approx \frac{ROC}{V} \tag{3.21}$$

Quality of the reduced gravity hold is determined by how well the aircraft can respond to small accelerations in any direction. These micro accelerations are generally caused by gusts or unsteadiness in the atmosphere and can be mitigated by control systems. The increased effect of gusts on smaller airframes forces the autopilot and control algorithms to be more robust on a UAS. Aircraft with a lower moment of inertial also require less control surface authority potentially making them more able to mitigate gust effects. Quality can be quantified by the average deviation from the targeted acceleration. For example, a Martian environment would be 0.38g and a C-9 aircraft can typically hold this with a residual acceleration accuracy of $10^{-2}g_0$ or $0.38g \pm 0.01g$. Where g_0 is the targeted acceleration. Quality of the free fall is significant to the experiment on board the vehicle.

Residual accelerations caused by the rotational rate of the aircraft are also important to consider so that the accelerations within the payload bay are as close to

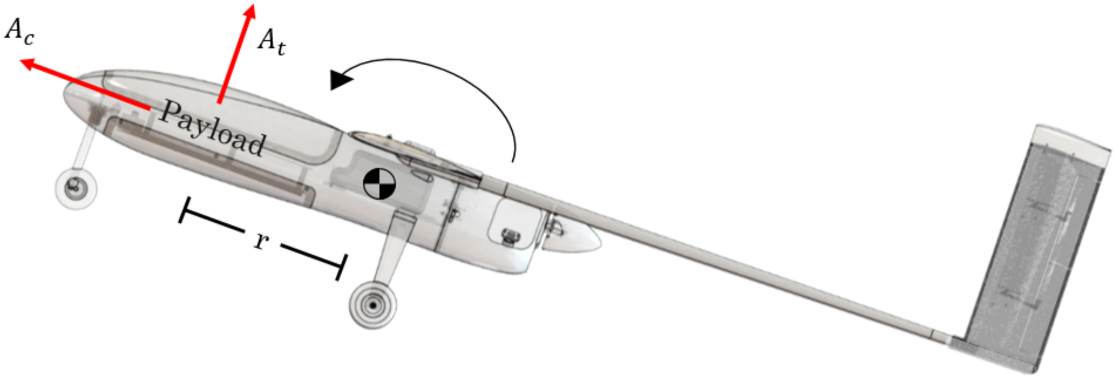

Figure 3.4: Effect of pitch rotation on local accelerations

the target as possible. During the maneuver, the aircraft is constantly pitching about its body frame y-axis causing a constant centripetal acceleration toward the interior of the aircraft. A forward payload bay would experience a reaction force toward the nose of the aircraft during a pitch down maneuver. Additionally, the payload will also experience a tangential acceleration A_t due to the the angular acceleration or pitch rate $\dot{Q}$ of the aircraft. A_t is also depends on distance from the rotational axis and will be the greatest at the beginning of the maneuver because the $\dot{Q}$ is largest. Both A_c and A_t are shown in figure 6.7.The dynamics of centripetal acceleration can be described in equation 3.22 where omega is the average angular velocity and **r** is the distance from the venter of rotation or CG. The dynamics of tangential acceleration is described in equation 3.23 where alpha is angular acceleration or $\dot{Q}$.

$$A_c = \omega^2 \mathbf{r} \tag{3.22}$$

$$A_t = \alpha \mathbf{r} \tag{3.23}$$

it is important to characterize the variation in local accelerations due to the pitch rate of the aircraft during the maneuver. An ideal case would be to have the on board experiment placed directly at the center of gravity of the aircraft. Otherwise, the experiment will experience centripetal and tangential accelerations during a pitch of the aircraft. The angular velocity due to pitch rate of the aircraft can not be avoided so to reduce local accelerations– the distance from the center of gravity must also be reduced. The exact amount of tangential and centripetal acceleration can be estimated due the fact the pitch rate is known. The path of a projectile is described in velocity components throughout the arc with projectile motion equations. The velocity components can then be used to calculate the angle of the craft relative to the earth which also known as flight path angle γ which is shown in figure 3.5. This can be used in calculation of $Q(\omega)$ and $\dot{Q}(\alpha)$ to determine A_c and A_t. Maximum Q is calculated as $24deg/s$ and max $\dot{Q}$ is 7 deg/s^2. Assuming a conservative distance of $0.5m$ from the center of gravity the maximum accelerations caused by Q and $\dot{Q}$ is $0.09m/s$ and $0.06m/s$ respectively. These accelerations are a small fraction of earth gravity so it can be concluded that the forces to follow are negligible.

3.2 Control

A background in basic control theory is important to the understanding of the microgravity controllers that are discussed in later chapters. In general, control theory is considered to be broken up into tow sections, the classical approach and modern control theory. The classical control approach is based on frequency response, root locus technique transfer functions and Laplace transforms which had its beginning in the 1930s [10]. Although the name suggests that classical control theory not used today, it is still very useful mainly because its simplistic. Classic control theory was the only answer to control prior to the introduction of computers. Modern control theory takes advantage of the power of computers by using state space modeling, state observers and ultimately allows for optimal control. Stability augmentation is one of the main uses of modern control which allows pilots to control aircraft that

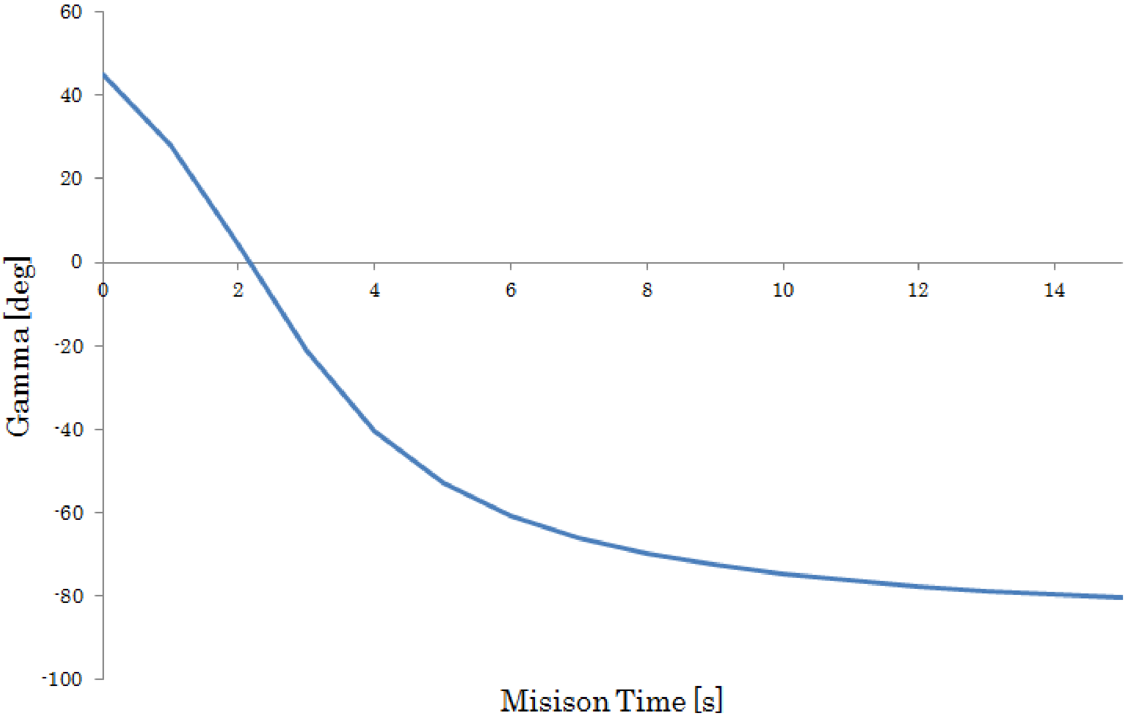

Figure 3.5: Flight path angle of a projectile in a ballistic trajectory

would normally be to unstable for reactionary piloting.

Most modern, high performance aircraft have operational envelopes that require feedback controllers with differentiating gains due to the large variations in dynamic pressure and Mach number. Gain scheduling is usually used to tune the controllers for these different flight conditions [12]. This is done so by increasing or decreasing the gains with variations in Mach number. In lower performance aircraft with relatively narrow flight envelopes (like UAVs), it is not as crucial for control gains to have the ability to change during flight. Dissimilar UAVs will require different gains initially but it is acceptable to use the same gains through out each respective aircrafts flight envelope. For UAVs, the normal process is to flight test the controller gains that were estimated in simulation, then update the control gains for each successive flight test based off of how the aircraft responds. In this case, it is crucial that the remote pilot have the ability to take back control of the aircraft at any time when tuning gains

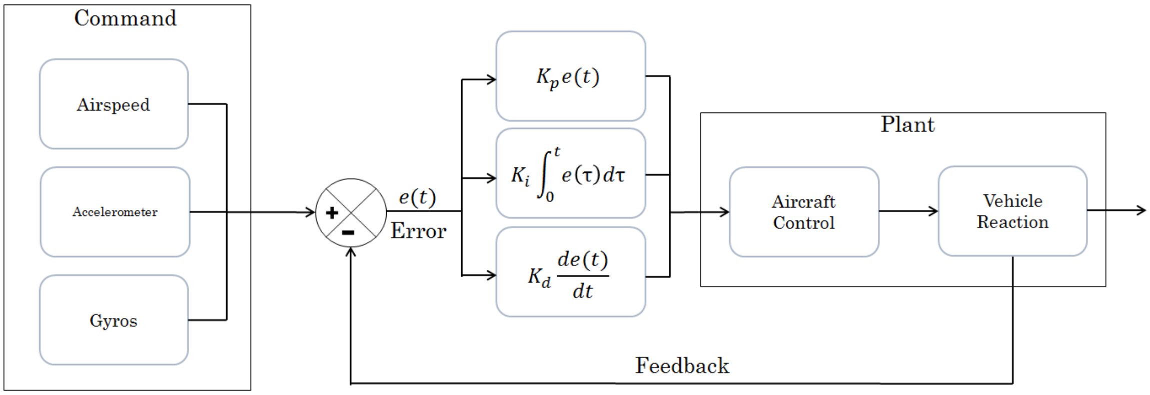

Figure 3.6: General PID controller

during flight tests. Pass through of the RC signal through the autopilot is needed to prevent loss of aircraft should the newly developed control algorithm fail.

Open loop is the most simple type of control. Here the input is directly fed to the controller then output to the system. In the open-loop system the control action is independent of the output. Open-loop control can be used for simple systems like a throttle controller. Closed-loop system the control action depends on the output of the system so it is more accurate [10]. Closed-loop is considered also known as feedback control.

3.2.1 Feedback control

PID (Proportional Integral Derivative) controllers are the most common type of feedback controller. A general PID controller can be visually referenced in figure 3.6. These types of controllers modify an error signal with three different controllers. Proportional controllers react to the error proportionally which is the most simple but creates a steady state error [10]. The integral gain mitigates the steady state error and causes the controller to react more quickly which inherently makes the it less stable. The derivative term mitigates overshoot and responds before error becomes large. Derivative controllers have issues with steady state error and signal noise. Fil-

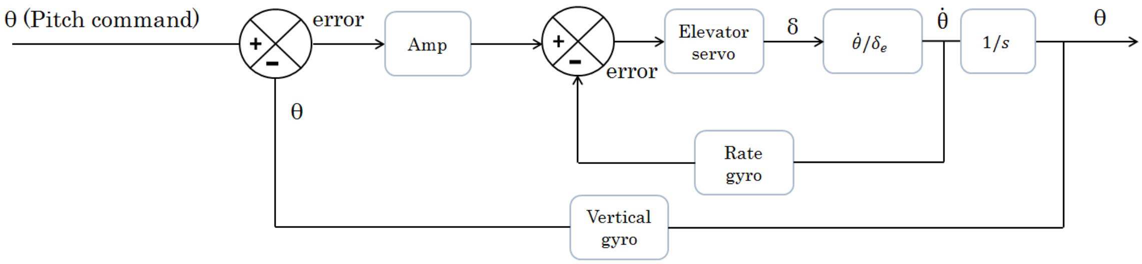

Figure 3.7: Pitch rate feedback controller [10]

ters can be used on error signals so that the derivative term does not amplify the noise. All three, P I and D controllers used together take of the slack of the others and result in a robust controller. In some applications it is better to reduce these controller to PI or PD controllers. It is also sometimes useful to limit the output of the controllers so that errors in throttle or elevator commands do not occur. Normally throttle commands range from 0-1 while control surface commands range from -1 to 1. This concept is important in both simulation and flight testing.

Displacement autopilots were one of the first types to be used in aircraft control [10]. Pitch displacement control is particularly important to the development of a microgravity control scheme as well. This type of control logic command elevator deflection depending on the displacement error between commanded and actual pitch of the aircraft. Pitch controllers have been used for different objectives like altitude hold, climb or aircraft attitude control. Normally, the control system uses a vertical rate gyro to feedback the current pitch of the aircraft shown in the outer loop of figure 3.7. To improve on damping, an inner loop which contains a gyro measuring pitch rate shown figure 3.7 can be added. The main issue with this is that gains must be tuned by trial and error until the desired response of the system is achieved.

Generally, closed loop controllers within aircraft include an outer and inner loop. The inner loop uses feedback compensation at a higher rate than the outer loop and is used in rate feedback of aircraft gyros or tachometer [12]. Rate feedback is usually only controlled with a proportional gain controller. This gain serves as the derivative gain for the outer loop controller where only a PI controller would be implemented. Together, the outer and inner loop contain a full PID controller. It is possible to control the aircraft in flight simulation will simple outer loop angle control, but during unsteady flight conditions rate compensation is needed. This type of controller will be needed to achieve the optimal pitch during a weightless maneuver.

3.2.2 Flight computer logic

In general, aircraft with lower moment of inertia need more responsive controllers to maintain the desired flight path. A microgravity vehicle is heavily effected by undesired changes in flight path due to the importance of experimental accuracy as described in previous sections. It is even more important then that the developed controllers be able to respond quickly and with minimal overshoot. Only in recent years, has autopilot technology become powerful and cheap enough to mitigate the effects of gusts. Also, it is important that the flight controller be able to direct the aircraft to achieve the longest duration microgravity period possible and this is increased with a initial upward velocity as described in previous sections. In this section we will assume logic for roll and yaw motion of the aircraft is already implemented because in most cases this flight logic has already been in developed. Assuming this also allows a more in depth description of the microgravity flight mode. There are multiple options for microgravity flight controllers of which will be described in this section. Each controller described will be verified in simulation and HIL before flight testing. It is important for the flight computer or the pilot of the aircraft to monitor flight speed. To low of a flight speed during the start of the maneuver could cause stall while too high of an airspeed towards the end would result in overspending of the airframe.

An acceleration feedback controller might be the most trivial to understand from

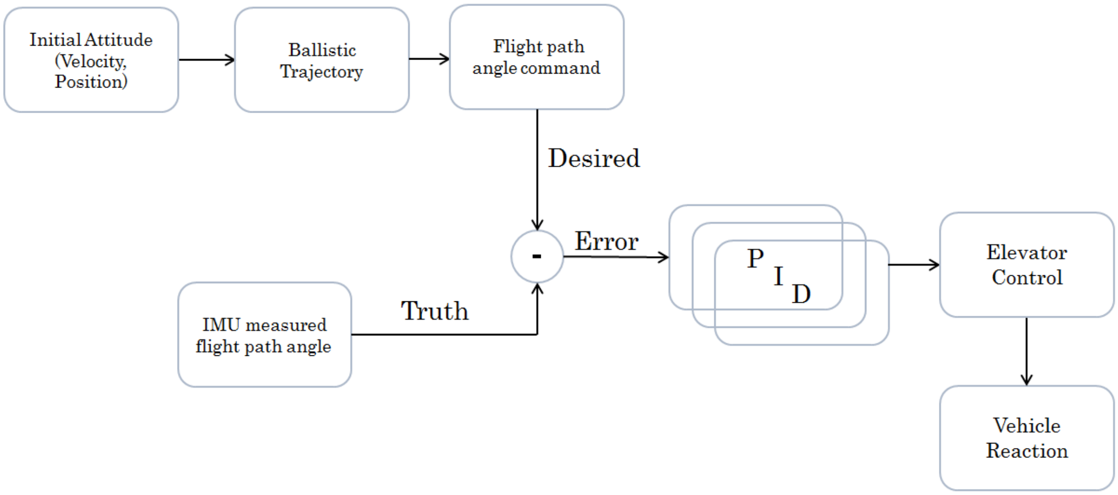

Figure 3.8: Alpha controller for ballistic trajectory path following

a broad perspective however it is difficult to design and implement. The idea is to obtain acceleration in both the X_B and Z_B axis of zero and control this with only elevator and throttle commands. Accelerometers on board the aircraft will measure the actual accelerations from the body frame of reference. This causes issues because the pitching of the aircraft creates acceleration of gravity in both X_B and Z_B body frame to change during the maneuver. Assuming that the attitude of the aircraft is known, the controller can command the desired component of gravity in each axis. The issue is that acceleration in the Z_B axis is not straight forwardly controlled by elevator command.

The main concept for control is described my ballistic motion which is known as projectile motion without the effects of aerodynamic drag. Objects that follow this path are introduced to a local net acceleration of zero as the body of the craft is allowed to accelerate with gravity. Therefore the main objective of this controller is to have the aircraft fly like a ballistic projectile which is not a normal flight mode. Based on projectile motion, there are couple different methods one can implement to control the aircraft in the desired flight profile.

Describing the desired path to follow is the more general of the two methods. Using the projectile motion equations described in equations 3.13, 3.14 and 3.15. From here we can derive the desired flight path angle γ and velocity. Calculation of γ and velocity desired can be done for the entire flight path based on the initial condition of the aircraft or calculated for each time step and updated accordingly. The continual calculation of desired γ and velocity allows for a more robust desired path which can respond better to gusts or perturbations although a feedforward flight path from the initial condition is easier for the controller to run at a high rate. γ is a parameter that can be determined by the INS (inertial navigation system) which is a system included in most autopilot controlled UAS. An error can then be generated between the desired γ and actual γ so that PID control can be used for α command. A visual representation of this controller is shown in figure 3.8. This concept controls γ with an commanded or desired alpha angle. Since the response between gamma and alpha commanded is not immediate in the real world, a transfer function was included to realistically delay the response. In operation, the controller will need to use elevator deflection in order to control α angle which introduces the need for another controller. This attitude controller will be nested within the flight path controller and will run at a faster rate.

Engine throttle control for this method is based on the concept that drag and thrust are the only two forces acting inX_B. For acceleration in X_B to be zero, the desired thrust is equal to the drag throughout the flight profile. PID control can be used based on the thrust of the previous step and a drag estimation based off of the current speed. A feedforward approach is more ideal for controller responsiveness although it is more reliant on an accurate drag estimate throughout the flight envelope. For a feedforward concept, velocity can be calculated for the whole flight path based off the initial condition which ballistic trajectory calculations as used earlier. Then, the drag can be estimated for the entire flight path based off of the velocity profile

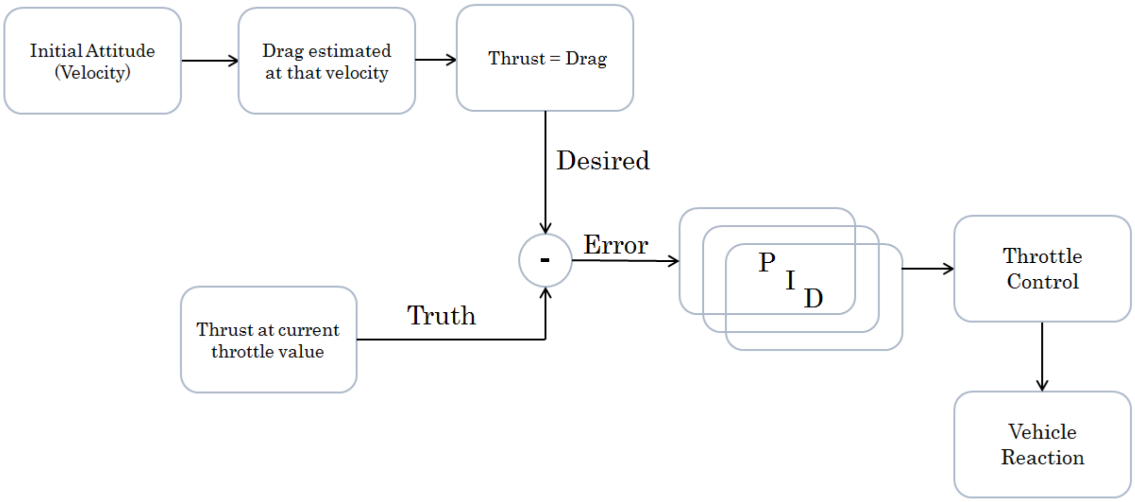
Initial Attitude (Velocity)
Drag estimated at that velocity
Thrust = Drag
Desired
-
Error
P
I
D
Throttle Control
Vehicle Reaction
Truth
Thrust at current throttle value

Figure 3.9: Throttle controller for ballistic trajectory path following

that is expected and a drag buildup of the aircraft. A visual representation of this controller is shown in figure 3.9.

The methods of control are currently reactive to the aircrafts starting velocity and position. For longer duration free fall the aircraft needs an initial upward velocity. This can be controlled manually by the manned pilot but also can be commanded via flight computer. An initial upward velocity allows a longer period before acceleration due to gravity requests a velocity that is not obtainable limited by either maximum engine thrust or maximum flight speed structurally. The maximum upward velocity is determined by aircrafts maximum ROC described in equation 3.21 but is usually at a 45 degree flight path angle. A 45 degree γ can be commanded by the elevator controller while throttle is increased to maximum until the highest ROC is achieved. Once in this state the previous logic can take over and control the aircraft into free fall maneuver. Once the microgravity maneuver is complete energy can be maintained through the next pull up phase to achieve a greater ROC. This method can be repeated for multiple maneuvers ultimately generating a sine wave flight path.

$$\begin{aligned} L - W_z = L - Wcos(\theta) = mA_z = m(1.8 - cos\theta)g \\ L = Wcos\theta + m(1.8 - cos\theta)g = W(cos\theta + 1.8 - cos\theta) = 1.8W \\ L = 1.8W \end{aligned} \tag{3.24}$$

$$\begin{aligned} L - W_z = L - Wcos(\theta) = mA_z = m(-cos\theta)g \\ L = Wcos\theta + m(1.8 - cos\theta)g = W(cos\theta + 1.8 - cos\theta) = 0W \\ L = 0W \end{aligned} \tag{3.25}$$

Another method of control is defined by Karmali and Shelhamer of which divides the complete maneuver(climb and descent) into magnitudes of increased and decreased lift of the wings [13] while maintaining thrust equal to drag in both phases. The two stages are pull up, where the occupants would experience positive g acceleration and the pitch over stage where the occupants would feel weightlessness. The dynamics are described by equations 3.24 and 3.25 below. Equation 3.24 describes the constant lift needed during the optimal pull up section of the maneuver while equation 3.25 describes the zero lift required through out the pitch over stage. Lift force is modulated by the angle of attack of the aircraft which is controlled with elevator deflection. True lift can be calculated with C_L, airspeed and angle of attack. A PID controller can be used to control the elevator deflection with error from the true lift and desired lift using equations 3.24 and 3.25. Desired lift is easily calculated by weighing the aircraft prior to testing. One issue with this type of controller is that the angle of attack must be known for lift calculations. α can be measured by multi hole Pitot probes or flag type AOA sensors. Multi hole Pitot probes can be manufacture relatively cheaply with current additive printing technology but they require extra logic to calculate estimated α. Flag type AOA sensors are usually not included on small UAS and can be quite expensive to the underfunded researcher.

CHAPTER 4

Methodology

This chapter discusses the modeling and simulation tools that were used to develop and evaluate the various methods of controlling a microgravity vehicle. In industry, the development of new aircraft and flight controllers are heavily dependent on the success of the modeling and simulation step. For each model and simulation, there is different ranges fidelity. High fidelity aerodynamic models are generated by wind tunnel testing and CFD, while low fidelity aircraft models are generated with X-Plane and Datcom. Researchers with less funding are usually constrained to lower fidelity models for simulation purposes. Additionally, simulations for low budget researches are less perfect. In industry for airliners and military aircraft, modeling and simulation would normally be tasked by a team of engineers so that the highest fidelity model and simulator was developed before flight testing. A high importance is placed on simulation accuracy due to loss of aircraft being unacceptable and the significance of vehicle design for these applications. Although it is still important for relatively cheap UAVs, it is acceptable to preliminarily use lower fidelity modeling and simulation techniques prior to flight testing.

Figure 4.1 represents the methodical approach that was taken to achieve the final goal of flight testing a microgravity vehicle. The process starts off at the definition of the aircraft which is used for generating an aerodynamic model. This step is basically gathering information for the aircraft and preparing it for the text based Datcom import. A CAD (computer aided design) file of the aircraft is very helpful for the aircraft description due to the detail in geometry that it provides. The Datcom a tool used to model the aerodynamics of the aircraft and is explained in more detail in the following section. A pre-requisite to this step is the selection of an aircraft for modeling and this process will be described in a following section. The flight profile for each respective aircraft is also important to be knowledgeable of because it will be an important input into the Datcom program. The Datcom outputs the aerodynamic coefficients, both static and dynamic, stability derivatives of the aircraft that can then be used in simulation programs like JSBsim, X-Plane and Simulink. The simulators rely on numerous models including atmospheric conditions, engine powerplants, sensors and controllers to estimate a realistic system. The simulators are used to develop and judge control concepts and logic as well as grade the ability of the vehicle to generate microgravity. The simulation results are then determined and a decision is made to either re-define the aircraft (chose a new aircraft), modify control logic or continue on to vehicle integration for flight testing. MATLAB or Simulink is able to converted to a C programing language and then implemented onto an a micro controller/autopilot. Once the flight is implemented onto a working autopilot, HIL tests can be conducted. HIL is generally done with a robust flight simulation program like X-Plane which generates a fully dynamic model of the aircraft and environment. The HIL step is important for testing the entire system together, debugging flight code, determining gust response of the aircraft and tuning gains. Once the HIL tests are completed the aircraft and autopilot is ready for its main challenge, flight testing.

4.1 Modeling

the Modeling process collects and collates information about a system and then constructs representations of that system [14]. In this section, the modeling of the Penguin-B aircraft will be discussed using different methods. These methods include the Digital Datcom and X-Plane. Platform selection will be discussed later sections but a vehicle must be selected initially in order to describe the modeling

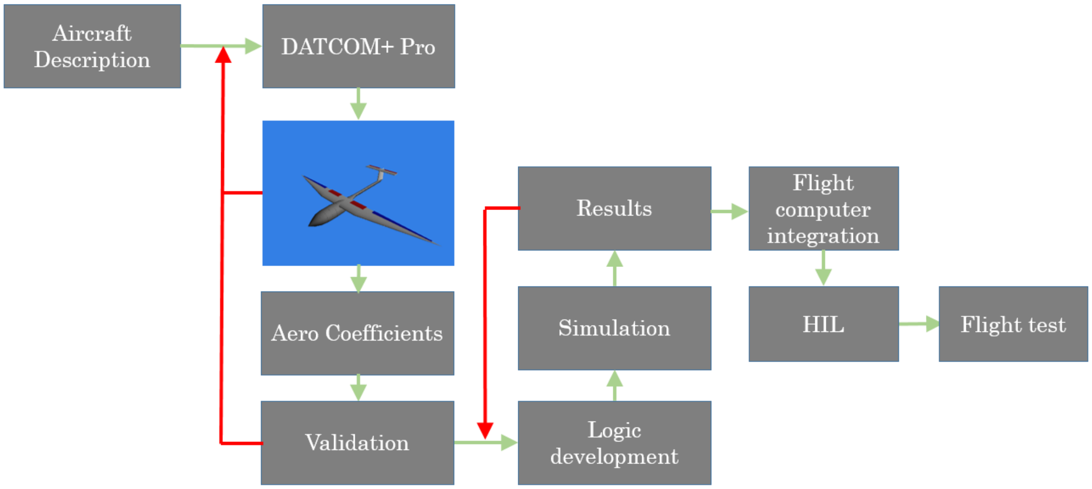

Figure 4.1: Methodology for modeling and simulation

process. The author has selected the Penguin-B aircraft designed by UAV Factory due to availability of important design parameters. UAV Factory has supplied the author with a CAD model of the aircraft as well as data sheets for mass moment of inertia which made the modeling process easier. In most cases, with cheaper airframes, the manufacture will not CAD, and inertial data. This makes the modeling process a more difficult although these parameters can be estimated. The Penguin-B is a classified as a twin boom inverted V-tail STUAV (small tactical unmanned aerial vehicle). STUAVS are sized between small and medium UAVs. The airframe has a 3.3m wing span and maximum take off weight of 21.5kg. The Penguin-B has a stall speed of 13 m/s and a max level speed of 36m/s and uses the 28cc internal combustion engine made by 3W. The engine can produce up to two and a half pounds of horse power, generating up to 10 lbs of thrust. The Penguin-B has a large payload bay like most twin boom tail airframes and mediocre performance characteristics. The aircraft is designed for long duration flights and is able to achieve an endurance of 20 hours with its high aspect ratio wings. An image of the Penguin-B aircraft can be

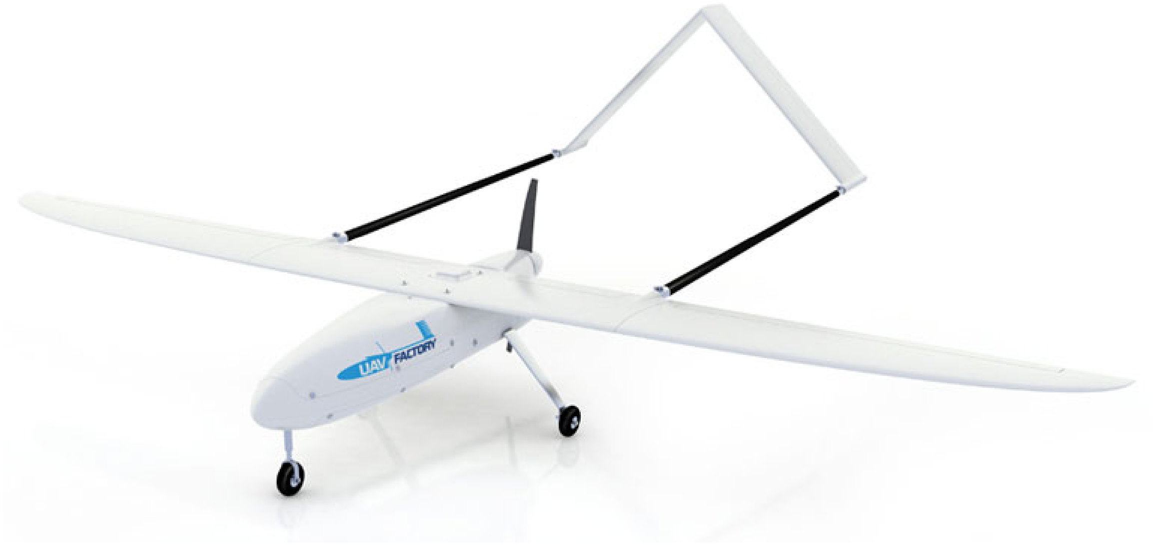

Figure 4.2: Penguin-B airframe developed by UAV Factory

referenced in figure 4.2.

4.1.1 Digital Datcom

The digital Datcom (data compendium) was created from the original paper version of the Datcom which was developed by the United States Air Force (USAF). The digital program calculates the static stability, control deflection effects and the dynamic derivatives of different aircraft geometry. It was first released in November of 1978 by the McDonald Douglas company and many updated versions have been released since then. It was also originally developed to provide rapid stability and control characteristics for preliminary design of fixed wing aircraft [15]. Although the program was written in the outdated programing language of Fortran, It still serves the same purpose today. Other programing languages like C and python are much more common but the Datcom has never been converted to these types because the user does not need a strong Fortran background in order to use the program effectively. The program is run as a executable file which will request a text file upon opening. The text file is the only way that the user can interface with the Datcom which contains the aircraft geometry and flight conditions.

The imported text file is set up with a structure of namelists that include, FLTCON, OPTINS, SYNTHS, BODY, WGPLNF, HTPLNF, VTPLNF and SYNFLP. The text file that created the Penguin-b aircraft model is included in figure 4.3 for reference. The FLTCON and OPTINS namelists describe the flight conditions and options respectively. Referring to the input file in figure 4.3, the flight conditions include multiple Mach numbers, multiple altitudes and multiple angles of attack. The Datcom has a systematic way to work through these conditions and can be varied using the "Loop" command. Loop = 1 changes Mach and altitude together while Loop = 2 only varies Mach at a fixed altitude then continues to the next altitude condition. Loop = 3 varies altitude at a fixed Mach number. It is important to note that each case is run for each angle of attack as well. This feature makes it easier to receive the coefficients for multiple flight conditions without entering multiple Datcom input files. The options section is where the user defines the aircrafts reference lengths, SREF is the wing reference area, CBARR is the reference wing chord and BLREF is the reference wing span. The SYNTHS namelist refers to synthesis parameters which included CG, wing, vertical and horizontal tail locations in the aircrafts X and Z-axis.

The BODY namelist is the most time consuming to complete depending on the type of aircraft fuselage. For these parameters, the user must describe the number of fuselage crossections and the geometry/location of each. WGPLNF, HTPLNF and VTPLNF are the body, wing horizontal and vertical tail parameters respectively. These namelists included the same general parameters to describe each. CHRDR is the respective chord at the root of the object. CCRDR is the respective root chord. CHRDBP defines the chord length at a wing breakpoint (multiple breakpoints can be added for more complex geometries). SSPN and SSPNE and SSPNOP are the semi-

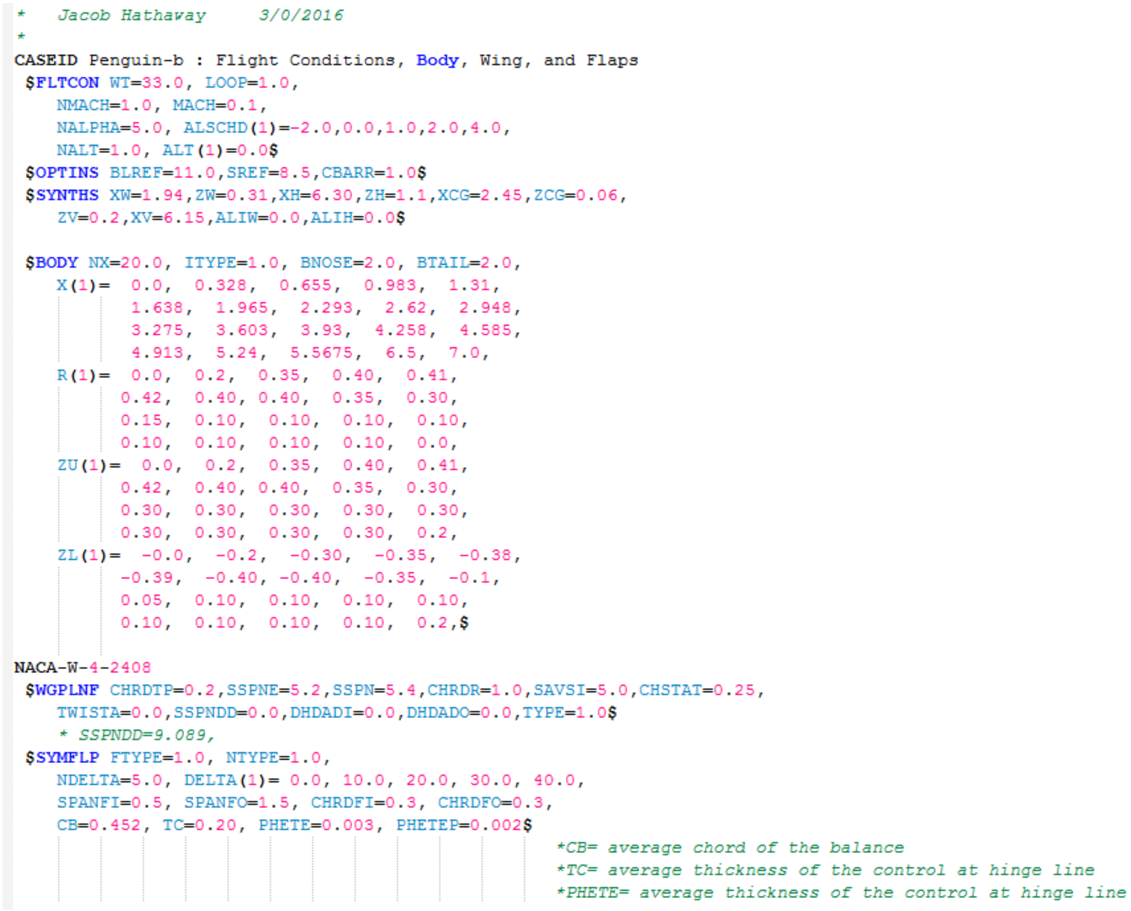

```
*   Jacob Hathaway     3/0/2016
*
CASEID Penguin-b : Flight Conditions, Body, Wing, and Flaps
 $FLTCON WT=33.0, LOOP=1.0,
    NMACH=1.0, MACH=0.1,
    NALPHA=5.0, ALSCHD(1)=-2.0,0.0,1.0,2.0,4.0,
    NALT=1.0, ALT(1)=0.0$
 $OPTINS BLREF=11.0,SREF=8.5,CBARR=1.0$
 $SYNTHS XW=1.94,ZW=0.31,XH=6.30,ZH=1.1,XCG=2.45,ZCG=0.06,
    ZV=0.2,XV=6.15,ALIW=0.0,ALIH=0.0$

 $BODY NX=20.0, ITYPE=1.0, BNOSE=2.0, BTAIL=2.0,
    X(1)=  0.0,  0.328,  0.655,  0.983,  1.31,
           1.638,  1.965,  2.293,  2.62,  2.948,
           3.275,  3.603,  3.93,  4.258,  4.585,
           4.913,  5.24,  5.5675,  6.5,  7.0,
    R(1)=  0.0,  0.2,  0.35,  0.40,  0.41,
          0.42,  0.40, 0.40,  0.35,  0.30,
          0.15,  0.10,  0.10,  0.10,  0.10,
          0.10,  0.10,  0.10,  0.10,  0.0,
    ZU(1)=  0.0,  0.2,  0.35,  0.40,  0.41,
          0.42,  0.40, 0.40,  0.35,  0.30,
          0.30,  0.30,  0.30,  0.30,  0.30,
          0.30,  0.30,  0.30,  0.30,  0.2,
    ZL(1)=  -0.0,  -0.2,  -0.30,  -0.35,  -0.38,
          -0.39,  -0.40, -0.40,  -0.35,  -0.1,
          0.05,  0.10,  0.10,  0.10,  0.10,
          0.10,  0.10,  0.10,  0.10,  0.2,$

NACA-W-4-2408
 $WGPLNF CHRDTP=0.2,SSPNE=5.2,SSPN=5.4,CHRDR=1.0,SAVSI=5.0,CHSTAT=0.25,
    TWISTA=0.0,SSPNDD=0.0,DHDADI=0.0,DHDADO=0.0,TYPE=1.0$
    * SSPNDD=9.089,
 $SYMFLP FTYPE=1.0, NTYPE=1.0,
    NDELTA=5.0, DELTA(1)= 0.0, 10.0, 20.0, 30.0, 40.0,
    SPANFI=0.5, SPANFO=1.5, CHRDFI=0.3, CHRDFO=0.3,
    CB=0.452, TC=0.20, PHETE=0.003, PHETEP=0.002$
                                                  *CB= average chord of the balance
                                                  *TC= average thickness of the control at hinge line
                                                  *PHETE= average thickness of the control at hinge line
```

Figure 4.3: Digital Datcom input file for Penguin-B aerodynamic coefficients

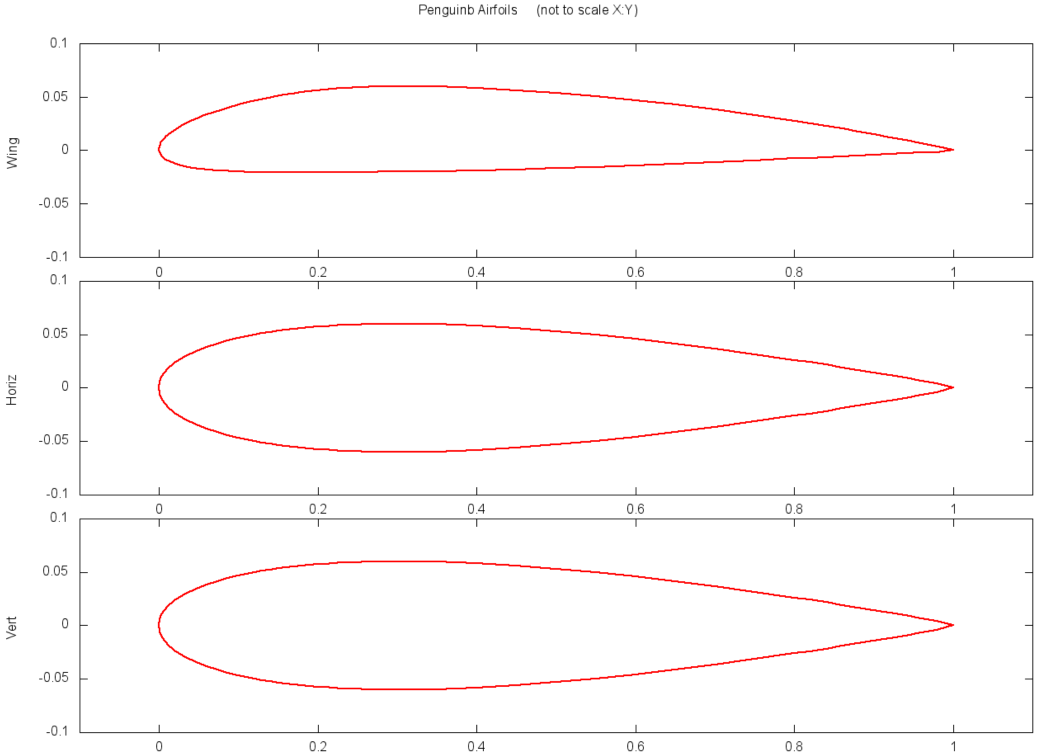

Figure 4.4: Airfoils imported into the digital Datcom for the Penguin-B model

span, exposed semi-span and semi-span from the breakpoint respectively. Dihedral, sweep and twist of the surface are defined by the parameters DHDADI, TWISTA and SAVSI/SAVSO respectively. The modeled aircraft for the microgravity vehicle have some wing sweep but do not have dihedral or wing twist which means these parameters generally have a value of zero. The last namelist used in the Datcom input file is SYMFLP and is where the user will define the control surface geometry. Ailerons and flaps can easily be defined as well as a multitude of deflection angles in which Datcom will run cases for. Within SYMFLP, the CB and TC parameters is are the average chord of the balance point and the average thickness of the control surface at the hinge point respectively. Lastly, the airfoils for the wing, horizontal and vertical tails are defined in a NACA four digit code at the end of the input text file.

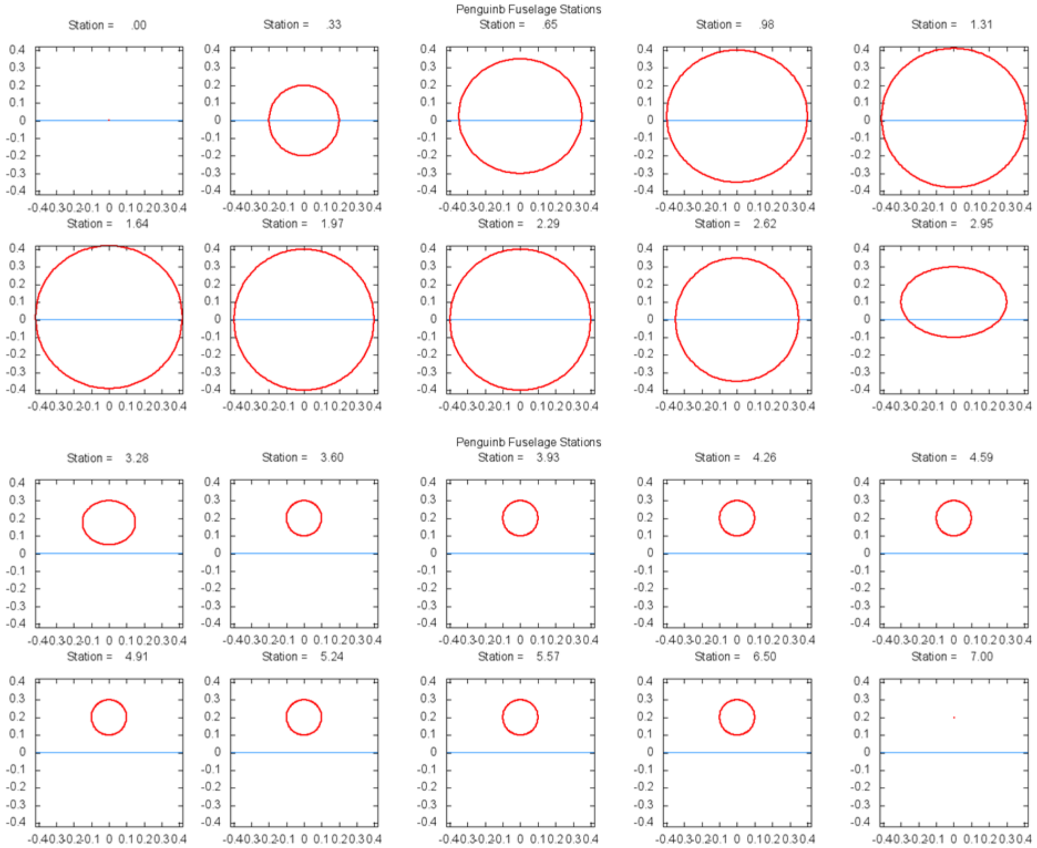

Figure 4.5: Fuselage crossections of the Penguin-B Datcom model

The aerodynamic coefficients are output through another text file. A list of some of the important coefficients are included in the following. The static stability coefficients are C_D, C_L, C_M, C_N, C_A as well as the dynamic derivatives $\partial C_l/\partial\alpha$, $\partial C_m/\partial\alpha$, $\partial C_y/\partial\beta$, $\partial C_n/\partial\beta$ and $\partial C_l/\partial\beta$. These coefficients are further defined in the list of symbols. The program can also calculate the downwash effects on the tail due to wing lift.The text file can be imported into Matlab using multiple matrices and arrays. Matlab stores each stability and control derivative so that they may be implemented into a Simulink model.

Datcom+ Pro was developed by Holy Cows Inc. to help students and professionals pick up the program more efficiently rather than encountering a steep learning curve [16]. The updated version includes add on programs that feature AC3D (Aircraft 3-d) and MATLAB for aircraft visualization feedback. The program is also able to output the cross sectional geometry of the fuselage sections and airfoils selected. An example of the fuselage sections is shown in figure 4.5 and an example of the airfoil visualization in figure 4.4. The control surfaces are also shown in the 3-D rendering tools which is very useful for geometry verification. Another useful addition of DATCOM+ Pro is the ability to separate the output values with commas for ease of importation to MATLAB/Simulink. The aerodynamic coefficients can now be imported into excel or MATLAB more easily. Datcom+ Pro has also been re-programed to interface with JSBsim as an .XML (Extensible Markup Language) for easy flight simulation.

There are quite a few significant limitations to the digital Datcom program so it is important to remember that it is just a tool to use for preliminary design and simulation. In order to generate the most accurate stability and control coefficients, extensive experimental testing (both wind tunnel and CFD) needs to be completed. This subsection will walk through each of the limitations that are significant to simulating a microgravity vehicle and how the author changed the design to accommodate for the restrictions. There is currently no way to define a rudder in the Datcom but if we are considering pure longitudinal motion there will be no calculations that consider ruder control effects. One major limitation is the ability to model only cruciform and T-tail configurations. There are other configurations like H and V tails that are aerodynamically different from a normal tail and can also not be modeled in Datcom. The changes in aerodynamics are relatively small between configurations so a V-tail can be estimated as a T-tail of the same volume and control surface sizing. A V-tail with the same size and control authority as a T-tail, provides a small decrease in interference drag due having one less connection point between the rudder and elevator. However, the coupling of rudder and elevator mean that some efficiency will be lost in pure pitching or yawing control. Additionally, tail configurations will be influenced differently by propeller wash. These issues differences are considered negligible in the Datcom modeling of the Penguin-B. Another limitation is lack of twin boom fuselage modeling. This is particularly important to UAVs where using booms to support a tail is becoming a common design. The twin boom design allows the airframe to have a larger payload bay and a more ideal location for camera systems forward of the propellers with little aerodynamic differences. Modeling the fuselage does not pose as big of an issue as the does the tail configuration. Twin booms can be modeled aerodynamically as a long slender fuselage/empennage seen in figure 4.6.

4.1.2 Model Comparison

As mentioned previously, A CAD file from UAV Factory was used to build a model of the Penguin-B through an specialized text file in the Fortran language which was input to Datcom. In order to maintain the same tail volume, it was calculated and using equations 4.1 and 4.2. Equation 4.1 represents the horizontal tail volume where S_H is the horizontal tail area, L_H is the distance from the tail aerodynamic center to the CG of the aircraft, S_W is the wing area and MAC is the mean aerodynamic chord. Equation 4.2 represents the vertical tail volume where b is the wing span. For

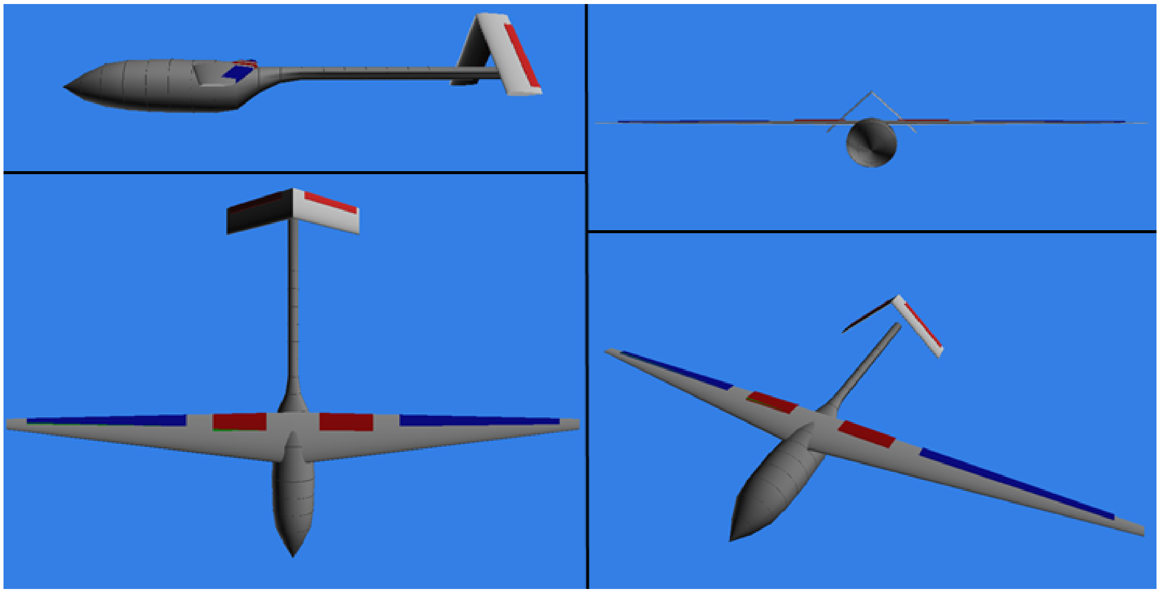

Figure 4.6: Digital Datcom output AC3D render

the case of a V-tail configuration, a horizontal and vertical tail must be arbitrarily selected. Placement of the T-tail is crucial to creating an accurate model and was done by matching the volumetric center for both tail and control surfaces. Aft and vertical tail distance are both important in longitudinal aircraft motion. Once the tail conversion is made and is placed in the correct location, the empennage is mostly complete. Twin boom effects were modeled by creating a thing fuselage with the same surface area. This will account for the effects of friction drag but may not include pressure drag due to separation in high angles of attack. However, in Datcom, there is currently no other options for modeling twin boom tails so this is an accepted inaccuracy. Datcom does not include the inertial mass data because no moments or forces are calculated. Inertial data will be mentioned in simulation.

$$V_H = \frac{S_H L_H}{S_W MAC} \tag{4.1}$$

$$V_V = \frac{S_V L_V}{S_W b} \tag{4.2}$$

After these changes have been made, the Datcom model is now used to calculate the aerodynamic derivatives for the 3 DOF simulation of the aircraft. Since the output file is usually multiple pages of data, an example of the output for the penguin-B will be included in the appendix figure **??**. Before this step, output of the modeled aircraft should be evaluated to show that Datcom has accepted the imported geometry and flight conditions. Although it would be quickly realized once testing began, verifying the stability prior to testing eliminates yet another variable during de-bugging of the software. The data used to create figures 4.7, 4.7 and 4.7 was taken from the Datcom output file at a Mach number of 0.1 and $300m$ altitude. Figure 4.7 shows the lift coefficient change with angle of attack. Angle of attack verses alpha plots show that the lift curve slope is correct and also reveals the zero lift angle of attack. Zero lift angle of attack is an important value for some of the microgravity control logic that is discussed later. Figure 4.8 includes the moment coefficient verses angle of attack plot otherwise known as the static longitudinal stability of the aircraft. A negative slope intersecting at a negative angle of attack indicates a stable aircraft in pitch. Graphs of some these simple aircraft parameters demonstrate that Datcom has modeled the aircraft as intended.

The root locus plot in figure 4.10 plots the stability modes of phugoid and short term longitudinal motion visually using real and imaginary components of the A matrix roots. The root locus plot was developed using the state space representation of the aircraft explained in equation 4.3. The A matrix is shown in equation 4.4, the B matrix is shown in equation 4.7 while x and η are shown in equations 4.5 and 4.6 respectively. x is the state vector, η is the control vector and the matrices A and B contain in the aircraft's dimensional stability derivatives [10]. The A matrix with the values from the Datcom model is shown in equation 4.8. The eigenvalues of the A matrix are then computed using the MATLAB function "eig()". A root locus plot can be constructed by plotting the real and imaginary values of the eigenvalues shown

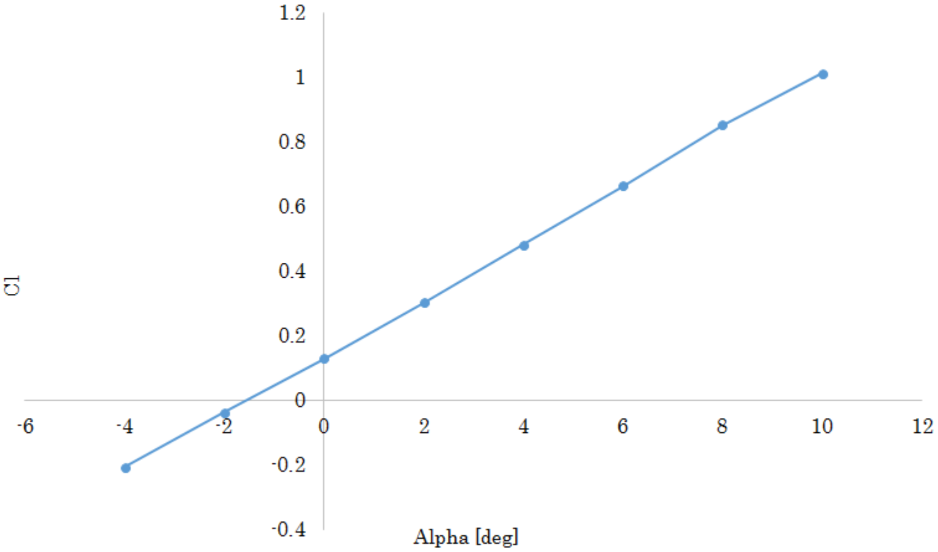

Figure 4.7: Lift coefficient verses angle of attack

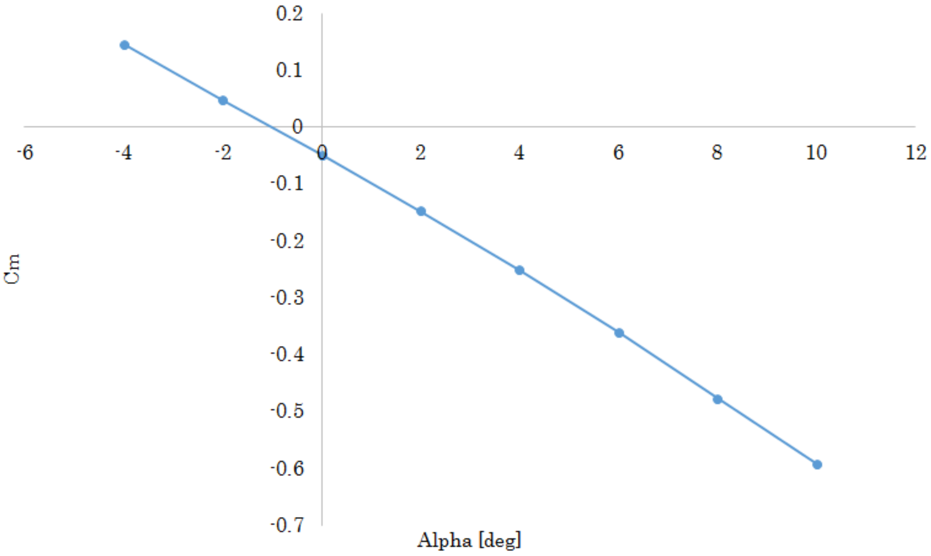

Figure 4.8: Moment coefficient verses angle of attack

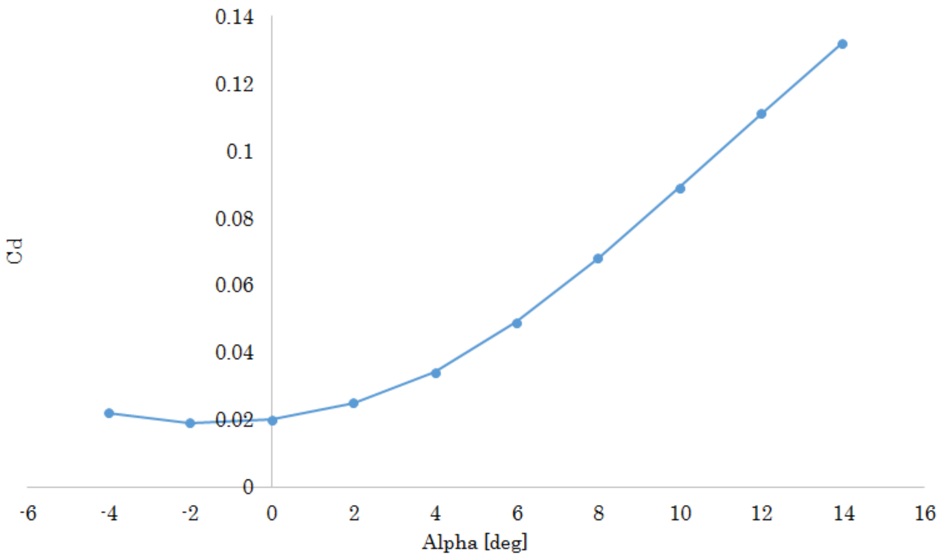

Figure 4.9: Drag coefficient verses angle of attack

in 4.10.

$$\dot{x} = Ax + B\eta \tag{4.3}$$

$$A = \begin{bmatrix} X_u & X_w & 0 & -g \\ Z_u & Z_w & u_0 & 0 \\ M_u + M_{\dot{w}} Z_u & M_w + M_{\dot{w}} Z_w & M_q + M_{\dot{w}} u_0 & 0 \\ 0 & 0 & 1 & 0 \end{bmatrix} \tag{4.4}$$

$$x = \begin{bmatrix} \Delta u \\ \Delta w \\ \Delta q \\ \Delta \theta \end{bmatrix} \tag{4.5}$$

$$\eta = \begin{bmatrix} \Delta \delta \\ \Delta \delta_T \end{bmatrix} \tag{4.6}$$

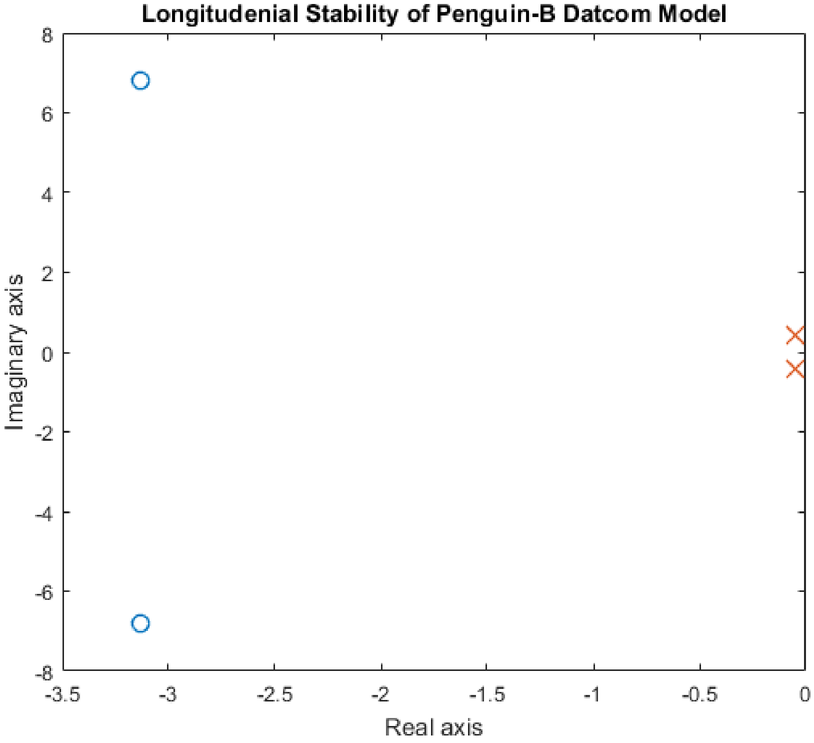

Figure 4.10: Dynamic longitudinal stability of Penguin-B datcom model

$$B = \begin{bmatrix} X_{\delta} & X_{\delta_T} \\ Z_{\delta} & Z_{\delta_T} \\ M_{\delta} + M_{\dot{w}} Z_{\delta} & M_{\delta_T} + M_{\dot{w}} Z_{\delta_T} \\ 0 & 0 \end{bmatrix} \tag{4.7}$$

$$A = \begin{bmatrix} -0.110 & -0.022 & 0 & -32.2 \\ -0.613 & -3.812 & 111.6 & 0 \\ 0.015 & -0.420 & -2.439 & 0 \\ 0 & 0 & 1 & 0 \end{bmatrix} \tag{4.8}$$

The rate of grown or decay of the oscillation is determined by the sign of the real part of the complex root. A negative real part produces a decaying oscillation [10] which is ideal a stability aircraft. From figure 4.10, it is seen that the model is stable in both the short and long (phugoid) period modes. The exact period of each mode is calculated in order to describe how the aircraft will respond to a step input. The equations used to calculated the period of the modes are shown in equation 4.9 where ω is the imaginary part of the eigenvalues. The period is calculated to be 0.92 and 14.89 seconds for short and long term respectively. The time to half amplitude is a measure of damping ratio and is written in equation 4.10 where η is the real part of the eigenvalues. The long term and short term modes have $t_{1/2}$ equal to 16.23 and 0.22 seconds respectively. The results are positive with the short and long term modes having a relatively high frequency and lower damping. It is now concluded that the Penguin-B Datcom model is stable and will now be used in simulation with confidence of aircraft stability.

$$Period = 2\pi/\omega \tag{4.9}$$

$$t_{1/2} = 0.69/|\eta| \tag{4.10}$$

Datcom models from professional model creators were used to further validate model accuracy. The two models chosen are for the Cessna-172 and Boeing 737-300 airframes and are visually shown in figures 4.11 and 4.12 respectively. The reason for choosing these two aircraft is because of the accessibility of general aerodynamic characteristics of each to compare the Datcom output with. These models are also publicly available in a repository of the Digital Datcom+ Pro file location. The Cessna 172 mode shown in figure 4.11l was created by a masters thesis student then modified for accuracy by Datcom+ Pro developer Bill Galbraith. The Boeing model shown in figure 4.12 was created by Marie-Louise Roy and Steven M. Sliva. The Boeing model shown in figure 4.12 came from a NASA technical document written in 1983 by Marie-Louise Roy and Steven M. Sliva [17]. The model was then updated from a B737-200 to a B737-300 series and entered by Bill Galbraith.

A comparison between Aerodynamic data from the Cessna 172 is widely public

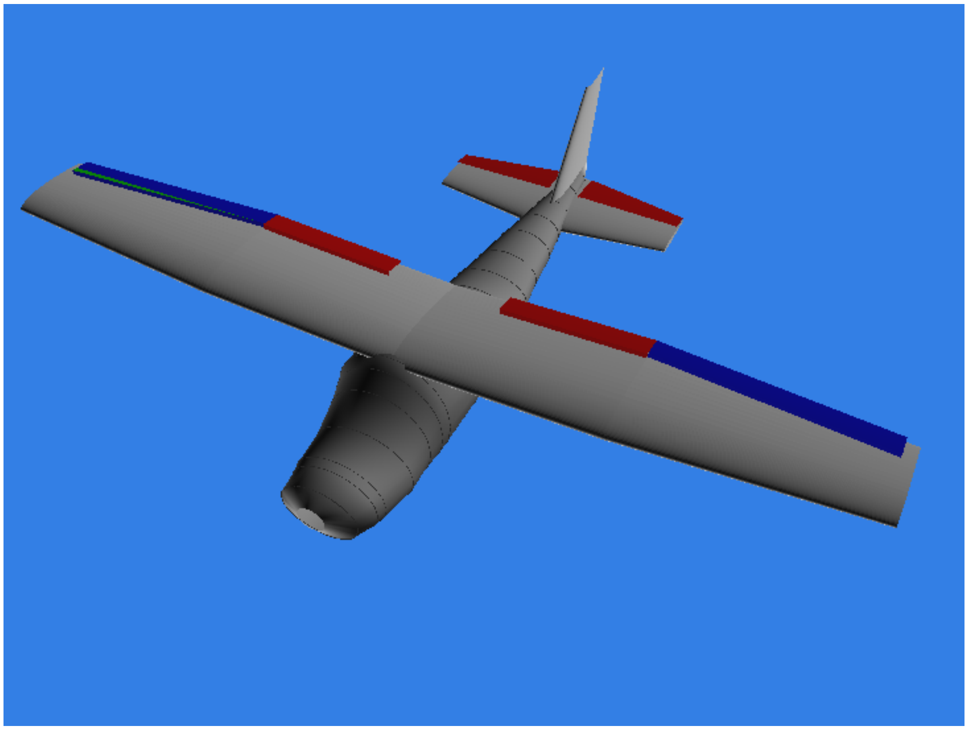

Figure 4.11: Cessna 172 Datcom model [16]

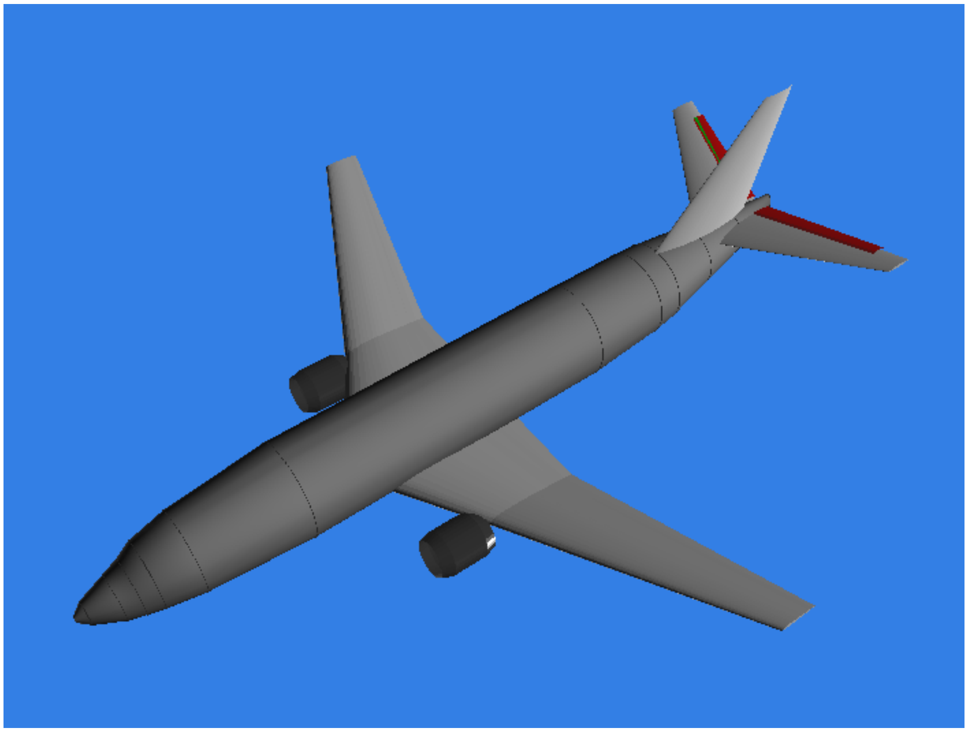

Figure 4.12: Boeing 737-300 Datcom model [16]

and can be obtained in aerospace textbooks. The aerodynamic data from the Boeing 737 was obtained form the manufactures data package for a flight simulator [16]. With the accuracy of this data assumed to be correct, a valid comparison to Datcom values can be made. A validation chart of the two airframe models (among other models) was completed by Bill Galbraith in the Datcom+ Pro User Manual and is shown in figure 4.13 [16]. In this chart, the C_{L_α} value is very accurate on both Cessna 172 and 737 models. As mentioned in later sections, the lift and drag coefficient will be particularly important to ZrhoG MATLAB simulator. This data concludes that these models accurately represent the two aircraft.

4.1.3 X-Plane

X-plane is a subsonic flight simulator and aircraft modeler developed by Laminar Research. X-plane includes a fully developed earth environment 6-DOF simulation that models weather effects and even variations in gravity due to altitude. The X-Plane simulator is used in HIL testing and will ultimately help further verify robustness of the flight controller prior to flight testing. X-Plane uses classic blade element theror to break the airframe into different components. Blade element theory is robust aerodynamically but is only as accurate as the aircraft model created. In this section we will discuss the process that X-Plane uses to model the aircraft and the techniques the software uses for simulation. the models are created in a separate program called X-plane Maker also developed by Laminar Research. It has user interface that makes designing and building new aircraft a better process than the Digital Datcom. Also, X-plane Maker is able to create a wider range of aircraft geometry including twin boom tail aircraft which was not possible in the Digital Datcom as mentioned previously. Almost any aircraft geometry imaginable is able to be created in X-Plane Maker4.14. The the more important aspects of the Penguin-B aircraft modeling in Plane Maker will be discussed in the following but the details for Plane Maker can

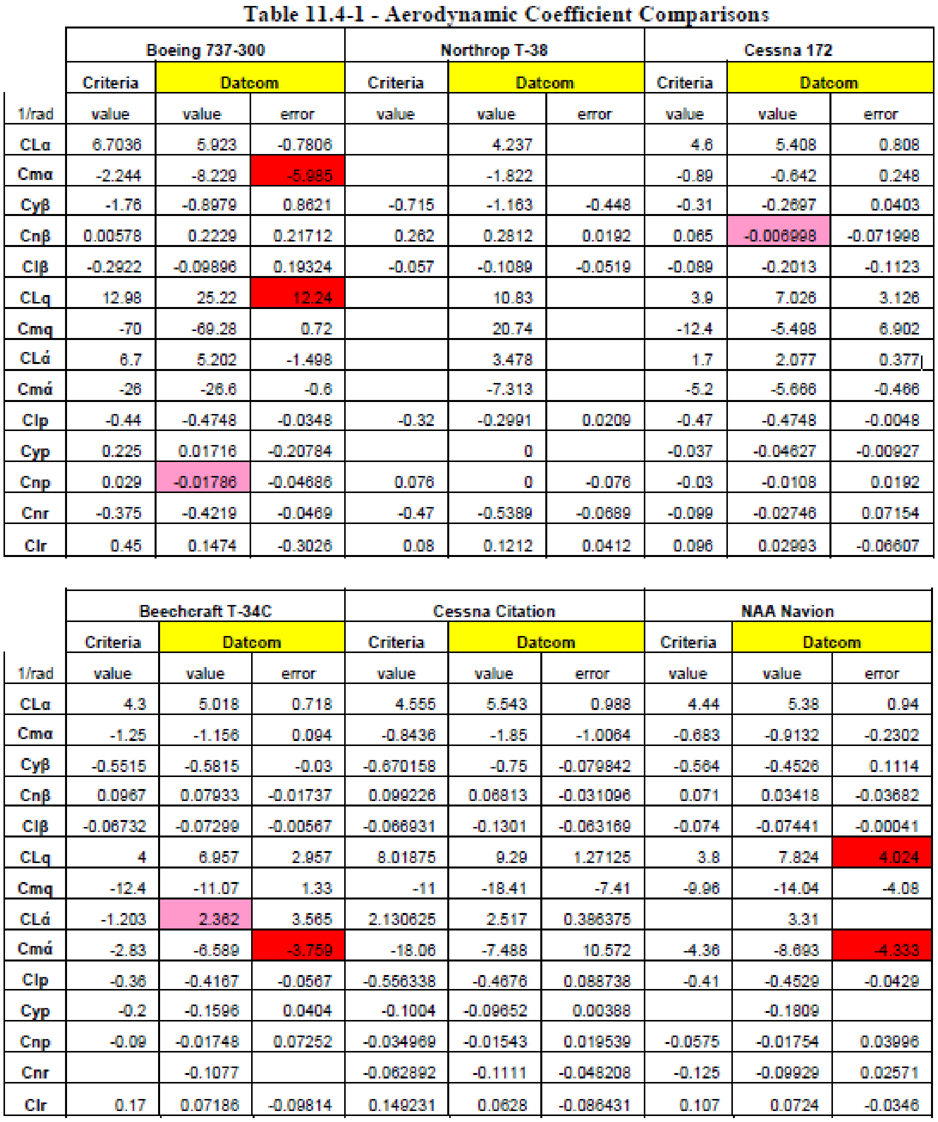

Table 11.4-1 - Aerodynamic Coefficient Comparisons

	Boeing 737-300			Northrop T-38			Cessna 172		
	Criteria	Datcom		Criteria	Datcom		Criteria	Datcom	
1/rad	value	value	error	value	value	error	value	value	error
CLα	6.7036	5.923	-0.7806		4.237		4.6	5.408	0.808
Cmα	-2.244	-8.229	-5.985		-1.822		-0.89	-0.642	0.248
Cyβ	-1.76	-0.8979	0.8621	-0.715	-1.163	-0.448	-0.31	-0.2697	0.0403
Cnβ	0.00578	0.2229	0.21712	0.262	0.2812	0.0192	0.065	-0.006998	-0.071998
Clβ	-0.2922	-0.09896	0.19324	-0.057	-0.1089	-0.0519	-0.089	-0.2013	-0.1123
CLq	12.98	25.22	12.24		10.83		3.9	7.026	3.126
Cmq	-70	-69.28	0.72		20.74		-12.4	-5.498	6.902
CLά	6.7	5.202	-1.498		3.478		1.7	2.077	0.377
Cmά	-26	-26.6	-0.6		-7.313		-5.2	-5.666	-0.466
Clp	-0.44	-0.4748	-0.0348	-0.32	-0.2991	0.0209	-0.47	-0.4748	-0.0048
Cyp	0.225	0.01716	-0.20784		0		-0.037	-0.04627	-0.00927
Cnp	0.029	-0.01786	-0.04686	0.076	0	-0.076	-0.03	-0.0108	0.0192
Cnr	-0.375	-0.4219	-0.0469	-0.47	-0.5389	-0.0689	-0.099	-0.02746	0.07154
Clr	0.45	0.1474	-0.3026	0.08	0.1212	0.0412	0.096	0.02993	-0.06607

	Beechcraft T-34C			Cessna Citation			NAA Navion		
	Criteria	Datcom		Criteria	Datcom		Criteria	Datcom	
1/rad	value	value	error	value	value	error	value	value	error
CLα	4.3	5.018	0.718	4.555	5.543	0.988	4.44	5.38	0.94
Cmα	-1.25	-1.156	0.094	-0.8436	-1.85	-1.0064	-0.683	-0.9132	-0.2302
Cyβ	-0.5515	-0.5815	-0.03	-0.670158	-0.75	-0.079842	-0.564	-0.4526	0.1114
Cnβ	0.0967	0.07933	-0.01737	0.099226	0.06813	-0.031096	0.071	0.03418	-0.03682
Clβ	-0.06732	-0.07299	-0.00567	-0.066931	-0.1301	-0.063169	-0.074	-0.07441	-0.00041
CLq	4	6.957	2.957	8.01875	9.29	1.27125	3.8	7.824	4.024
Cmq	-12.4	-11.07	1.33	-11	-18.41	-7.41	-9.96	-14.04	-4.08
CLά	-1.203	2.362	3.565	2.130625	2.517	0.386375		3.31	
Cmά	-2.83	-6.589	-3.759	-18.06	-7.488	10.572	-4.36	-8.693	-4.333
Clp	-0.36	-0.4167	-0.0567	-0.556338	-0.4676	0.088738	-0.41	-0.4529	-0.0429
Cyp	-0.2	-0.1596	0.0404	-0.1004	-0.09652	0.00388		-0.1809	
Cnp	-0.09	-0.01748	0.07252	-0.034969	-0.01543	0.019539	-0.0575	-0.01754	0.03996
Cnr		-0.1077		-0.062892	-0.1111	-0.048208	-0.125	-0.09929	0.02571
Clr	0.17	0.07186	-0.09814	0.149231	0.0628	-0.086431	0.107	0.0724	-0.0346

Figure 4.13: Validation of Datcom models to actual airframe aerodynamic data [16]

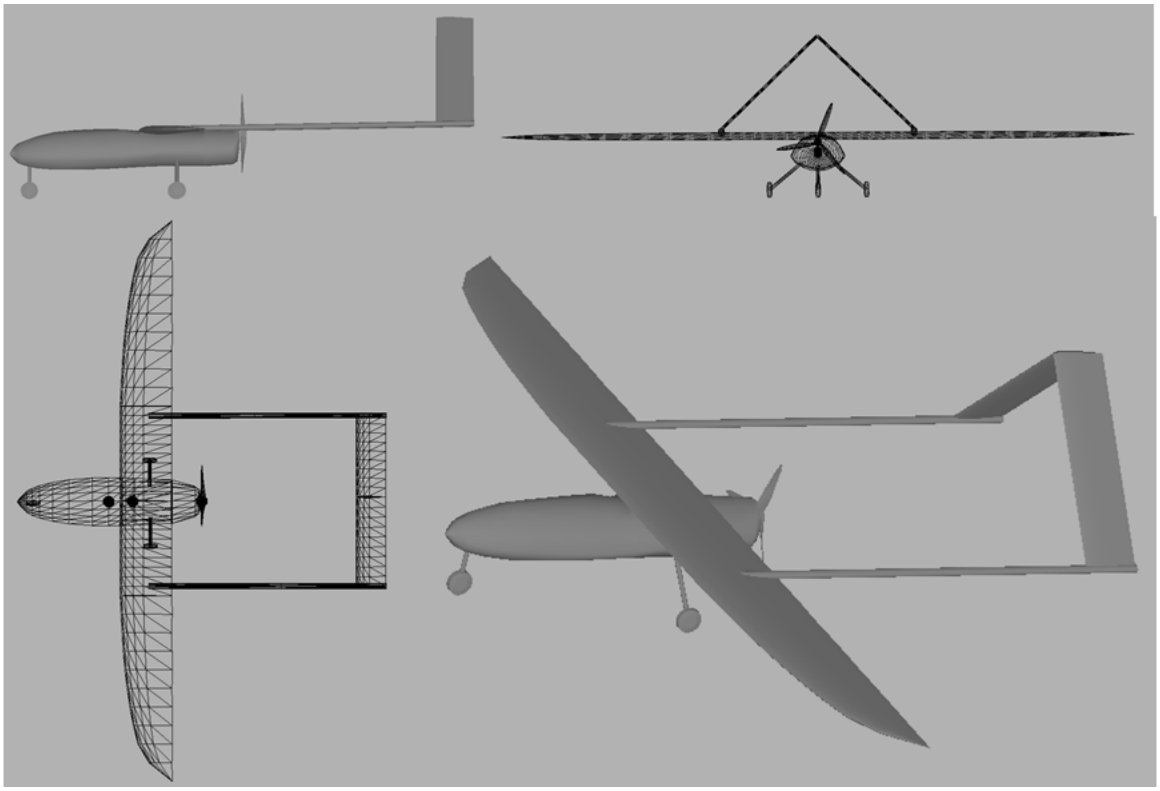

Figure 4.14: Plane Maker model of the Penguin-B aircraft

be found in the manual [18]. The final result is the model shown in figure 4.14.

The modeling process usually begins with major aerodynamic surfaces like the wing, fuselage and tail of the aircraft. Plane Maker has tools for importing images that help with tracing and aligning of these components. Much like the Digital Datcom, Plane Maker models the fuselage by defining multiple crossections geometry along the length of the body. The crossectional modeler is shown in figure 4.15. Plan-form and side views can be imported to define the outer most point of the cross sections which is important for scaling. The top and side views of the fuselage modeler is shown in figure 4.16. Once the outer most point on the crossections are defined, the remaining crossectional geometry can be estimated using a CAD software. In CAD, sectional cuts can be made at every crossection then used to update Plane Maker. CAD also allows the user to take images at any orientation which is ideal for platform

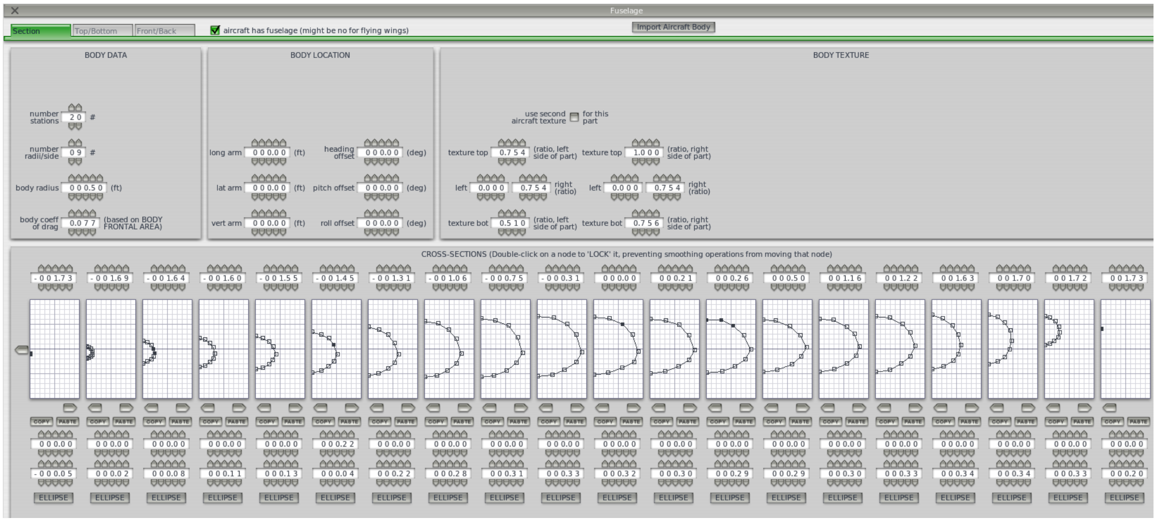

☑ aircraft has fuselage (might be no for flying wings)

number stations 20 #

number radii/side 09 #

body radius 000.50 (ft)

body coeff of drag 0.077 (based on BODY FRONTAL AREA)

long arm 000.00 (ft) heading offset 000.00 (deg)

lat arm 000.00 (ft) pitch offset 000.00 (deg)

vert arm 000.00 (ft) roll offset 000.00 (deg)

use second aircraft texture □ for this part

texture top 0.754 (ratio, left side of part) texture top 1.000 (ratio, right side of part)

left 0.000 0.754 right (ratio) left 0.000 0.754 right (ratio)

texture bot 0.510 (ratio, left side of part) texture bot 0.756 (ratio, right side of part)

CROSS-SECTIONS (Double-click on a node to 'LOCK' it, preventing smoothing operations from moving that node)

-001.73	-001.69	-001.64	-001.60	-001.55	-001.45	-001.31	-001.06	-000.75	-000.31	000.00	000.21	000.26	000.50	001.16	001.22	001.63	001.70	001.72	001.73
000.00	000.00	000.00	000.00	000.00	000.22	000.00	000.00	000.00	000.00	000.00	000.00	000.00	000.00	000.00	000.00	000.00	000.00	000.00	000.00
-000.05	000.02	000.08	000.11	000.13	000.04	000.22	000.28	000.31	000.33	000.32	000.30	000.29	000.29	000.30	000.33	000.34	000.34	000.33	000.20

Figure 4.15: Fuselage modeler within Plane Maker

and side view import.

Wing geometry is determined by also overlaying a scaled plan-form view to trace the outline. The wing airfoil can be selected from a database within X-Plane or uploaded from Airfoil Maker which is another add on software from Laminar Research. In Airfoil Maker, the user can define the desired performance characteristics then the software will generate airfoil geometry. The main characteristics for the airfoil are C_l, C_d and C_m verses alpha. For the Penguin-B, a sail plane airfoil would be a good estimate although the actual airfoil is the MH-32 (Martin Hepperle). We are able to model the airfoil in Airfoil Maker since the aerodynamic data for the MH-32 is available to the public. The gaol is to use the MH-32 wind tunnel tested data in creating similar plots in Airfoil Maker. The plot from the MH-32 is included in figure 4.17 at a Reynolds number of 200,000. A range of performance characteristics for the airfoil at different Reynolds numbers are produced so that X-Plane can model dynamics at different flight speeds. For the MH-32, performance modeling was done up to a Reynolds number of 1,000,000. More details of Laminar Researche's Airfoil Maker is included in the user manual [19].

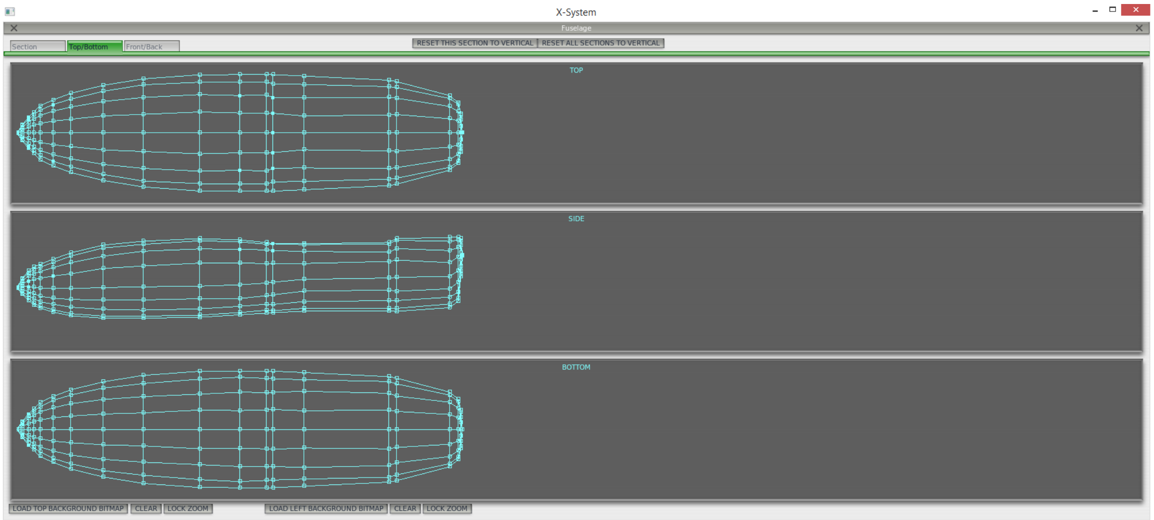
X-System
Fuselage
Section
Top/Bottom
Front/Back
RESET THIS SECTION TO VERTICAL
RESET ALL SECTIONS TO VERTICAL
TOP
SIDE
BOTTOM
LOAD TOP BACKGROUND BITMAP
CLEAR
LOCK ZOOM
LOAD LEFT BACKGROUND BITMAP
CLEAR
LOCK ZOOM

Figure 4.16: Fuselage modeler within Plane Maker

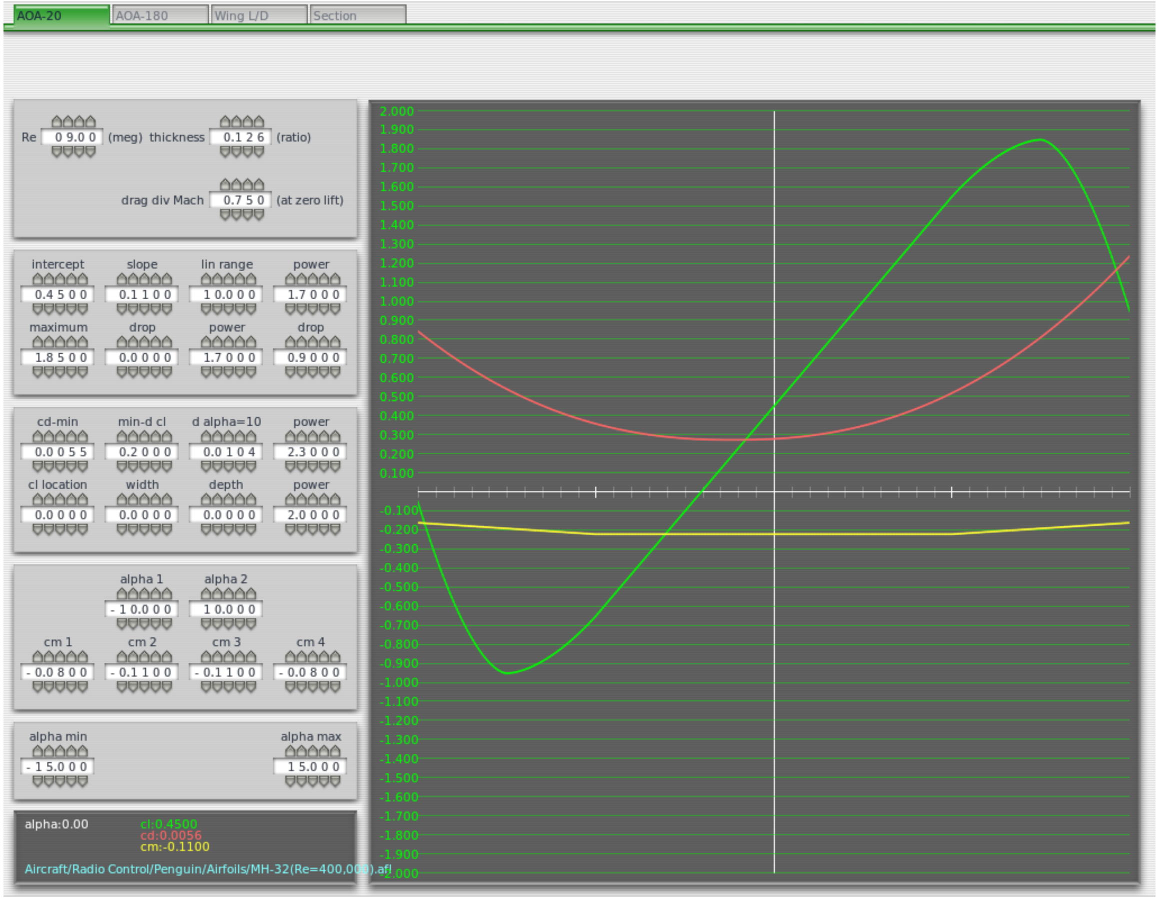

Re 09.00 (meg) thickness 0.126 (ratio)

drag div Mach 0.750 (at zero lift)

intercept	slope	lin range	power
0.4500	0.1100	10.000	1.7000
maximum	drop	power	drop
1.8500	0.0000	1.7000	0.9000

cd-min	min-d cl	d alpha=10	power
0.0055	0.2000	0.0104	2.3000
cl location	width	depth	power
0.0000	0.0000	0.0000	2.0000

	alpha 1	alpha 2	
	-10.000	10.000	
cm 1	cm 2	cm 3	cm 4
-0.0800	-0.1100	-0.1100	-0.0800

alpha min -15.000

alpha max 15.000

alpha:0.00

cl:0.4500
cd:0.0056
cm:-0.1100

Aircraft/Radio Control/Penguin/Airfoils/MH-32(Re=400,000).afl

Figure 4.17: MH-32 Airfoil modeled in Airfoil Maker

Engine modeling can also be done within the Plane Maker software. The 28i 3W engine is modeled with the most important parameters being horse power, maximum and min RPM and the propeller geometry. For this engine, a recommended three bladed propeller was installed to eliminate any issues with propeller strike during take off and landing. In more detail, the propeller is a 16 inch diameter blade with $10 inch/rev$ pitch in English units. Pitch is known as the pitch of the propeller blade at 75 percent of the radius where the angle is measured from the lower surface placed on a flat surface [5]. X-Plane does a good job estimating the thrust per throttle with these simple input parameters but there is room for finer tuning. For now, estimated engine parameters are modeled. Experimental testing with this engine can provide more realistic numbers for modeling but is relatively insignificant for simulation. Control surface area and deflection is important in modeling the control authority of the aircraft. The area of each control surface was measured by hand, recorded and applied to the Plane Maker model. Control surface deflections were measured from the vehicle by deflecting each servo fully and recording and applied to the model. Landing gear was modeled in the same way but is not as important in aircraft dynamics.

X-Plane uses the C_{l_α} C_{m_α} and C_{d_α} slopes for the wing and tail airfoils. The airfoil data entered in Airfoil Maker is 2-dimensional, so X-Plane applies finite wing lift-slope reduction, finite-wing $C_{L_{max}}$ reduction, finite-wing induced drag, and finite-wing moment reduction appropriate to the aspect ratio, taper ratio, and sweep of the wing, horizontal stabilizer, vertical stabilizer, or propeller blade in question [20]. The aerodynamics of the rest of the aircraft are then calculated using blade element theory (BET). BET is possible through the Plane Maker software which breaks up the aircraft model into sections of area. The forces on each section are then calculated and integrated to obtain the velocities and accelerations [20]. Propeller wash and down wash effects from wing lift are also considered in X-Plane.

$$C_M = m/(S_{ref}C_{ref}q) \tag{4.11}$$

Similar to the Datcom model, it is a good idea to determine if the aircraft model is stable and flying as expected prior to testing. It is more difficult to quantify this in X-plane because the software does not generate the aerodynamic coefficients for the entire aircraft directly. Multiple manual flight tests within the X-Plane environment were completed to verify the handling qualities of the aircraft. It was concluded by flight test pilots that the model flies similarly to the real aircraft. X-plane also has a function that aids in calculating C_M during flight. By trimming the aircraft at a steady flight condition, X-plane can perturb the aircraft one degree and calculate the restoring moment that reacts. The C_M is described in equation 4.11 where S_{ref} is area of the wing, C_{ref} is the average chord length and q is the dynamic pressure of the condition. In order to do that, the radius of gyration is estimated using volume and location of each part of the aircraft. Running the function at 0.1 Mach and zero pitch angle, (which is the same condition of the DATCOM model) the moment coefficient was calculated at -0.007251$/rad$. The corresponding C_M in shown in figure 4.8 is -1.71$/rad$. Although C_M is not equal for both models, it is negative for both which suggests a longitudinal stable aircraft. The accuracy of the X-Plane estimation for C_M includes error during initialization of level flight conditions conditions. Repeatability of this condition was low as results varied after sever attempts.

As mentioned previously, the X-plane environment is very detailed. One can simulate a range of weather effects like wind speed, gusts, or air turbulence as well as rainy conditions and variations in temperature and humidity. The most important parameters to the current simulation are wind speed and gusts which can be seen in figure 4.19. These parameters will allow the researcher to verify the UAS's ability to maintain zero gravity in different conditions.

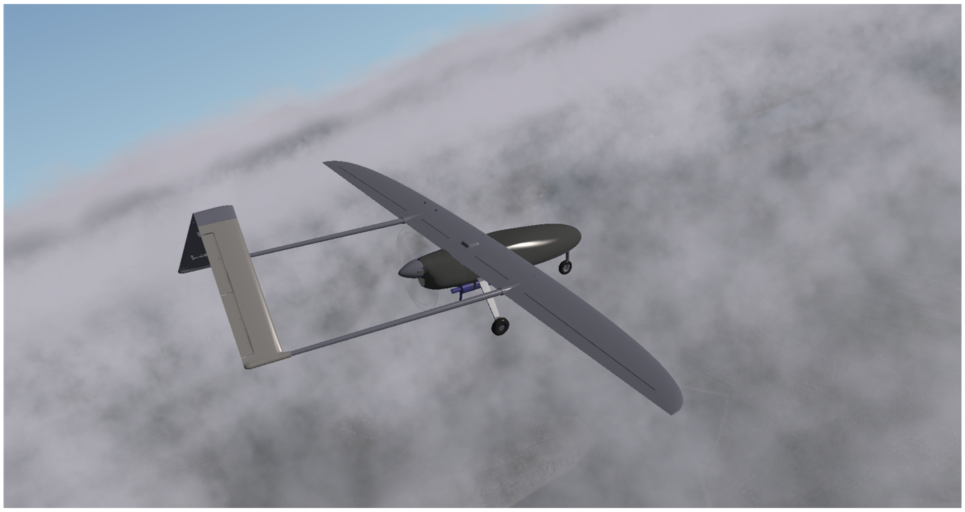

Figure 4.18: Final result of Penguin-B model flying in the X-Plane simulator

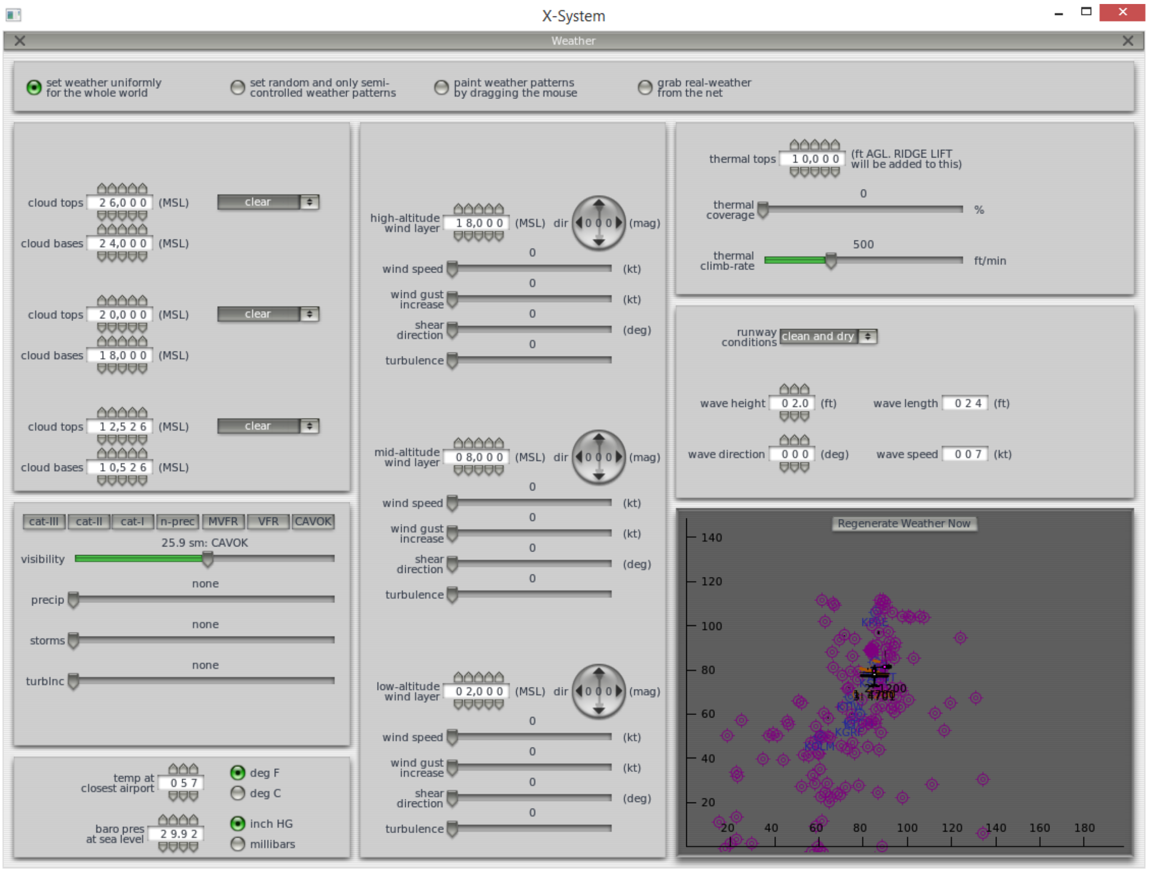

X-System

Weather

● set weather uniformly for the whole world
○ set random and only semi-controlled weather patterns
○ paint weather patterns by dragging the mouse
○ grab real-weather from the net

cloud tops 2 6,0 0 0 (MSL) clear
cloud bases 2 4,0 0 0 (MSL)

cloud tops 2 0,0 0 0 (MSL) clear
cloud bases 1 8,0 0 0 (MSL)

cloud tops 1 2,5 2 6 (MSL) clear
cloud bases 1 0,5 2 6 (MSL)

cat-III | cat-II | cat-I | n-prec | MVFR | VFR | CAVOK

visibility 25.9 sm: CAVOK
precip none
storms none
turbInc none

temp at closest airport 0 5 7 ● deg F ○ deg C
baro pres at sea level 2 9.9 2 ● inch HG ○ millibars

high-altitude wind layer 1 8,0 0 0 (MSL) dir 0 0 0 (mag)
wind speed 0 (kt)
wind gust increase 0 (kt)
shear direction 0 (deg)
turbulence 0

mid-altitude wind layer 0 8,0 0 0 (MSL) dir 0 0 0 (mag)
wind speed 0 (kt)
wind gust increase 0 (kt)
shear direction 0 (deg)
turbulence 0

low-altitude wind layer 0 2,0 0 0 (MSL) dir 0 0 0 (mag)
wind speed 0 (kt)
wind gust increase 0 (kt)
shear direction 0 (deg)
turbulence 0

thermal tops 1 0,0 0 0 (ft AGL. RIDGE LIFT will be added to this)
thermal coverage 0 %
thermal climb-rate 500 ft/min

runway conditions clean and dry

wave height 0 2.0 (ft) wave length 0 2 4 (ft)
wave direction 0 0 0 (deg) wave speed 0 0 7 (kt)

Figure 4.19: The X-Plane environmental tab

4.2 Simulation

Simulation is a computational task or or experiment that is initialized in a known condition and then is steered by stimuli that are applied at a system of boundaries [14]. Simulations are made up of multiple models that all together describe a system of importance. Simulators are commonly used in the aerospace industry today and are one of the best ways to verify the aerodynamic characteristics of aircraft prior to flight testing due to increased safety and variable controllability. There are some aerodynamic simulators available to the public but most companies will spend months of time and millions of dollars developing their own high fidelity simulators. Simulators serve many different roles in aerodynamics and aviation and come in a variety of detail and fidelity. For the purpose of initial testing of microgravity flight logic, lower fidelity simulation can be used like simple 3 DOF MATLAB. Not only do lower fidelity simulation take less time to develop, they also eliminate variables during the debugging process so that the researcher may focus on the flight logic. After logic has been confirmed on lower fidelity simulators it is a good idea to test more extensively in more conclusive simulation. Even while UAVs subtract the risk of human life should the autopilot fail, it is still not acceptable to lose vehicles due to lack of qualification. Secondly, It is important to characterize the aircraft and control algorithms prior to flight even more so when the goal is to complete such an aggressive maneuver as microgravity flight. This section will discuss the high and low fidelity simulation used to qualify the microgravity flight logic.

4.2.1 Matlab simulator

MATLAB, or matrix laboratory, was developed by MathWorks and initially released in 1984. Over the years it has had many revisions of which MathWorks has made it increasingly easy for scientist and engineers to design and analyze systems and products [21]. MATLAB uses a matrix-based language which is similar to C programing language which interfaces well with other softwares. Interface able languages include, C/C++, Java, Python and Microsoft Excel. The matrix-based language makes matrix math simple which is particularly useful to the aerospace engineer who uses high order matrices commonly in order to define the states of the aircraft. Although MATLAB language is ideally used for matrix math it has many functions and toolboxes that make systems analysis easier to complete as well. Additionally, the work flow of MATLAB makes it easy to develop new functions that can then be called and implemented into the main MATLAB script at any time. MATLAB is an good overall tool for any systems engineer to be familiar with. MATLABs sister program SIMULINK is a block diagram based program aimed at simulation and modeling design [22]. SIMULINK is integrated with MATLAB so that the two programs can cooperatively analyze systems and exploit each programs strengths. Full systems with multiple models can be developed in SIMULINK which is more ideal for simulation design although this program was not used in the initial development of the microgravity flight controller.

A lower fidelity simulator named “ZrhoG” by the author was developed using MATLAB and Datcom programs as described in previous sections. As mentioned, Datcom provided the basic aerodynamic coefficients used in simulation including C_{L_α} and C_{D_α}. The aerodynamic data was called into MATLAB as several large matrices then was looked up consistently during the simulation. The purpose of this simulation is to initially test and verify the different concepts of control for the MGUAS. Using MATLAB the author has developed a simplified flat earth, constant gravity, 3 DOF simulation that models aircraft longitudinal motion and aerodynamics. The complete MATLAB file can be found in appendix **??**. For the initial testing, the Penguin-B aircraft was modeled but the simulator is set up so that the user can change variables that define the vehicle as well as initial conditions like starting position and velocity of the aircraft. Other vehicles like the RMRC Anaconda, will be tested in this simulation

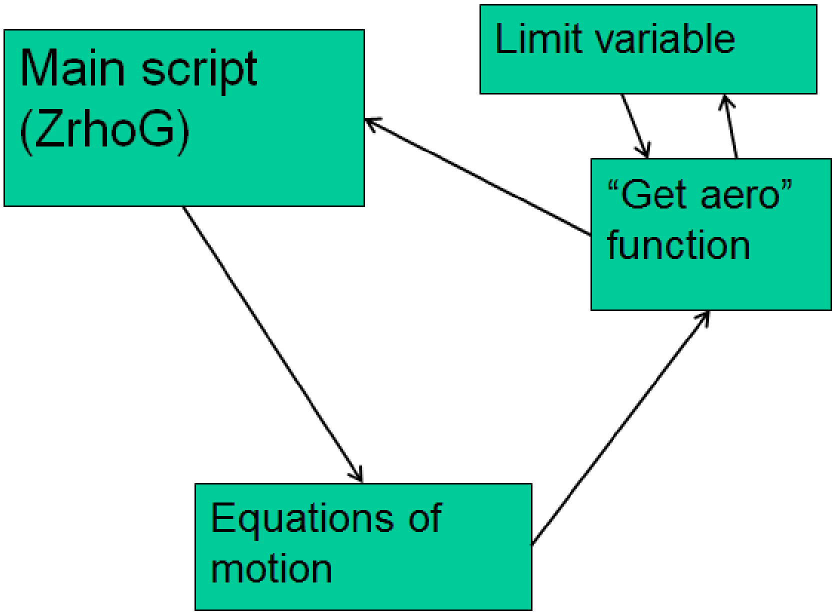

Figure 4.20: Schematic of 3 DOF Matlab Simulation ZrhoG

as well but for consistency and non redundancy, the description here will only include the Penguin-B setup. Also, aircraft models such as the Cessna 172 and Boeing 737 are included to compare results from simulation. The simulator is set up as a time dependent model with a 0.01 time step which can also be changed. The user can develop the flight computer logic within the time dependent for loop and view the response of the system using graphical output with MATLAB. A schematic of the scrips and subscips of the ZrhoG simulator is shown in figure 4.20.

The EOMs used in this simulator are described in equation 3.16 and 3.17. The EOMs are considered as non-linear and allow the simulation to describe the vehicles motion based off of lift, drag, thrust and gravity forces. From these EOMs, the vehicles motion is derived using the Euler method or (RK) Runge-Kutta first order [12]. This could ultimately be upgraded to an RK4 which is fourth order and is the most robust RK method. The accuracy gained from increasing to a 5th order system is minimal compared to the increase in computational power needed.Pitching moment was not included in the governing equations of motion for further simplification. Pitch moment can be accounted for with the equation $M = I_{yy}\dot{q}$ where I_{yy} is the moment of inertia of the aircraft about the aircraft y-axis and $\dot{q}$ is pitching acceleration. This concept requires moment of inertia data for each respective aircraft. In general, COTS UAV manufactures do not provide the moment of inertia data. There are experimental methods that can estimate moment of inertia of the aircraft. These methods included mass and distance from CG and a oscillatory pendulum or spring experiment however they are very time intensive and for initial flight logic testing are not required. Another component of pitch moment modeling is elevator deflection. Instead of modeling pitching moment due to elevator deflection $C_{m_{\delta e}}$ and the change in lift due to elevator deflection, a transfer function was derived to model the pitch response of the entire aircraft with a commanded α. Since all of the autopilot controllers to be tested on this simulator ultimately command a angle of attack, it is a practical approach to represent the system as a estimated response model.

Engine thrust is modeled with a lookup table that relates a throttle command of 0 to 1 with a output thrust value. The thrust values are estimates of what the engine is expected to produce with a given throttle input. In reality, there is a delay between throttle command and thrust output, so this is modeled as a second order response using a transfer function. For this model, natural frequency ω_n and damping factor ζ are $(5)2\pi$ and 0.7 respectively. The response of the system also depends on the engine type so an estimate of similar rise time and damping ratio were used. Engine dynamic estimates could be improved by dynomometer and wind tunnel testing but the current estimated lookup table is practical for initial testing of control concepts.

This simulation uses the data obtained by United States Standard Atmosphere 1976 for the atmospheric model [23]. This part of the simulation is a separate function called “get aero” called on by the main script. A lookup table is generated from the data containing temperature, pressure, density and speed of sound at different altitudes ranging from SL (sea level) to 10,000[m] AGL (above ground level). This altitude is obviously above the ceiling for most SUAS but for simulation purposes it is good practice to make the boundary's as large as possible. A simple "if, else if" structure is was created to call the correct drag and lift coefficients based on the current aircraft speed, altitude and angle of attack. This atmospheric model is important in the calculation of all aerodynamic forces and is especially important to microgravity vehicles due to the rapid change in altitude that is expected. Aerodynamic coefficients of C_L and C_D at different angles of attack are included. These coefficients were obtained and imported from the Datcom model. The coefficients are only imported for one Mach number and do not include effects of elevator deflection on C_L and C_D.

Gusts are a major contributor to the dynamics of MGUAS so the structure to model gust effects was added to ZrhoG. The major benefit of this is comparing how different airframes respond to these gusts and how well the zero g controller can maintain course. Gusting effects can be introduced from the atmosphere in multiple ways such as down bursts, thermals and general atmospheric turbulence. From a simulation point of view, these gust effects can be modeled by a simple step input type of gust. This gust parameters can then be varied in magnitude, direction and point in time which the gust is created. All gust parameters impact the duration and acceleration quality during the maneuver. Ultimately, a range of acceptable gust parameters will be chosen from this simulation. The gust simulation structure was set up in the main script of the ZrhoG code. Here, a simple if then statement was created to generate a perturbation in true velocity of the aircraft at a chosen time. Depending on the airframes size, mass and drag coefficients, a estimated velocity perturbation was chosen to match a certain gust velocity. A change in velocity up or down simulates a up or down draft while a forward or aft velocity change creates a head or tail gust respectively. The elementary drag equation was used along with newtons second law to estimate gust effect on the airframe. These equations are shown in 4.12 and 4.13 respectively. For simulation, A typical range of gust velocities include zero to a maximum of 20 knots in any direction and time.

$$D = \frac{C_d \rho V^2 A}{2} \tag{4.12}$$

$$F = m\frac{dv}{dt} \tag{4.13}$$

4.2.2 Monte Carlo Simulation

MC (Monte Carlo) simulation is a brute force method for testing nonlinearities and random effects of simulated systems. It is commonly used in the aerospace industry to estimate overall success of the mission as a percentage value. MC simulation is used extensively for launch vehicle trajectory analysis [24]. It is most useful when the inputs or processes are not completely deterministic, when the outcome is too complicated to calculate easily and when a simple worst-on-worst approach is either too difficult or too expensive to achieve [24]. The worst-on-worst approach is completed by choosing the extreme value of each input parameter and showing success for the combination of these worst values.

The process for MC simulation is shown visually in figure 4.21 by Hanson et. al. The process begins with randomly generated parameters that are ran through simulation. Results are collected then a new set of input parameters are again randomly generated and ran through simulation. A large compilation of results from each loop will

In this study, gust effects are particularly important and of high influence on the system. Because of the stochastic nature of the phenomena, the Monte Carlo approach will yield the most realistic assessment [25].

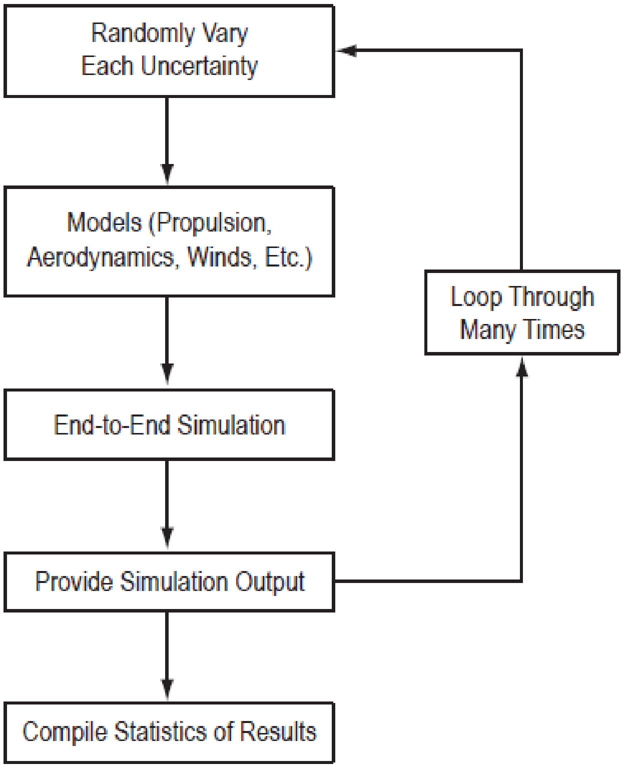

Figure 4.21: Monte Carlo process schematic [24]

CHAPTER 5

Experimental testing

In this chapter, the author will discuss the experimental setup and testing method used to validate and qualify the microgravity system. These overall test system includes the three testing phases that NASAs Unmanned Microgravity program suggested. To re-iterate the three methods included, complete manual flight, semi-autonomous flight and complete autonomous flight. During each of these phases HIL and flight testing will be tested with two airframes, the Penguin-B and the Anaconda. The MATLAB control logic was implemented into the Stabilis autopilot firmware for HIL tests. The results from this section will be included in chapter 6 and will be used to judge both the aircraft and the flight control logics ability to maintain microgravity. Experimental flight testing is normally the last step in certifying new technologies and aircraft. The HIL testing was not completed to the extent needed for flight testing so it is even more important for the author to explain the setup and methodology for other researchers to build on.

The Anaconda COTS airframe will be used for initial flight testing of the ZrhoG control logic. Additionally this is the airframe that is tested in HIL prior to flight testing instead of the Penguin-B. The airframe was selected because of the overall price compared to the Penguin-B and the similarities between both platforms. The Anaconda is a manufactured by RMRC (ready made radio controlled) and is a foam structured airframe shown in figure 5.2. It is a twin boom, inverted V-tail pusher with a 2.06m wingspan and a forward to aft length of 1.41m [26]. The airframe is light, has a relatively large payload bay of L-66cm X W-15cm X H-8cm and sporty

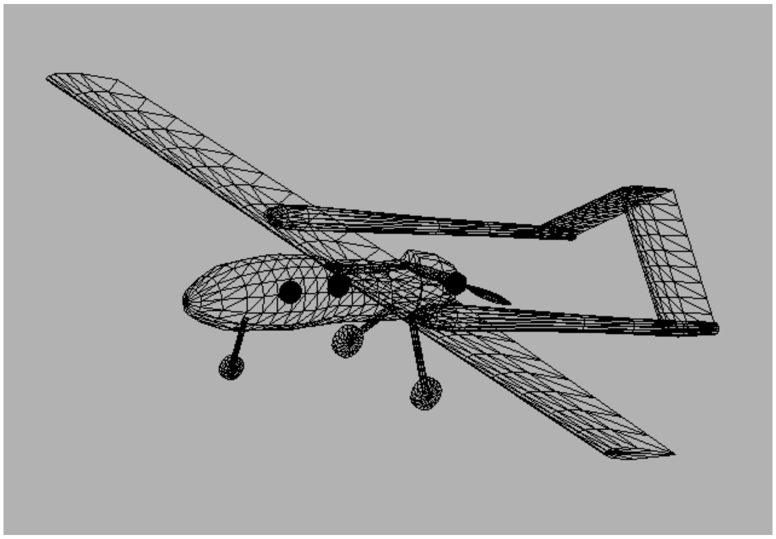

Figure 5.1: X-Plane Maker model for the Anaconda airframe

performance characteristics. The Anaconda supports a 80 Amp electric brush-less motor that can produce up to $35N$ of static thrust with a 15X4E propeller. It has a relatively low aspect ratio of 7.5 compared to the Penguin-B's 11. It also has a higher thrust to weight ratio than the Penguin-B.

The penguin-B airframe is also available for later flight testing but the cheaper Anaconda is more expendable should the unexpected happen. This is a good idea because developmental flight control can have bugs or issues that have not been addressed even with extensive HIL testing. The test conductor will take the safest precautions during initial flight testing but this will be spoken about in later sections in more detail. Even though the airframe is more expendable, the same precautions should be taken for both to ensure safe flight. The same methods were used to verify the Anaconda models aerodynamic derivatives and flight characteristics as was used for the Penguin prior to HIL. The Datcom model, state matrix A and root locus plots are included below in figures 5.3 5.1 and 5.4 accordingly.

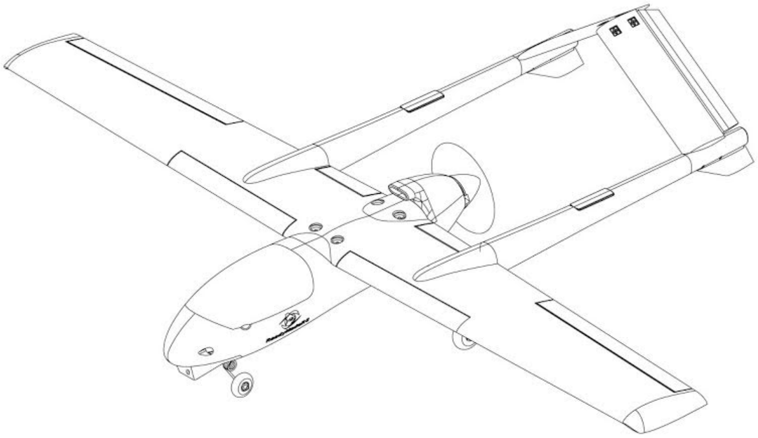

Figure 5.2: Ready Made RC Anaconda airframe [26]

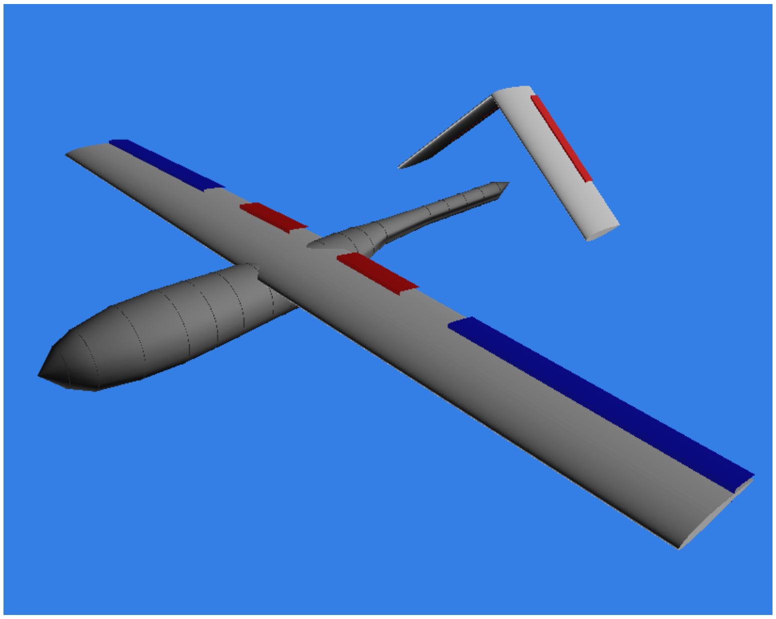

Figure 5.3: Datcom model for the Anaconda airframe

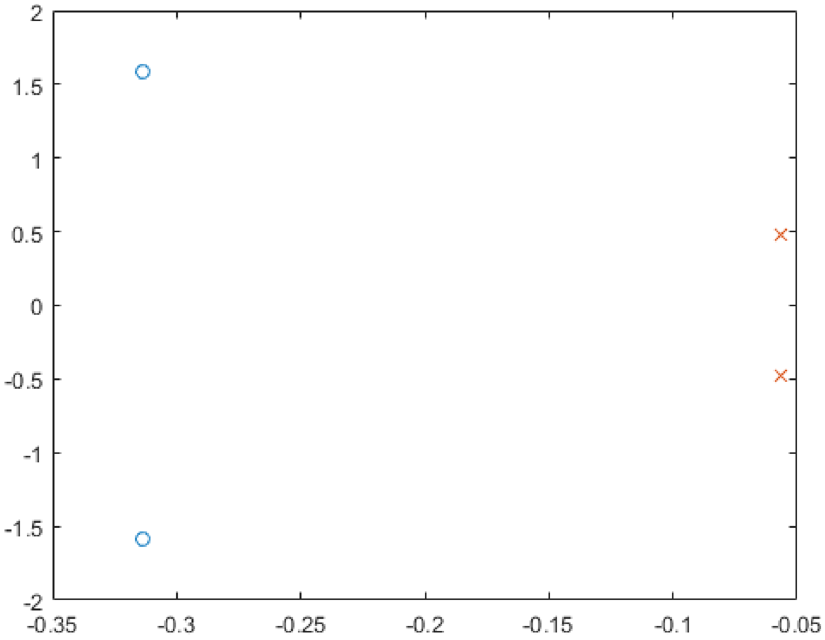

Figure 5.4: Root locus plot for the Anaconda Datcom model

$$A = \begin{bmatrix} -0.125 & 0.179 & 0 & -32.2 \\ -0.382 & -0.152 & 55.7 & 0 \\ 0.003 & -0.048 & -0.464 & 0 \\ 0 & 0 & 1 & 0 \end{bmatrix} \tag{5.1}$$

5.1 Hardware in the loop

When it comes to verifying newly developed flight control logic prior to flight testing there are two options including software in the loop (SIL) and HIL. SIL only tests the autopilot firmware and control logic on a computer (usually a desktop) that is not planned to be implemented on the vehicle but is robust enough to handle high processing loads. The control logic was essentially tested and verified in SIL during MATLAB simulation where the controller is proven to work. The logic still needs to be integrated into the rest of the autopilot firmware as well as the flight computer which

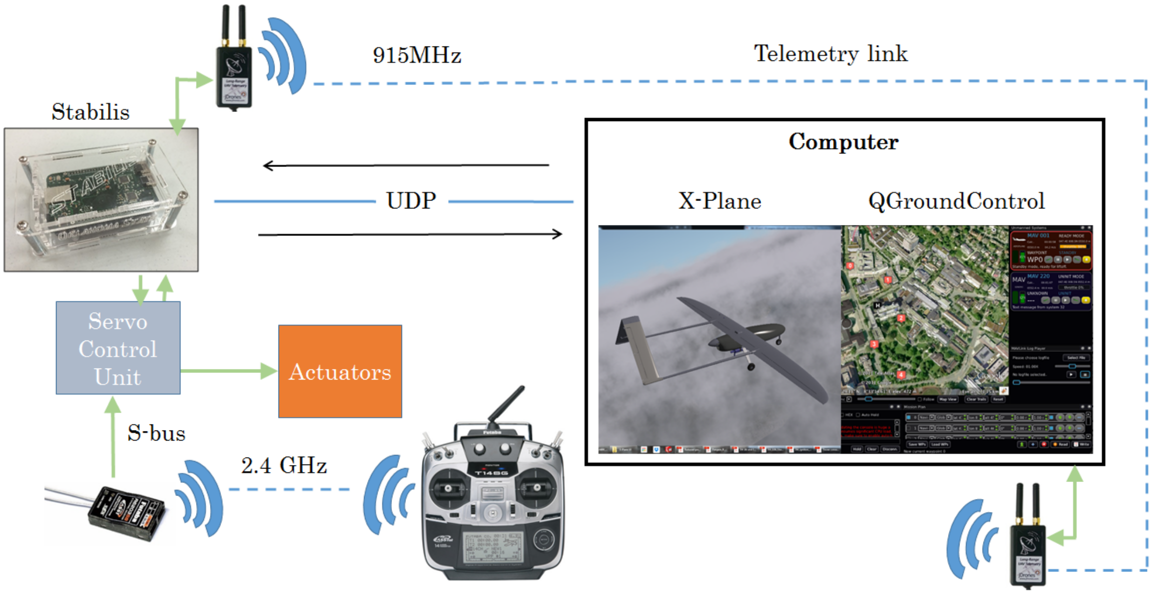

Figure 5.5: Layout for HIL testing

is generally less powerful than the one used in SIL. Since the controllers developed in 3 DOF MATLAB simulation only included pitch and throttle control, this logic needs to be implemented over a current autopilot that controls roll and yaw as well. The HIL allows for debugging of both software and hardware during testing which makes SIL somewhat redundant. HIL simulations are commonly used to check out the performance of the systems hardware and software before flight testing [25]. Since flight testing the system is the ultimate goal, HIL is a major objective.

5.1.1 Setup

The HIL layout is shown in figure 5.5. In HIL X-Plane provides the autopilot with the simulated telemetry data that basically feeds the flight computer fake sensor information. The autopilot treats the telemetry data as input from the on board sensors then uses it for the control system. Then, instead of outputting command signals to the actual control surfaces and engine throttle, these signals are sent to X-plane and the simulation responds according. The loop continues as long as the simulation runs. X-plane and the micro controller communicate through a UDP (User Datagram Protocol) connection which sends and receives commands between autopilot and. The telemetry data to ground control station is made with UART (universal asynchronous receiver/transmitter) telemetry transmitter. Here, the J-Drones long range RFD900s are used that communicate over a 915 MHz frequency [27]. The BeagleBone Black is the on board flight computer that is integrated with Stabilis autopilot firmware. The flight computer communicates with a separate servo control unit which commands the airframe actuators and shown as a gray box in figure 5.5. The Servo control board is separate from the flight computer and receives commands from the RC controller for failure scenarios in the autopilot. If the firmware crashes or flight computer freezes, a direct link from RC controller to servo control unit is available so that the Pilot can take over manual control at any time. The manual take over concept is particularly important in testing of developmental autopilots.

MAVlink (micro air vehicle communication protocol) was first developed in 2009 by Lorenz Meier [28]. It is a communication language that sends data between ground control station and flight computer. The two most popular ground control station softwares that use MAVlink are QGroundControll and MissionPlanner. They are quite similar programs that are used to develop missions and waypoint courses prior to flight testing. Both programs are free to download and interface well with a variety of off the shelf autopilots due to using the same MAVlink protocol. Over the years MAVlink has been updated with new functionality but the flight computer for micro-gravity UAS currently interfaces with an older version of MAVlink. QGroundControl has been selected in HIL and flight testing because it works with older versions of MAVlink where as MissionPlanner does not. QGroundControl is known for its ability to control multiple UAS at a time and could eventually be used to command multiple microgravity UAS. These ground control station softwares interface well with X-Plane in HIL and can be used to tune gains mid flight [28]. It is only recommended that control gains be tuned mid flight in simulation and not actual flight testing.

For RC control, the Futaba R6303SB was chosen for its relatively small size and S-Bus capability. The R6303SB communicates with a Futaba controller over the 2.4GHz frequency [29] The RC controller is the same as used in flight testing to maintain the same V-tail mixing and channel outputs as in HIL. This controller was used to complete manual, semi-auto and completely autonomous HIL testing.

The Stabilis autopilot has been in development at Oklahoma State university since 2014 and has been tested in multiple fixed wing aircraft. Stabilis software is integrated into the BeagleBone Black flight computer which includes a relatively powerful $1GHz$ processor, $2GB$s of flash memory and $512M$B of random access memory (RAM). For comparisons, the popular 3DR Pixhawk autopilot includes a $0.168GHz$ processor with $2GB$ of flash memory and $266MB$ of RAM. The more powerful flight computer is not necessarily needed for microgravity flight because of the simplicity of the control logic. The quicker processor allows for more snappy reactions to gusts effects. The BeagleBone board runs off a $5.5V$ input voltage and is W $7.6cm$ X L $12.2cm$ X H $4.6cm$ in volume and weights $2.5oz$ so it can easily be integrated into a SUAS. The autopilot has proven to work in stabilize mode which is a attitude hold controller. It maintains a zero roll, yaw, and pitch angle with This mode is the most important mode of the autopilot to microgravity flight although Stabilis has demonstrated waypoint navigation modes as well. A manual passthourhg mode has also been tested to work in flight which allows the RC pilot to take over control at any point during the mission should the autopilot computor fail. A seperate servo control board allows RC pilot to maintain controll at all times. Shown in figure 5.5.

5.2 Flight testing

Flight testing is always the final test of the aircraft system before it goes into use or production. There are no simulations or models that can fully compare to actual flight test data because of the nature of aerodynamic and fluid modeling. After extensive flight testing, most of the variables will be tested and issues resolved, creating a robust system that can repeatibly produce microgravity environments for on-board experiments.

5.2.1 Airframe modifications

Prior to flight testing a few modifications to the Anaconda airframe were made so that it would fly more reliably during the higher stress maneuver. Fluttering of the wing was observed in high gust weather during high speed flight. Reinforcements spars in the wing and tail were added to mitigate these effects. The reinforcement spars are a solid carbon fiber rectangular crossection and were epoxied into a grove towards the outboard section of each wing shown in figure 5.6. The crossection was oriented to take advantage of the rectangular shapes ability to resist bending moment in the wing lift direction. Servo to control surface connections were replaced with stronger steal rods and more reliant mechanism. In the past, the airframe has had issues with aileron control rail breaking in flights so this is an attempt to reduce failure.

5.2.2 Systems Layout and Sensors

The flight test system is presented in figure 5.8. The entire system runs off a 5v powers supply which usually regulated from a 4 cell (11V) battery using a BEC (battery eliminator circuit). The current configuration uses a 6,600 MAh battery for all systems including propulsion which is regulated with 60-80 Amp ESC (Electric speed controller). Its estimated that with the current draw from all systems that a full battery would last up to 15 minutes depending on motor throttle and actuator usage. The ground control station remains similar to the setup for HIL testing with the addition of a video receiver. The FPV (first person view) camera was added so that the RC pilot could fly the aircraft with higher efficiency and also for using OSDs

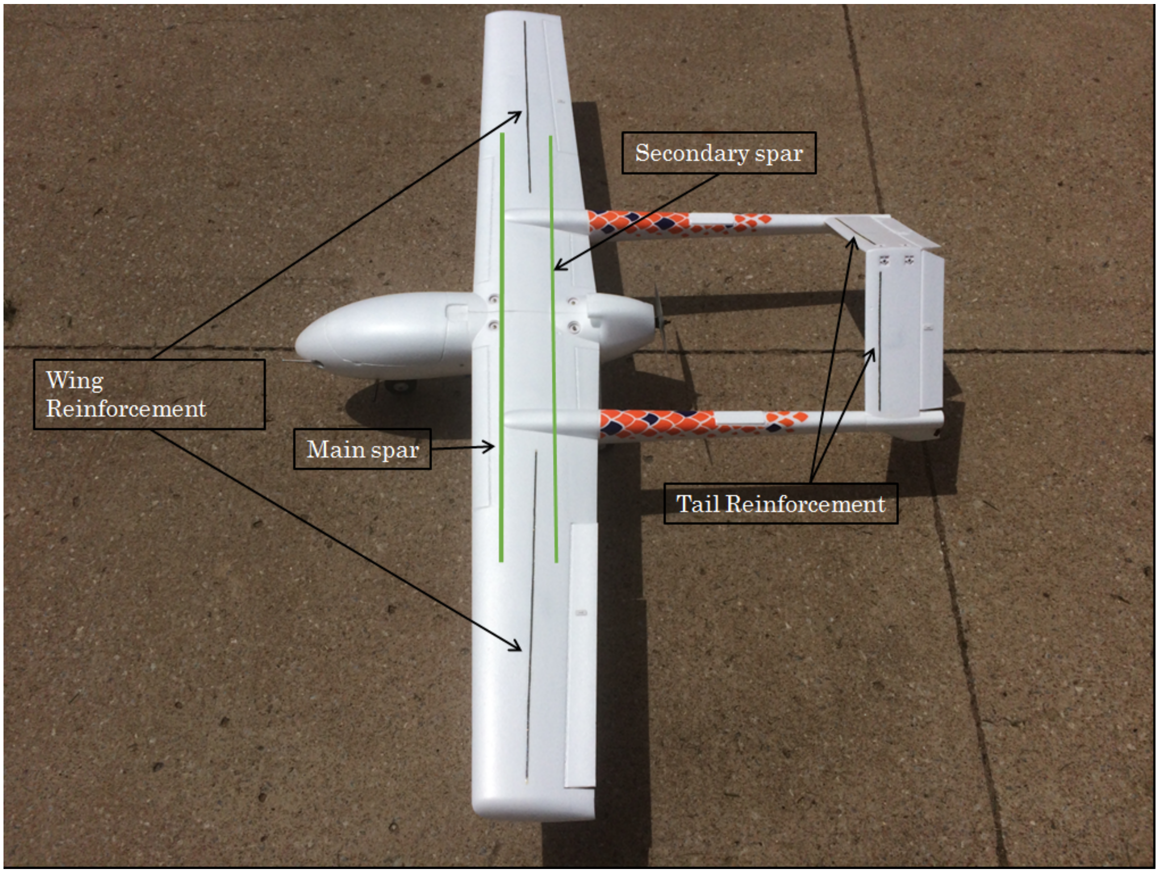

Figure 5.6: Spar layout modifications for Anaconda airframe

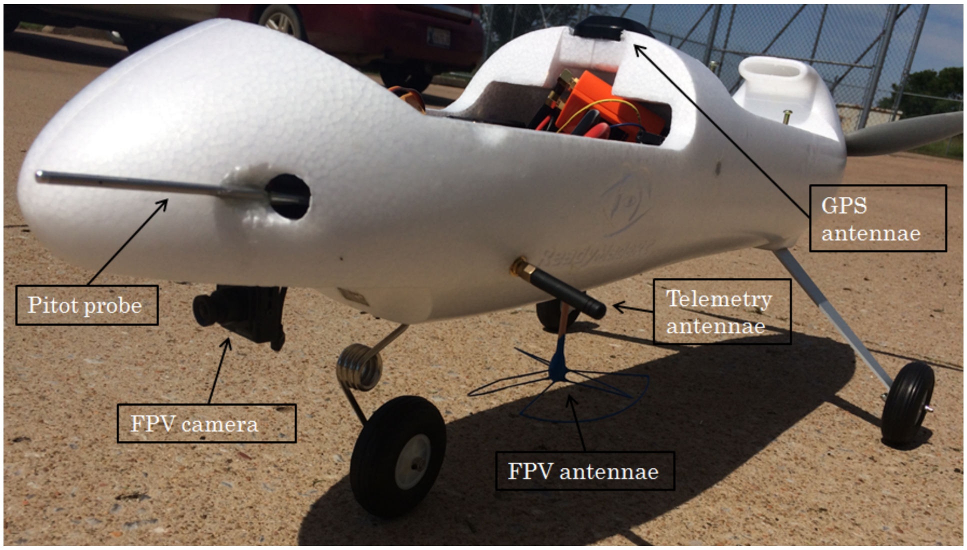

Figure 5.7: Sensors and components on the anaconda fuselage

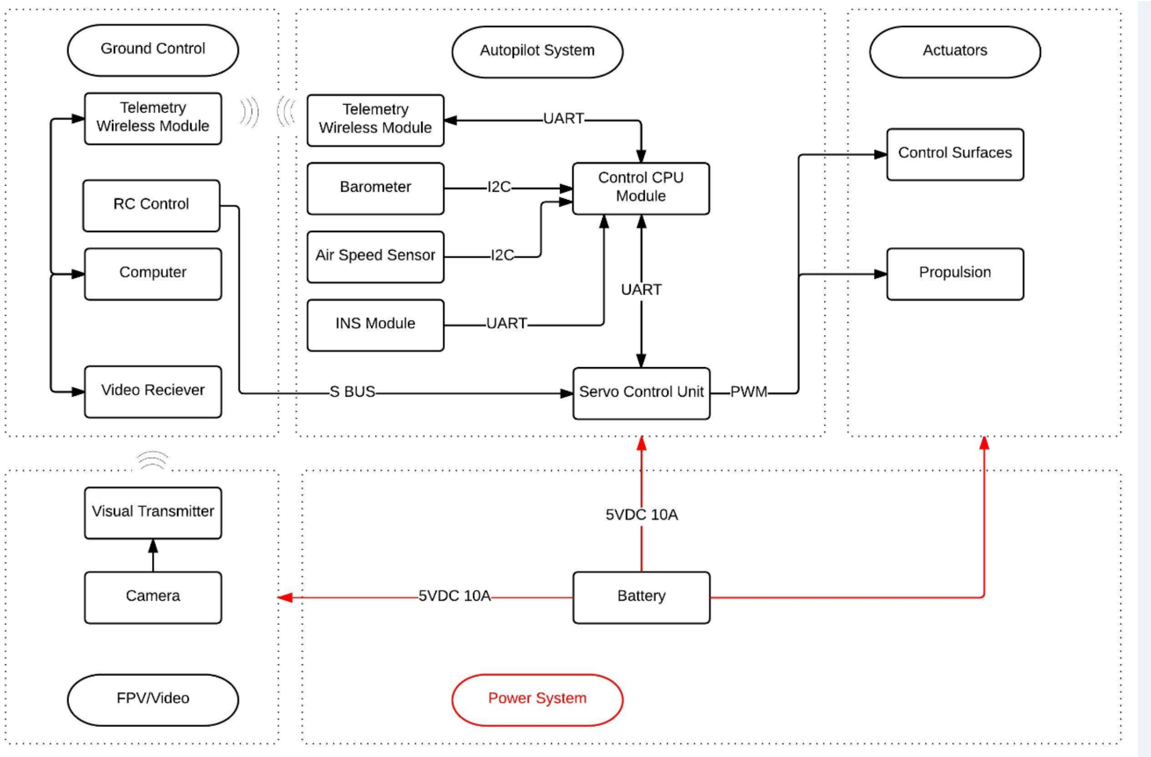

Figure 5.8: Block diagram for the flight computer

(on screen display) for visual telemetry feedback. The OSD will also allow visual feedback of accelerometer data so the pilot can fly manual and semi-auto microgravity maneuvers without looking at the ground station computer screen. Sensors on board the airframe included the VN-200, Pitot probe, and barometer for pressure altitude. The VN-200 is a GPS (global positioning satellite) aided INS (inertial navigation system) that combines MEMS (micro electro mechanical system) inertial sensors, high-sensitivity GPS receiver and Kalman filtering algorithms to provide optimal estimates of position, velocity and orientation [30]. The INS is relatively small and is separate from the rest of the autopilot which makes it easier to mount at the center of mass of the aircraft. A picture of the layout within the airframe is included in figure 5.9.

A separate Arduino Uno system was used to record local accelerations within the payload bay. The the system included the Arduino Uno board, a micro SD

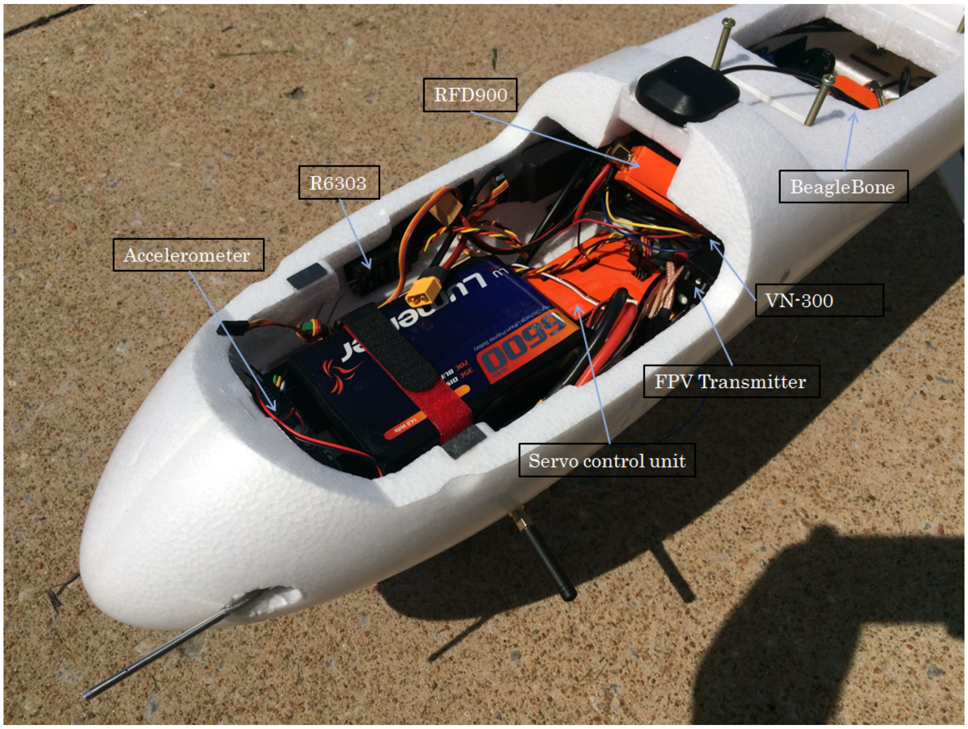

Figure 5.9: Systems layout Anaconda Platform

breakout board and an ADXL345 three axis accelerometer. Simple data logging code was loaded onto the Arduino read and record the accelerometer data.The installed system is shown in figure 5.10.

5.2.3 Flight testing

Although an initial flight testing setup was discussed in chapter 5, no actual flight tests were completed during the authors work. The extensive work on airframe and flight test readiness was completed so that the system could go directly into flight testing after successful HIL. The flight test plan is shown visually through test cards for each successive test in figures 5.11, 5.12 and 5.13.

Flight one in the test campaign of the MGUAS includes a maiden flight of the RMRC Anaconda Airframe in a manual RC piloted flight. The test would verify that modifications to airframe and build quality was successful so that further testing can

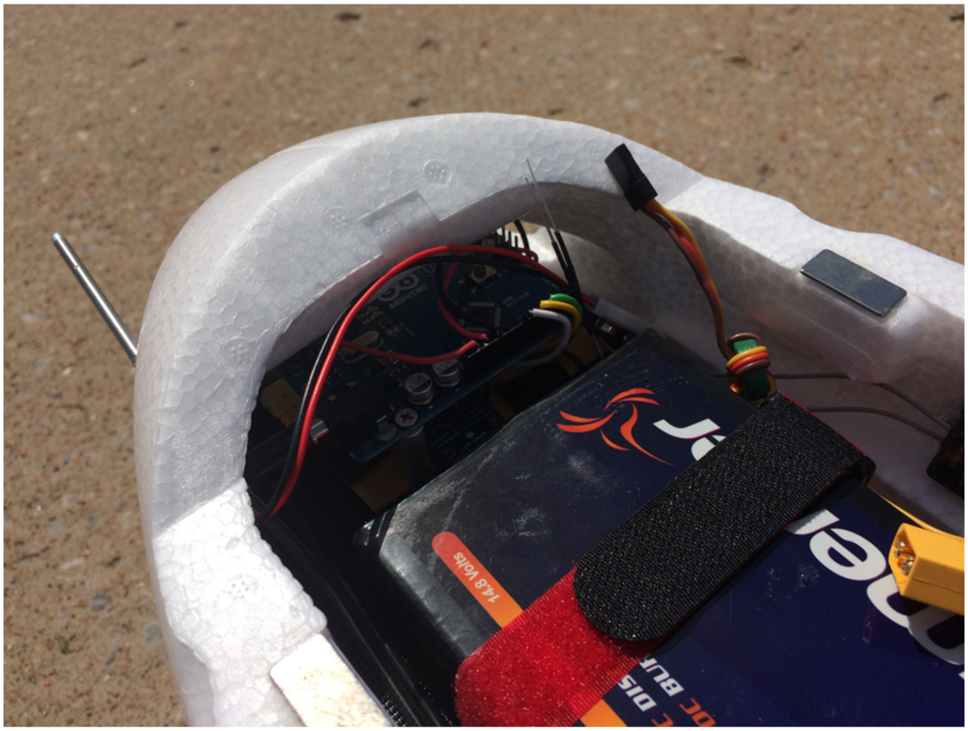

Figure 5.10: Forward payload bay with Arduino Uno accelerometer system

proceed. The method of testing is explained in the test card but essentially the pilot should take off, move all control surfaces and throttle commands to make sure the airframe and system is responding as expected then land.

Flight two in the test campaign includes the first flight that the ZrhoG autopilot will be used on. Initially the stabilize flight mode on the autopilot should be tested so that the RC pilot is confident in the switch from auto to manual control. Stabilize mode can also tests the autopilots ability to hold wings level while maintaining a direct heading. After this mode is verified the ZrhoG mode can be tested. The pilot should initially take off with the manual pass through mode active then switch to ZrhoG mode once the aircraft is at least to 400 ft AGL and in the required "safety zone". The safety zone ensures that the aircraft is not in a location of harm should something go wrong. At 400 ft AGL, the pilot should have 3 seconds until takeover is needed. At this time the aircraft should still be above the "never go below" altitude of

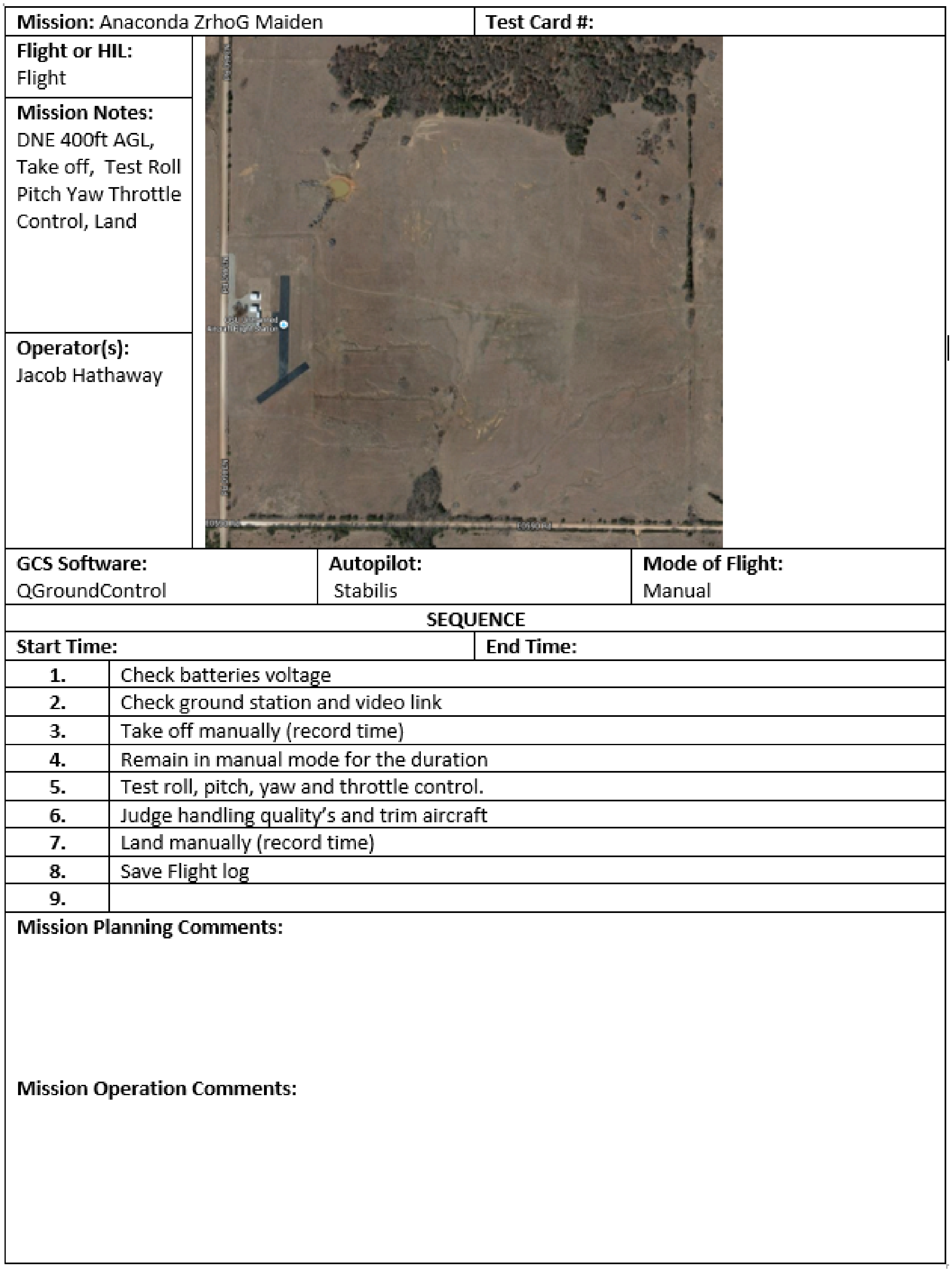

Mission: Anaconda ZrhoG Maiden

Test Card #:

Flight or HIL:
Flight

Mission Notes:
DNE 400ft AGL, Take off, Test Roll Pitch Yaw Throttle Control, Land

Operator(s):
Jacob Hathaway

GCS Software:
QGroundControl

Autopilot:
Stabilis

Mode of Flight:
Manual

SEQUENCE

Start Time:

End Time:

1.	Check batteries voltage
2.	Check ground station and video link
3.	Take off manually (record time)
4.	Remain in manual mode for the duration
5.	Test roll, pitch, yaw and throttle control.
6.	Judge handling quality's and trim aircraft
7.	Land manually (record time)
8.	Save Flight log
9.	

Mission Planning Comments:

Mission Operation Comments:

Figure 5.11: Maiden flight of the Modified Anaconda Vehicle

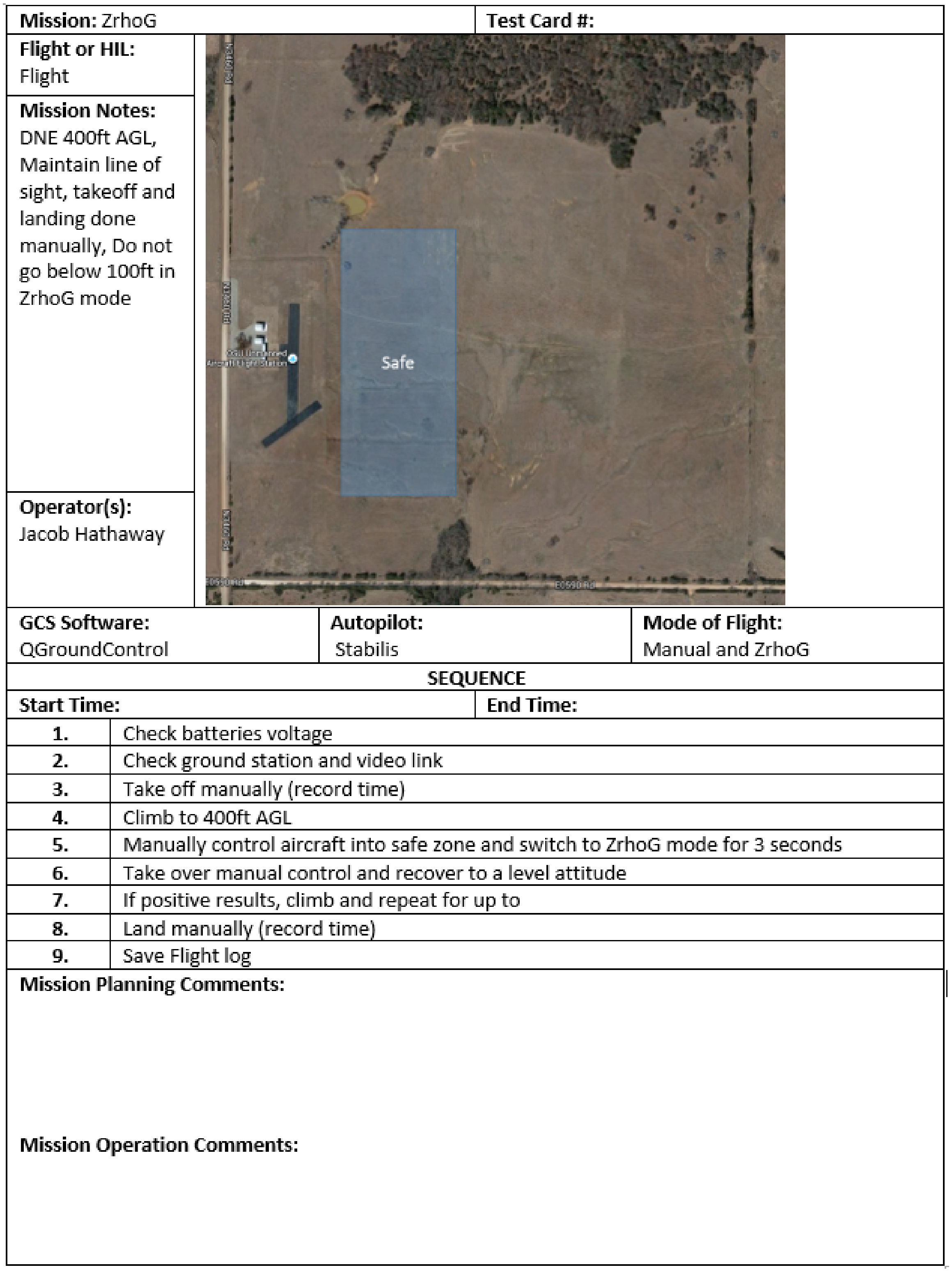
Safe
OSU Unmanned Aircraft Flight Station
E0550 Rd

Mission: ZrhoG

Test Card #:

Flight or HIL: Flight

Mission Notes: DNE 400ft AGL, Maintain line of sight, takeoff and landing done manually, Do not go below 100ft in ZrhoG mode

Operator(s): Jacob Hathaway

GCS Software: QGroundControl

Autopilot: Stabilis

Mode of Flight: Manual and ZrhoG

SEQUENCE

Start Time:

End Time:

1.	Check batteries voltage
2.	Check ground station and video link
3.	Take off manually (record time)
4.	Climb to 400ft AGL
5.	Manually control aircraft into safe zone and switch to ZrhoG mode for 3 seconds
6.	Take over manual control and recover to a level attitude
7.	If positive results, climb and repeat for up to
8.	Land manually (record time)
9.	Save Flight log

Mission Planning Comments:

Mission Operation Comments:

Figure 5.12: First flight of the ZrhoG control mode

100 ft. The never go below altitude is only used while in ZrhoG mode and ensures that the pilot has sufficient time to recover the aircraft without overloading the airframe in a steep pull up. This flight test campaign should serve as an outline for future research to be completed.

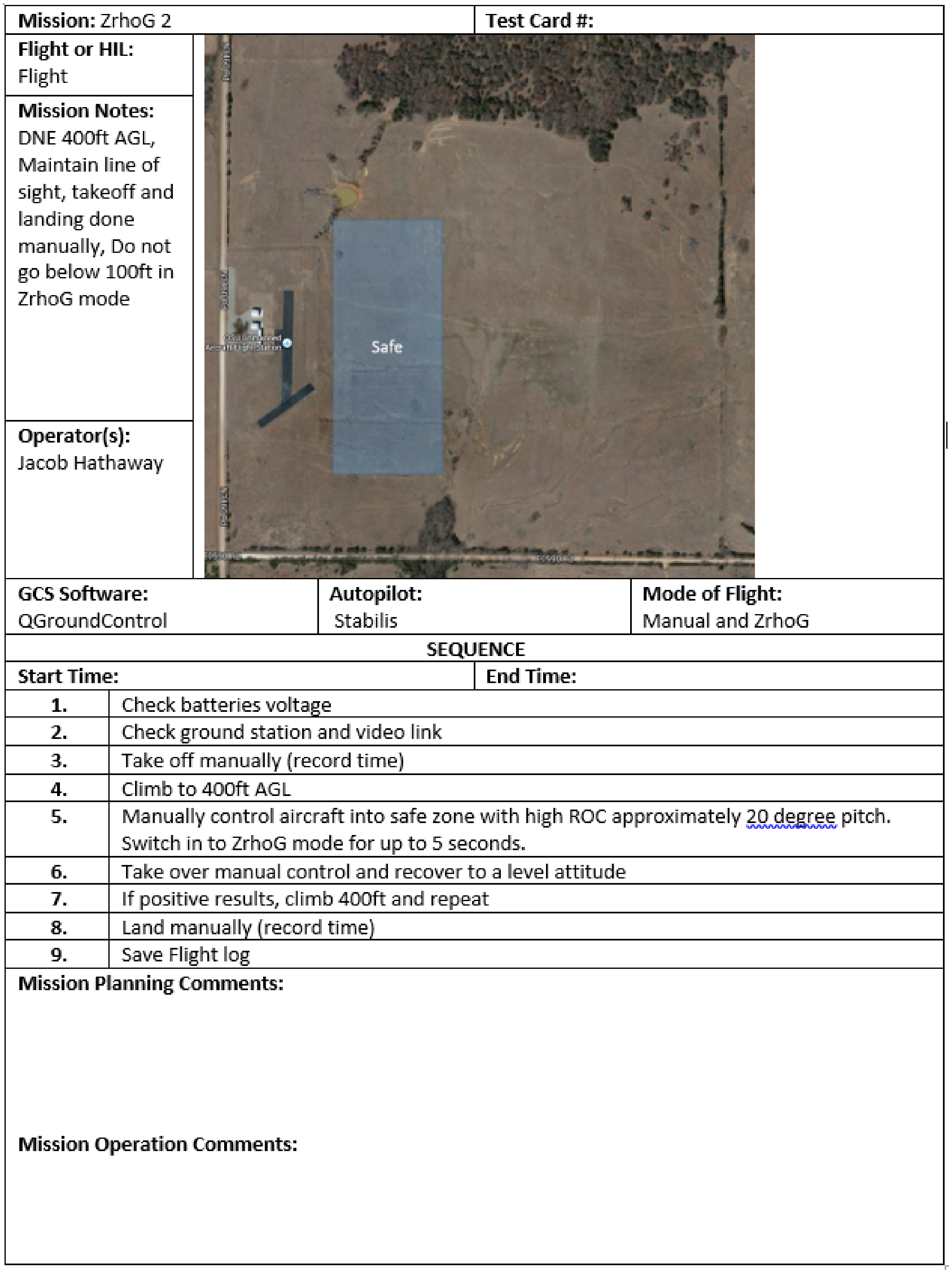

Mission: ZrhoG 2	**Test Card #:**

Flight or HIL:
Flight

Mission Notes:
DNE 400ft AGL, Maintain line of sight, takeoff and landing done manually, Do not go below 100ft in ZrhoG mode

Operator(s):
Jacob Hathaway

GCS Software: QGroundControl	**Autopilot:** Stabilis	**Mode of Flight:** Manual and ZrhoG

SEQUENCE

Start Time:	**End Time:**
1.	Check batteries voltage
2.	Check ground station and video link
3.	Take off manually (record time)
4.	Climb to 400ft AGL
5.	Manually control aircraft into safe zone with high ROC approximately 20 degree pitch. Switch in to ZrhoG mode for up to 5 seconds.
6.	Take over manual control and recover to a level attitude
7.	If positive results, climb 400ft and repeat
8.	Land manually (record time)
9.	Save Flight log

Mission Planning Comments:

Mission Operation Comments:

Figure 5.13: Second flight of the ZrhoG control mode

CHAPTER 6

Results

6.1 MATLAB simulation results

6.1.1 Initial ZrhoG Simulation Tests

Results from the MATLAB simulator ZrhoG are presented in this section. All airframes were tested in ZrhoG but the results from the Penguin-B aircraft parameters are shown initially. The author chose the Penguin-B for the initial results of the simulation for consistency with setup method and modeling. The input parameters include, but are not limited to, wing area S_{ref}, aircraft mass m, initial flight velocity V_0 and initial attitude (θ and $\dot{\theta}$). Since the manufacture of the Penguin-B did not provide the aerodynamic coefficients, they were determined by the Digital Datcom and then read into MATLAB. This simulation tests the ability to maintain microgravity of the projectile motion based controller mentioned in previous section. Increasing the duration is mostly affected by the vehicle and not the control method. Using simulation and estimated engine thrust data, we are able to predict the maximum free fall duration of the vehicle given different launch angles. With an initial launch velocity of 30 m/s (the Penguin-Bs cruise speed) at 45 degree flight path angle, the altitude desired and altitude actual are shown in figure 6.1. Altitude desired is not used in controller logic but is used here to show what the optimal path would be. The actual altitude path stops populating at 14 seconds due to lack of available thrust from the engine causing the zero acceleration to be un-achievable. This shows that we can expect a maximum duration of around 15 seconds depending on initial V_y.

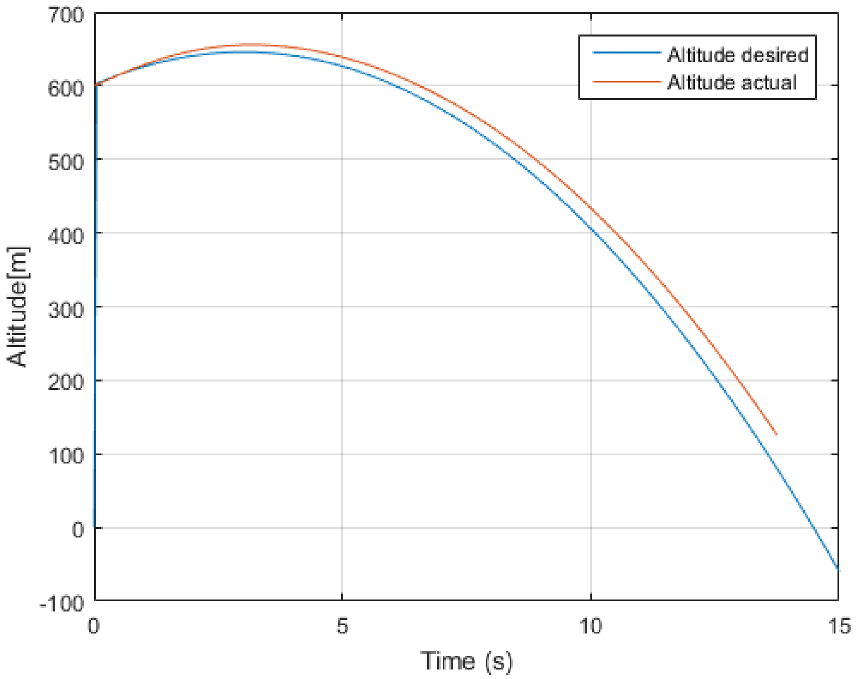

Figure 6.1: Desired Vs actual Altitude

Figure 6.2 shows the desired and actual γ. Desired γ was calculated from the projectile motion equations and γ actual was determined by the attitude of the aircraft in the current state. In this figure, γ actual overshoots in the beginning due to the response of the aircraft in pitch then converges on the desired flight path angle. The error between γ desired and γ actual is plotted in figure 6.3. This is the difference of the two lines plotted int figure 6.2. Error plots show the responsiveness of the controller to commands and ultimately should go to zero with as little overshoot and the highest response possible. Figure 6.4 shows the aircrafts angle of attack for the duration of the flight path. It is important to note that this measurement is what will be used for elevator deflection in HIL and flight testing control logic.

Figure 6.5 shows the lift and drag forces during the maneuver. In this figure we can conclude the large importance of launch velocity and angle. With the parabolic increasing thrust force, it can be seen that even an doubling in maximum engine thrust

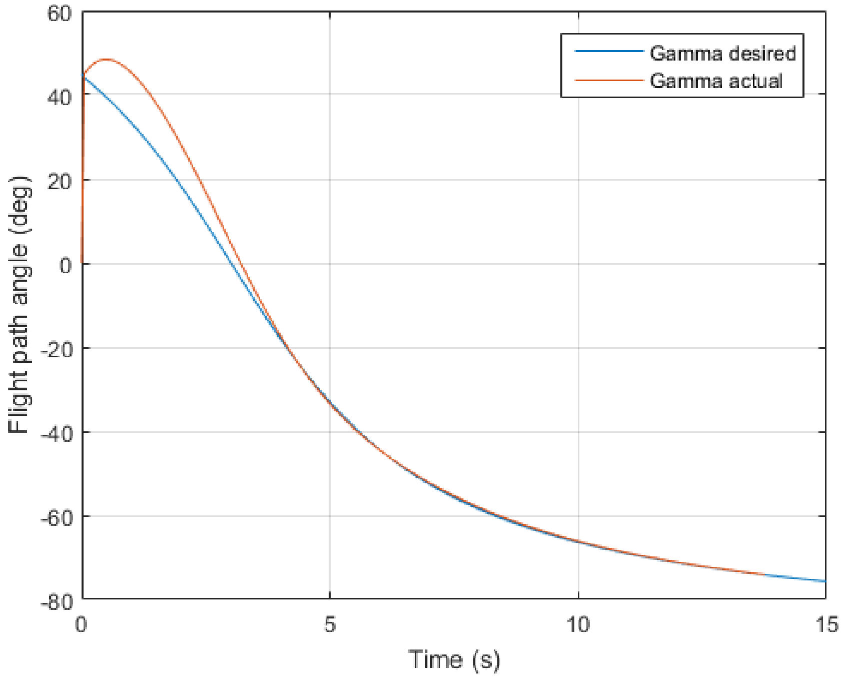

Figure 6.2: Gamma actual and gamma desired during

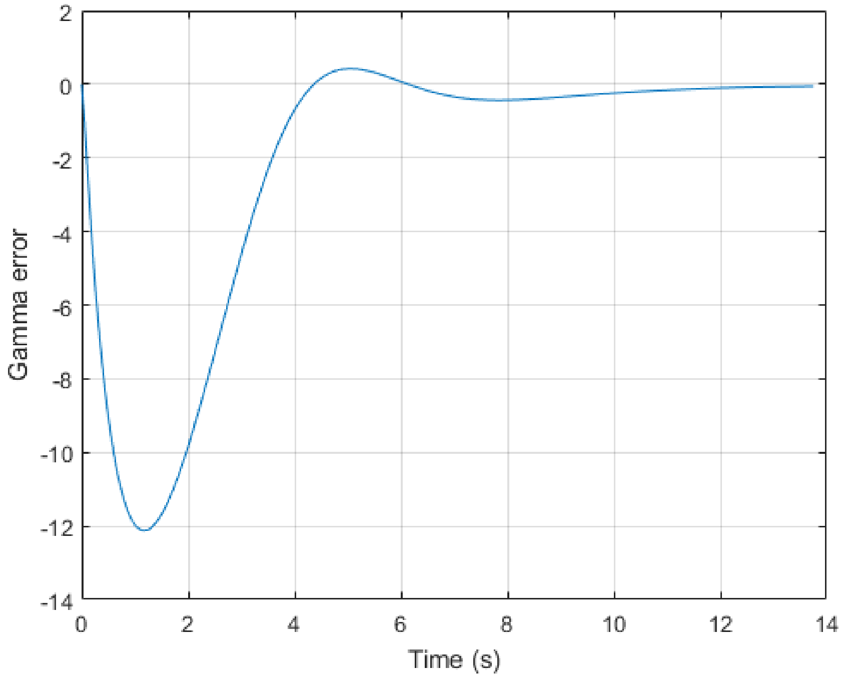

Figure 6.3: Error from gamma desired and gamma actual

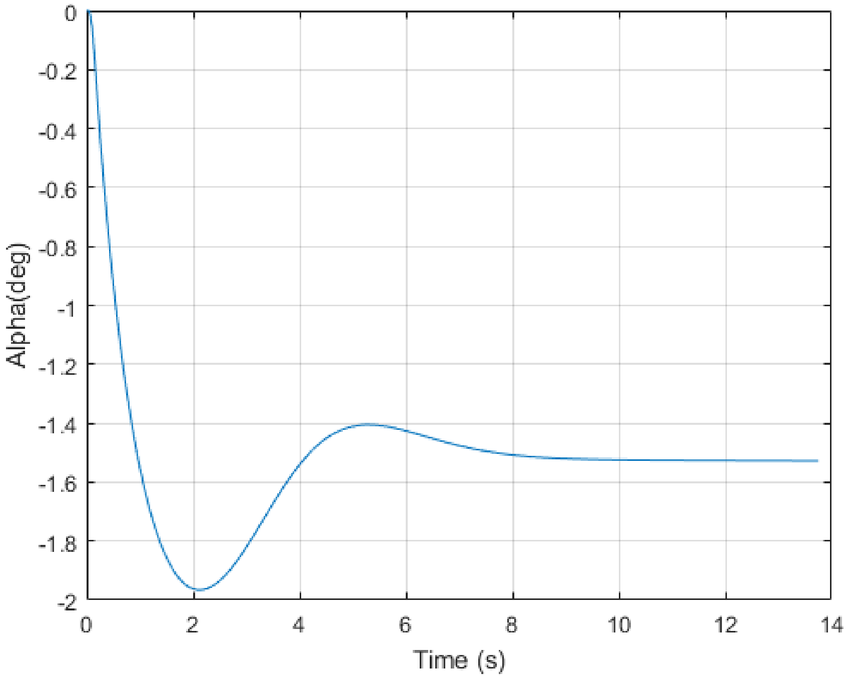

Figure 6.4: Angle of attack

would only extend the duration by a few seconds. Additionally, the figure shows that Karmali and Shelhamer's control logic is viable as the lift force is approaching zero when local accelerations are zero. Figure 6.6 is a plot of thrust desired (which is essentially predicted drag) and thrust actual. It shows the response of the thrust given an input throttle command and also shows that at 90 [N] thrust, the engine throttle is set to 1 and has more available thrust.

Acceleration magnitude in Figure 6.7 is one of the most important result of the testing. It shows the local acceleration of the aircraft based on the change in velocity during the maneuver. Acceleration due to gravity is measured at -9.81 or one earth gravity and the initial response produces a positive acceleration of about 4 m/s. This is a common overshoot where the objects within the aircraft would be lifted from the floor of the fuselage initially before weightlessness began. The response of this initial overshoot may be caused by the underestimation of pitch response

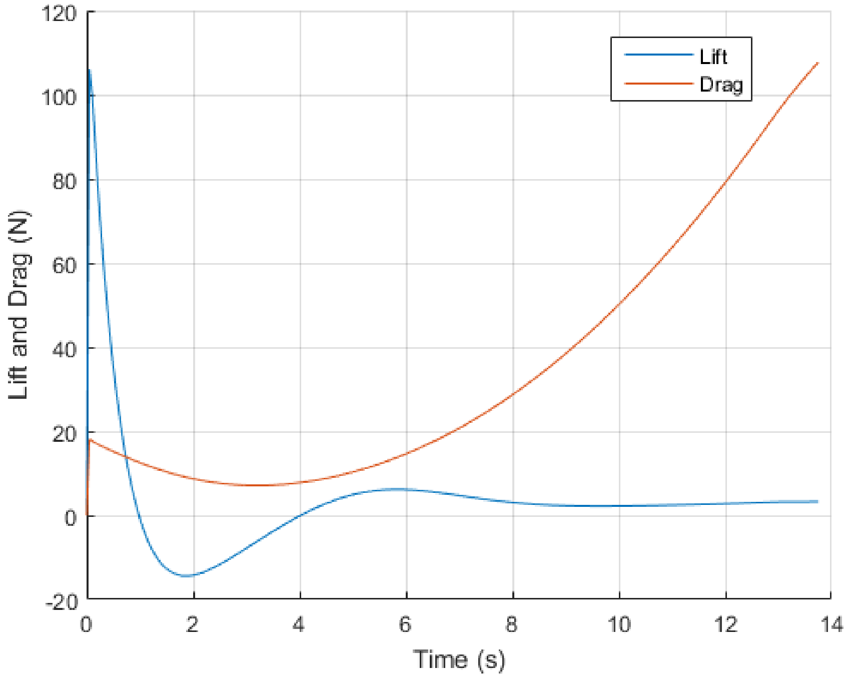

Figure 6.5: Lift and drag forces

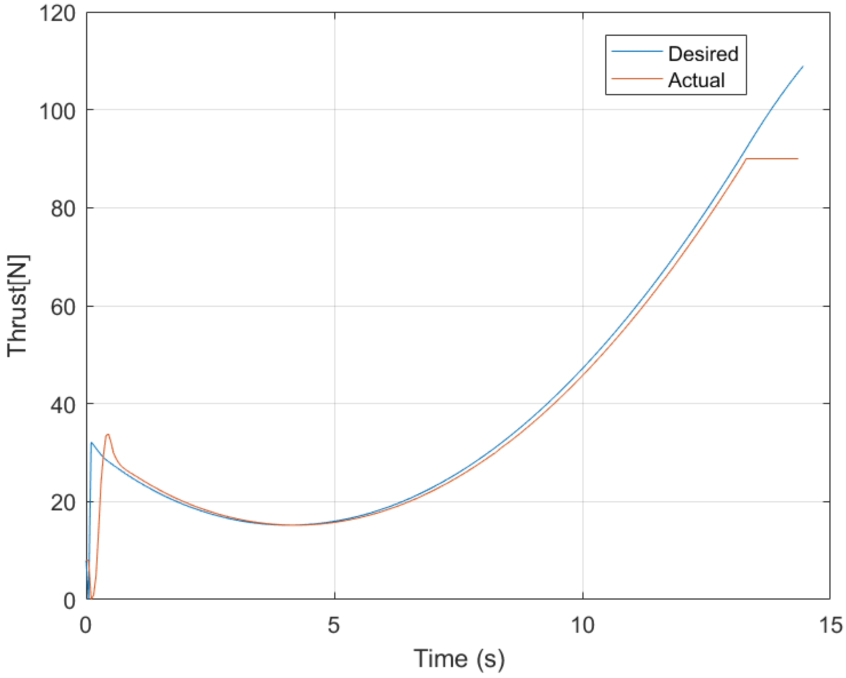

Figure 6.6: Thrust response

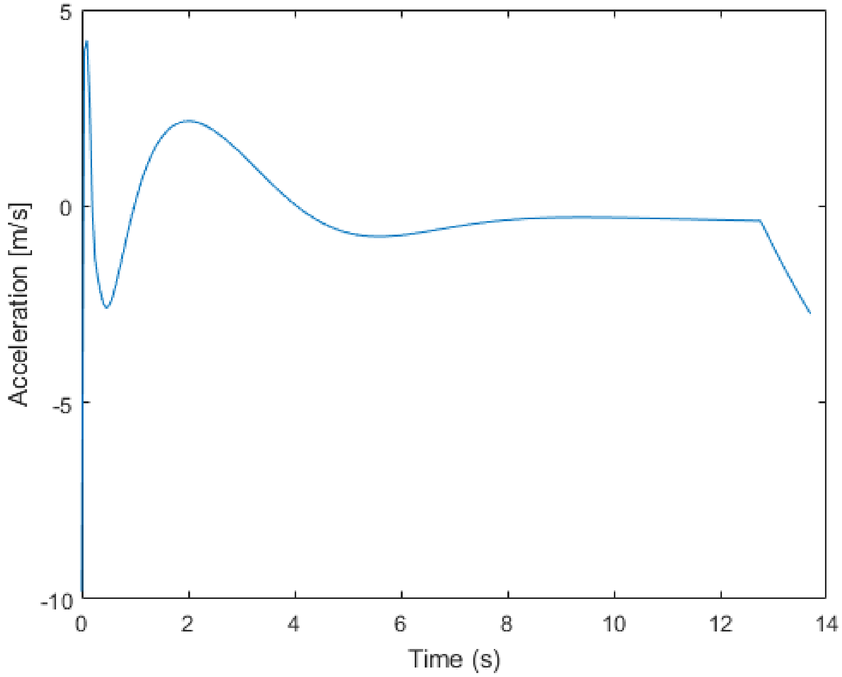

Figure 6.7: Net accelerations

described by the transfer function. Also, gains may be tuned more ideally to decrease settling time but were not tuned in this simulation. The controller eventually achieves weightlessness at about 5 seconds from the start time and continues until thrust available is saturated. The duration of testable microgravity is around 8 seconds. During this time, residual accelerations are maintained at 0.05 magnitudes of earth gravity on average. These are acceptable residuals for experimentation on board the aircraft although there is no unsteady atmospheric effects currently modeled. Gusts will effect the results significantly but this simulation shows that he controller does achieve zero acceleration. It is also seen in figure 6.1 that the aircraft is not following the desired path exactly but is still managing to create a zero acceleration environment. It can then be concluded that the flight controller can accept steady state error from altitude desired and still work.

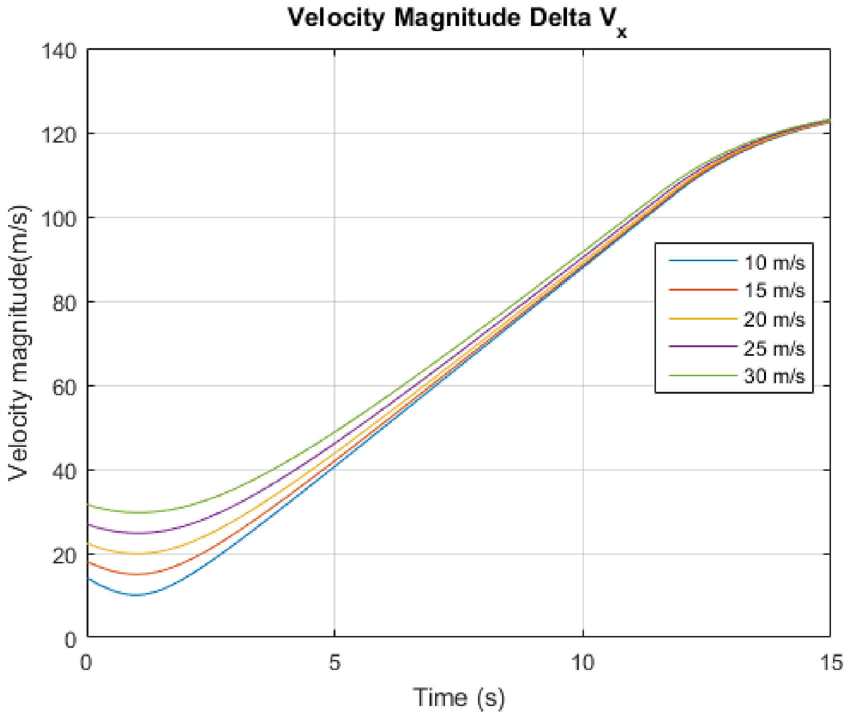

Figure 6.8: Velocity magnitude with changing initial horizontal velocity

6.1.2 Trajectories

As mentioned in previous sections, the starting conditions have large effects on duration of weightlessness. Using the ZrhoG simulator, plots were created with multiple variations in initial velocity magnitude and direction. Plots of velocity magnitude are presented because micrography duration is influenced mostly by drag or V_{NE} of the aircraft which are directly correlated to velocity. The test ran where all conducted with the same starting altitudes of 2000 meters. The aircraft that provided the following plots was the Penguin-B model and the variation in starting velocity began at $10m/s$ which is the airframes cruising velocity. This velocity was increased in one component at a time. First V_x was increased by $5m/s$ up to $30m/s$ while V_y remained constant at a starting velocity of $10m/s$. Then, V_y was varied while V_x remained constant at $10m/s$. This is a systematic approach for determining the effects of variation of velocity in each component.

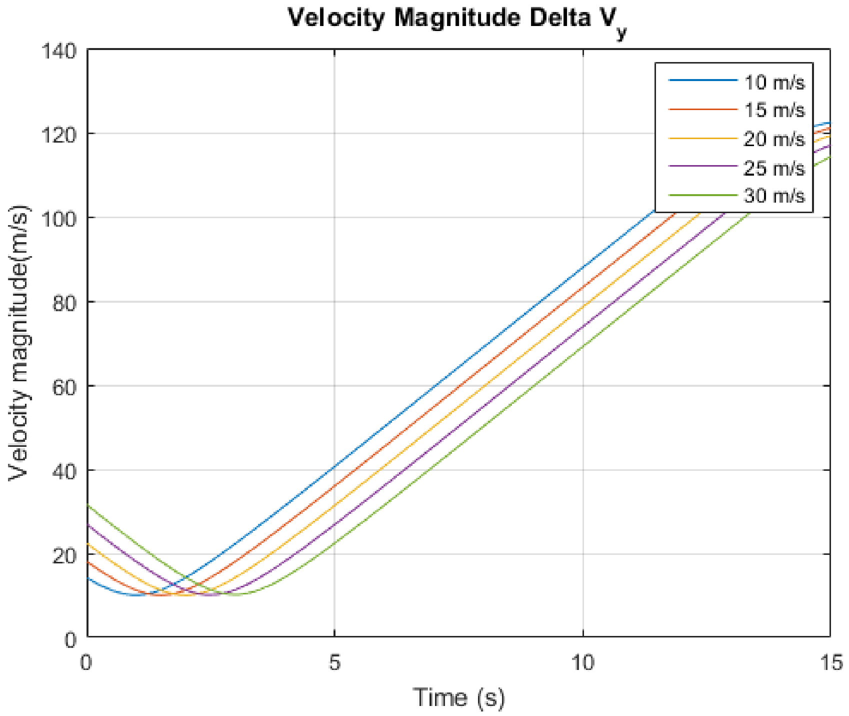

Figure 6.9: Velocity magnitude with changing initial vertical velocity

As we can see from figure 6.8, the x velocity change as little effect on the overall magnitude later in the maneuver. It is however more impact full in the early stages due to the velocity component being mostly in the X direction. Changing V_x allows the pilot to increase lowest speed of the aircraft during the maneuver so that the wings do not stall. It is not crucial to maintain lift in the wings assuming the pitch rate is advantageous so that the airframe begins to pick up speed at a ideal angle of attack. This is a similar dynamic to a gravity turn used in rocketry. With that in mind, it is concluded that the V_x variation does not have a large impact on the maneuver.

Figure 6.9 represents the aircrafts velocity in the vertical direction. Here, the effect of increased vertical velocity is noticed to shift all velocity profiles further to the right while maintaining the same profile. This ultimately extends the allowable duration of free fall.

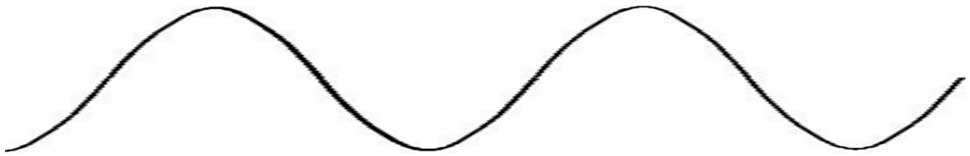

Figure 6.10: Sinosoidal path to follow for energy management

The Penguin-B aircraft does not have a climb rate of $30m/s$. However, if energy from the last maneuver is used, a greater upward velocity can be achieved. This is the case for NASAs weightless wonder where a sinusoidal path is followed like the one shown in figure 6.10. This includes a flight path of multiple zero g manuevers which each successive parabola generates more energy for the next.

6.1.3 Gust effects

Results from the gust effect structure that was presented in previous sections is included here. Plots where created with gusts varying from 0 (for a neutral) to a maximum of 20 m/s and a starting velocity of V_y 30 m/s and V_x 10 m/s as shown in figure 6.9. This equates to around a 40 knot wind which is quite large from SUAS. These gusts were applied to all airframes but for initial presentation the Penguin-B results are shown. Figure 6.11 shows how different strength of head and tail gust effect the overall acceleration during reduced gravity portion. A gust from this direction shows to have little effect on the quality of the maneuver and only perturbs the acceleration magnitude by 0.3 m/s or 0.02 percent of one gravity. This is a very minimal effect from head on or tail gust of a relatively high magnitude. The duration is more impacted by gusts in this direction which is also shown in figure 6.11. Duration is determined by how long the system is able to maintain close to zero acceleration. To understand this dynamic, it is important to realize that the gust simulation was done by adding a velocity step to airframe continually after 5 seconds. This adds and

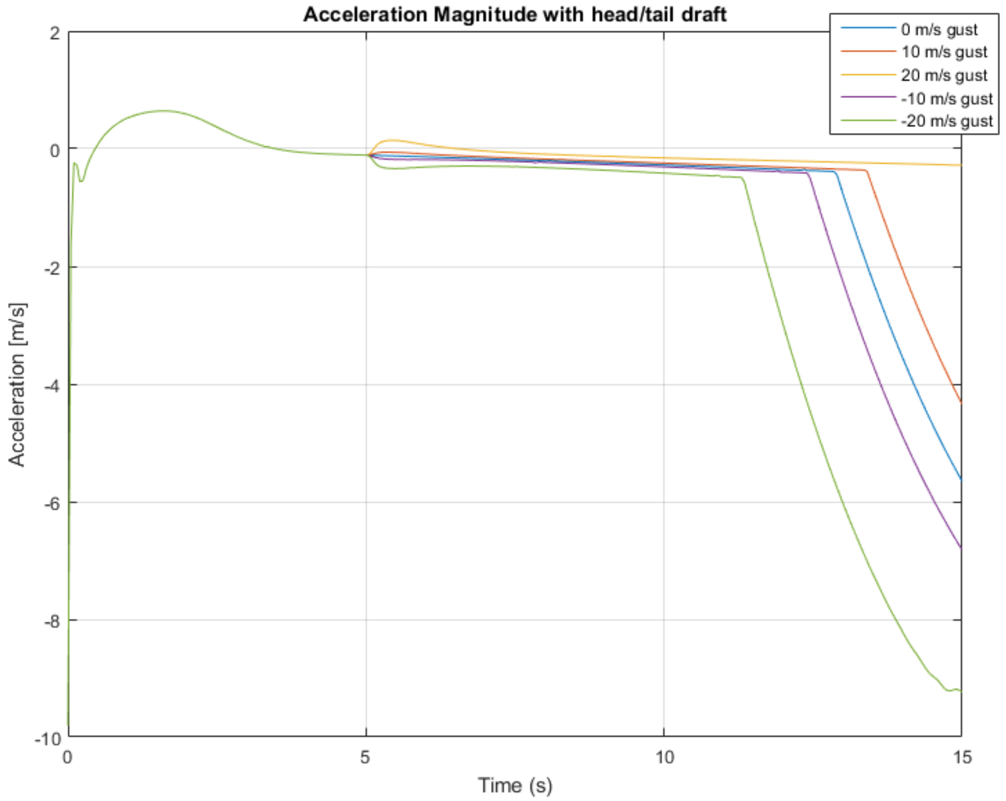

Figure 6.11: Acceleration magnitude do to head and tail wind of varying strength at 5 seconds simulation time

subtracts from the total velocity in the forward and aft directions so the maneuver is able to be held for longer periods of time with tail wind. On the other hand, the duration is shortened by a direct head wind due to the drag build up and thrust available.

Figure 6.12 represents the response from a Up/down draft of different magnitudes. Here, a positive velocity gust would be acting in the upward direction where as a negative value would represent a downward gust. These type of gusts have a much greater effect on the acceleration magnitude of the airframe and causes the controller to react to the offset. The worst condition occurs at an upward gust of 20 m/s (yellow line) which causes a 1 gravity acceleration upward. It is difficult for the controller

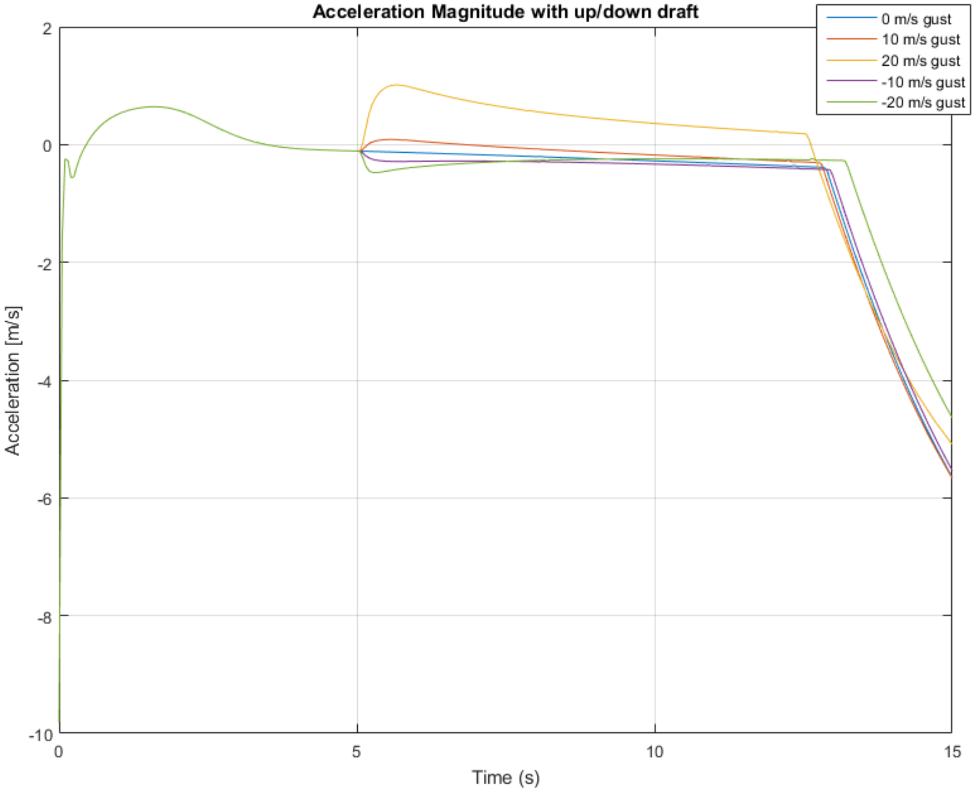

Figure 6.12: Acceleration magnitude do to up and down draft of varying strength at 5 seconds simulation time

to react to such a strong offset which but begins to level out after 5 seconds to zero acceleration. Other gust strengths in this direction are easily corrected by the controller which responds within 1-2 seconds. Neither up nor down draft have a large impact on duration.

The next test was to see if time of gusting had an effect on how difficult it was for the controller to respond. In figures 6.13 and 6.14 the gust time was changed from 5 seconds to two simulation time. The change shows large effects in both up/down and forward/aft gust conditions. In fact, in the forward gust condition of 20 m/s goes beyond the angle of attack values recorded from the Datcom model of the aircraft. It stops the simulation for that condition shortly after because there are no further

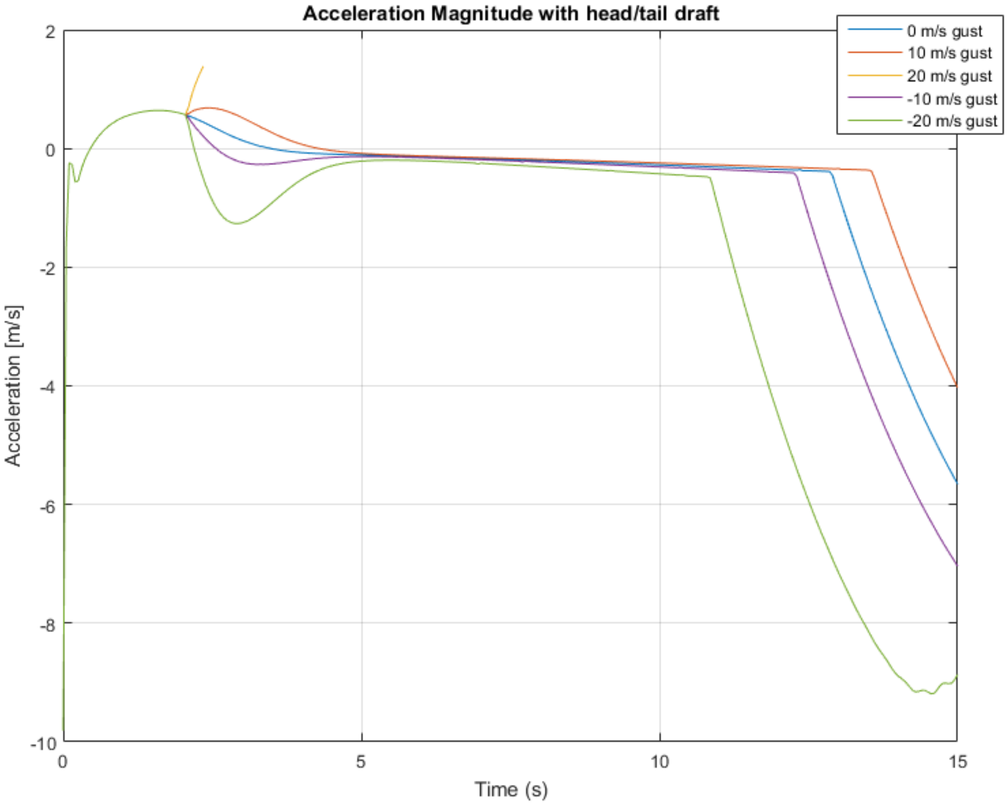

Figure 6.13: Acceleration magnitude do to head and tail wind of varying strength at 2 seconds simulation time

C_D and C_L values to use in the equations of motion. The impact on duration from a head/tail gust also is magnified with a 2 second gust. At two seconds, the conditions of the aircraft is high pitch rates and low relative velocities. Applying velocity changes at this point causes a larger error perturbation from the commanded value which. Ultimately this causes a large effect to the overall acceleration and makes it more difficult to recover from. These higher pitch rate and lower velocity conditions can be referred to in figure 6.4 and 6.9. It is also important note that a large aft gust of 20 m/s has a large initial effect but is well corrected for by the controller.

Figure 6.14 presents the effects of the 2 second up and down drafts on the system. In this figure, all responses from the system are acceptable other than the 20 m/s

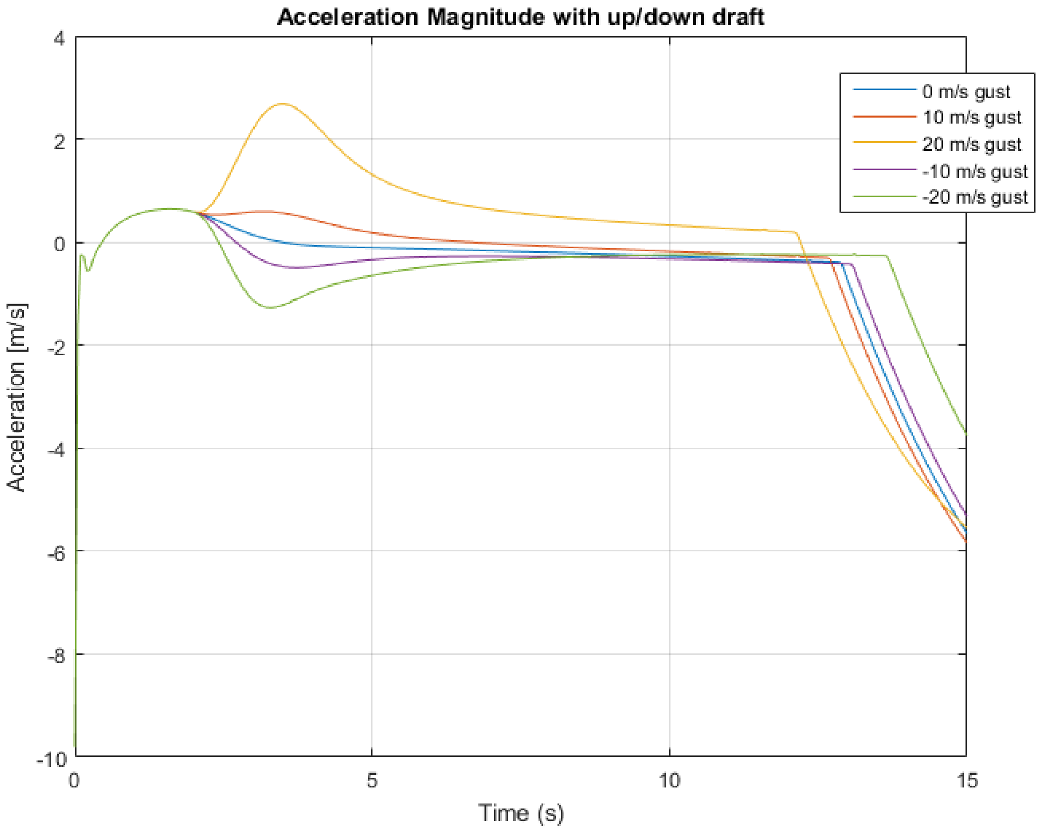

Figure 6.14: Acceleration magnitude do to up and down draft of varying strength at 2 seconds simulation time

updraft. Similarly to the previous Up/down draft scenario, these drafts have large effects on the overall acceleration response. Additionally, in this case the duration is also increased with larger magnitude gusts downward.

The figures show that the airframe and controller system is more than capable of handling gusts up to 10 m/s. Although gusts of $20m/s$ were controlled well, the initial response of the airframe would be too large for the experimentation on board. It is possible that a gust at this speed would just be a non-reocurring instance so that follow up zero gravity periods could continue as normal. $10m/s$ is a significant gusting condition that would only be exceeded in extreme weather conditions. These results also show that the controller is viable as just an “initial condition controller” as opposed to a controller that continuously calculates the desired state. The former is much less computationally intensive and means that the controller could be implemented on a less powerful flight controller.

6.1.4 Comparing airframes in simulation

Different airframes were analyzed in order to compare the effects of gusts and ZrhoG controller effectiveness. The pitch rate and throttle response time simulator was changed for both the Cessna 172 and Boeing 737 models. For the Cessna model, the damping ratio was left the same at 0.7, and the natural frequency was decreased from 31 to 19 seconds and decreased to 6 seconds for the B737 model. This models the higher response time for larger actuators and moment of inertia. The effects of similar gusting conditions are obliviously not as intense for larger airframes so the gust magnitudes were increased so that a similar conditions to the Penguin-b gust tests are maintained. It is already known that larger airframes are less affected by atmospheric gust but showing the response from a similar step input will help judge the controllers effectiveness on larger airframes.

The B-737 shows similar attributes to NASA modified 727 Weightless Wonder. The most revealing result is that the aircraft can hold a zero gravity condition for up to 35-40 seconds using a start condition of $V_y = 100$ and $V_x = 100\ m/s$ (a common cruise/climb condition). The repeatable duration of the 727 is also 35 to 40 seconds long.

spider plot

6.2 Hardware in the loop results

6.2.1 Manual and semi-manual maneuver

The manual maneuver was tested in X-plane with Futaba controller and receiver on a work station computer. X-plane, Stabilis autopilot and QGroundControl was

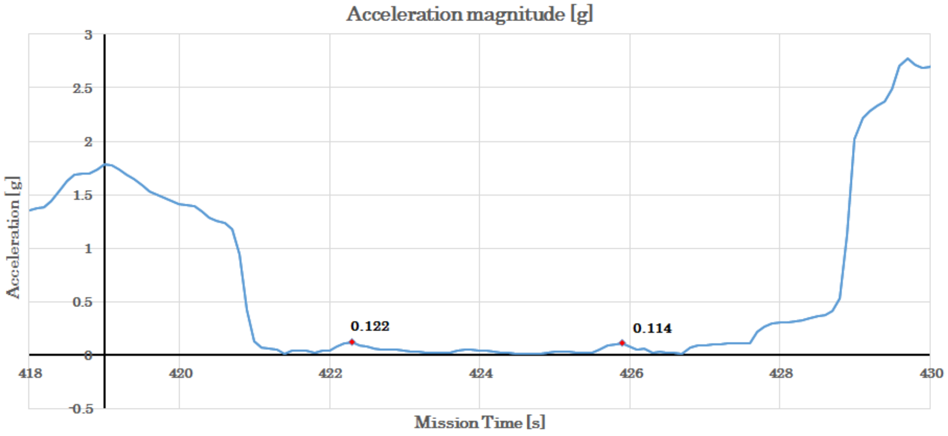

Figure 6.15: Acceleration magnitude achieved in HIL manual mode

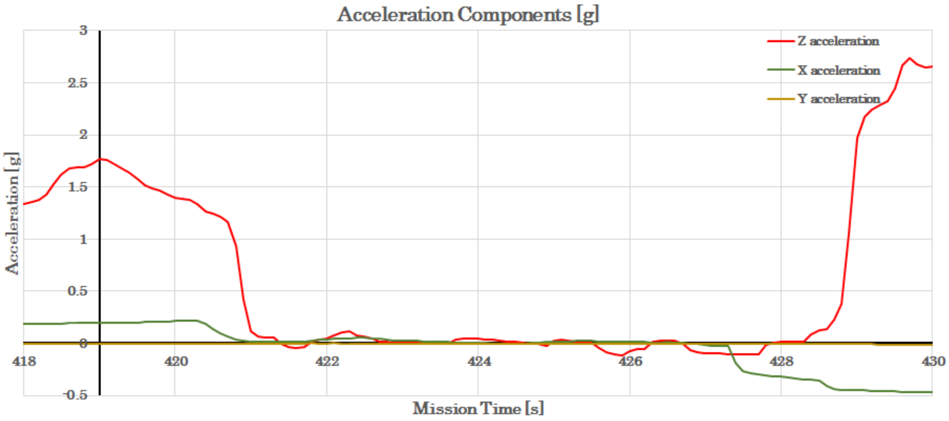

Figure 6.16: Component accelerations during manual mode HIL test

used in HIL as shown in figure 5.5. The X-plane data that was output included on the display was velocity, altitude and acceleration components for the pilot to read during the maneuvers. For these tests, the X-Plane simulation environment had steady atmospheric conditions (zero wind, gusts etc.) and the maneuver was attempted 30 times. There was some initial flight time prior to the 30 attempts to get the pilot antiquated with the maneuver dynamics. The best of the 30 attempts is shown graphically in the following figures.

Figure 6.15 represents the aircrafts acceleration magnitude during the flight. Here, as expected the local acceleration approaches zero for about 8 seconds but has sig-

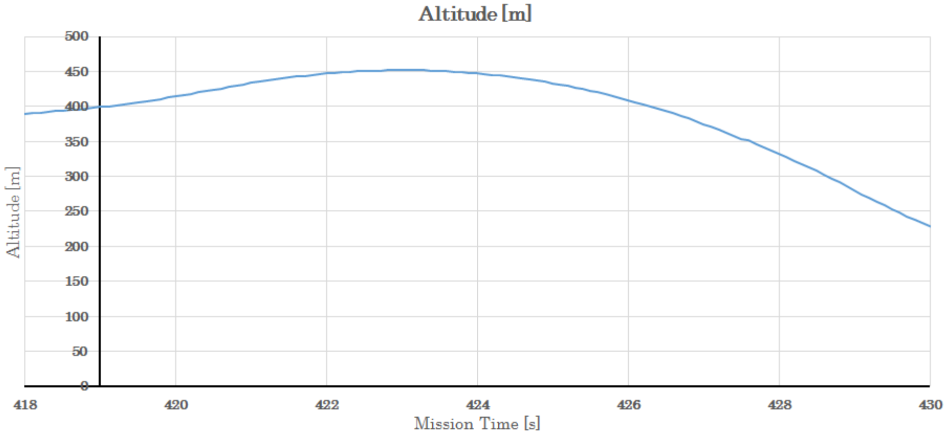

Figure 6.17: Altitude during manual mode HIL test

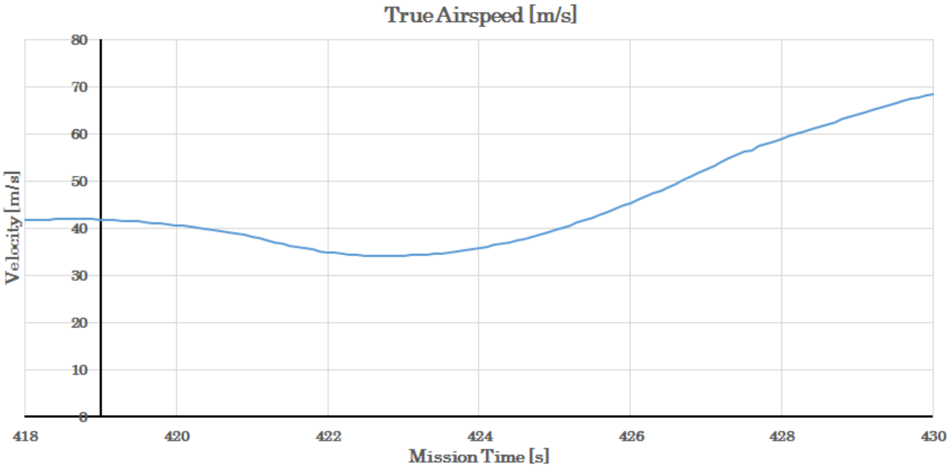

Figure 6.18: Velocity during manual mode HIL test

nificant residuals shown by the red diamonds. By looking at figure 6.16 where the acceleration is broken up into components, the problem points can be further identified. Accelerations in Y_b are almost non existent and do not add to the high residuals. X_b acceleration is controlled by throttle and is relatively well maintained throughout the parabola. Acceleration in Z_b has the largest impact on the magnitude of residuals. The pitch controller must be the most responsive in order to reduce these residuals.

The pilot must be aware of the velocity magnitude as well so that the V_{ne} is not exceeded. In X-plane simulation, the aircraft structure is not modeled so in theory, the aircraft is only limited in maneuver duration by thrust capacity. This effect is realized in figure 6.16 when the acceleration in X_b can no longer be maintained due to thrust available. The actual duration is shorter because the airframe V_{ne} is equal to 60 m/s We can conclude that the manual operation of the maneuver is unacceptable for experimental repeatability. Also, it is very draining on the pilot to control roll and yaw directions while also visually looking at x and y accelerations to change pitch and throttle commands. The response time of humans is too slow to create microgravity by simply using visual feedback of acceleration. It is then determined that there needs to be alternative methods for manual piloting to be effective. One option would be a display that shows the pilot a directed path to follow. This would help the pilot maintain a course instead of responding to numbers but such is not so easily done with developmental autopilots.

The Simi-manual maneuver showed that, even with the pilot only concentrating on throttle and pitch of the aircraft, it is difficult to achieve using an RC controller. The pitch rates from elevator control for a smaller UAV are higher than that of a airliner sized aircraft which requires the pilot to be more responsive while giving very small commands. The RC controller is also not ideal for small command input compared to a flight yoke or joystick. The results best from 30 attempts at maintaining weightlessness is shown in figure 6.19. It is clear immediately that the maneuver requires too much resolution from the RC pilot. With pilot practice, these maneuvers may be improved in quality and repeatability but at current conditions are unacceptable.

6.2.2 Fully autonomous

Fully autonomous flight was completed but did not work successfully enough for flight testing to commence. The ZrhoG flight control code was constructed based off of existing stabilize code on the Stabilis autopilot. Here, the commands for pitch and throttle were changed to incorporate the ZrhoG controller. The modified autopilot

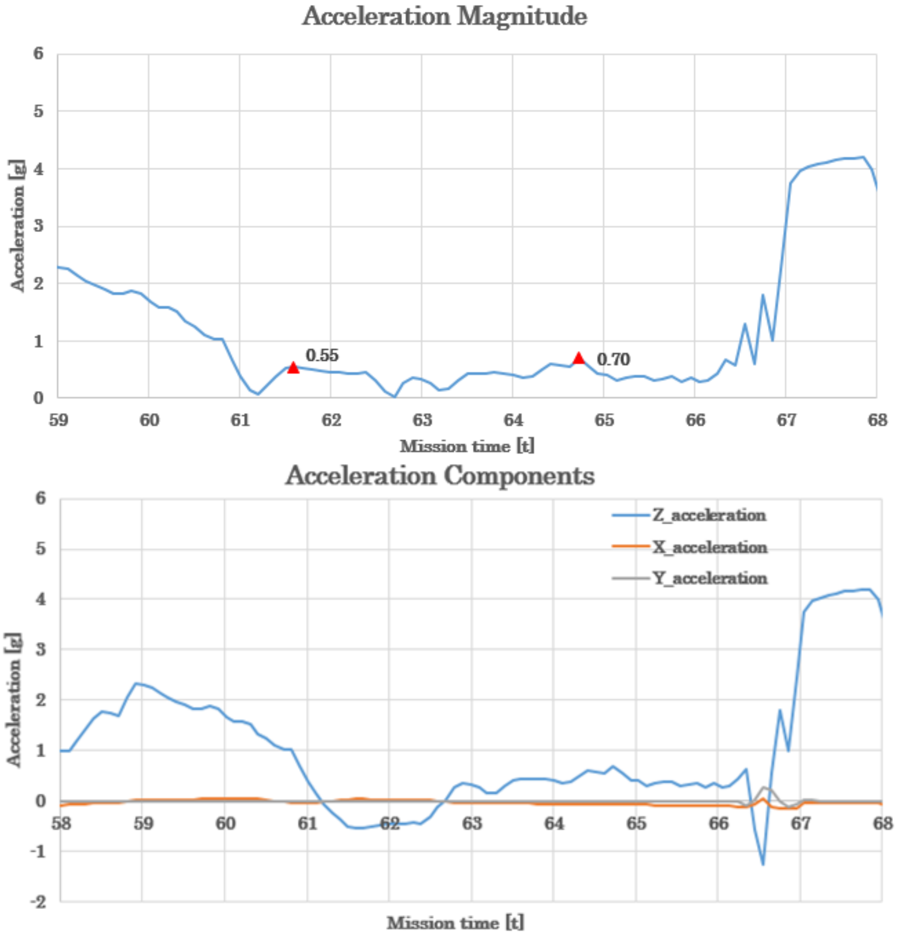

Figure 6.19: Acceleration reading during semi-manual microgravity attempt

code was having issues with the limiting parameters for fixed wing aircraft safety. These parameters include a maximum pitch rate and angle that the autopilot will allow. Changes were made to these parameters to allow the aircraft to pitch as fast as the airframe would allow and pitch downward at maximum of 70 degrees. These changes did not resolve the persistent issues so further debugging was done. The issues are not in the commanding of the controllers. Errors reside in the systems ability to achieve the commanded values.

CHAPTER 7

Conclusions

7.1 Summary

The major goals of developing a framework to evaluate models of MGUAS and validating the MGUAS prototype with HIL and flight testing have been addressed. In doing so the goal of creating a framework to develop MGUA has been accomplished. That framework included the development of Datcom models, development and discussion of flight control logic and the development of a simulator. Datcom models were compared to confirm accuracy. The simulator started off as a simple 3 DOF MATLAB code with separate functions for aerodynamic values or EOMs and was continually built on through out the research process. The ZrhoG MATLAB simulation was used to verify flight control logic as well test different parameters effect on the weightless maneuver. The ability to add gusts effects was eventually added to ZrhoG which increased the amount of parameters to study. To the authors knowledge, analysis of this type for a microgravity vehicle has never been accomplished and is a effective tool to use for current and future research. Gust research shows that on certain a MGUAS airframe, the maximum gust velocity that the system could handle was 20 m/s in magnitude and in the airframe body axis up direction. The goal of validating a MGUAS prototype was not fully accomplished however, large strides were made in the process. These strides include integrating an autopilot system with HIL functionality, implementing the ZrhoG flight code onto the autopilot, testing manual/semi-manual flight modes in HIL and developing a flight test plan. The major un-accomplished tasks have been added to the future work section and include more extensive HIL testing of the ZrhoG autopilot and Flight testing of the MGUAS prototype.

Major conclusions in this work include, the success of both airframe and flight control method to create a weightless environment. The Penguin-B airframe and ZrhoG flight controller were able to maintain up to a 10 second free fall duration with no residual accelerations in a non gusting condition. The zero residual acceleration is a result of the simulation environment. In reality, atmospheric unsteadiness and control surface slop would influence quality significantly. The work has shown that the control concept also works on larger airframes and produces similar results to that of NASAs Boeing 727 Weightless wonder. The flight controller concept that was selected is an initial state measurement that produces a commanded path for a PID controllers to follow through out the duration. This method is different from a continual feedback path in that it only runs a projectile motion calculation once. This reduces the load on the processor and ultimately means that the flight computer can be less powerful. The largest contribution of this research work is the foundation for future researchers to build on.

7.2 Recommendations

Maximum flight speed needs to be determined to safely push the boundary for maximum duration. Although structural strengthening was added to the Anaconda airframe the never exceed speed has yet to be quantified. Failure tests can be conducted on similar wings to determine the maximum aerodynamic loading. Then, by estimating drag at certain airspeeds, the maximum recommended speed of the airframe can be quantified. For some airframes, a more accurate estimate of maximum airspeed may only be increased by a few meters per second. In increased duration this increase in speed would only allow for less than a second longer period of weightlessness. For others, this V_{NE} estimation could prove to add multiple seconds to duration. In any case, it is a relatively easy estimation process that should be done to optimize duration.

Eventually flight testing a more ideal airframe with lower aspect ratio. A lower aspect ratio wing improves the performance of a microgravity vehicle in two different ways. It increases the structural resistance to drag due to a smaller moment on the wing box ultimately leading to a longer duration. Shorter wings also decrease the effects of gusts which reduces residual accelerations during experimentation. Unfortunately, lower aspect ration wings decrease the endurance and range of the vehicle but this drawback is quickly out weighed by the gain. For quality and duration are both of higher importance to the generation of microgravity than endurance of flight time. Ideally, an airframe and propulsion system should be designed specifically for this mission profile if optimal microgravity conditions are to be achieved. The main parameter of the aircraft would be high performance, low drag, high structural strength for large velocities and a large payload bay that is somewhat close to the CG of the airframe.In the design, It is not crucial to reduce weight as much as other aircraft because it is momentum that helps the MGUAS maintain energy through to the next maneuver which ultimately extends free fall duration. A high performance engine of the jet engine type would be ideal because it reduces vibrations that would cause errors in the INS which would heavily impact the controller if acceleration feedback was used.

7.3 Future work

7.3.1 MATLAB simulator

Some improvements to the ZrhoG simulator could be made to further its use in research. As mention in previous sections, the truth dynamics calculator is based off of the Euler method and could be upgraded to RK4 integration. Engine models and accuracy could be improved which would give better estimates of duration. Also, instead of using a transfer function to model elevator pitch response, the actual dynamics could be included. The Datcom models were made with realistic control surfaces so C_l and C_d based on elevator deflection is included in the imported data file fore each aircraft. Once a longitudinal moment equation is added to the EOMs, elevator deflection effects should be easy to implement. Furthering pitch moment equations, the effects of pitch rate could also be modeled through C_{l_q}, C_{l_q} and C_{d_q} which are also included in the aerodynamic input file for each aircraft.

7.3.2 MGUAS Control

Some logic needs to be developed to command the airframe into the next parabola because currently it is just commanded to dive until simulation end. This structure could be used to evaluate optimal paths in between each maneuver which would increase the initial upward velocity of the next. The path of NASA 727 aircraft is determined by the maximum g load pull up that was desired. With in-experienced pilots on board the aircraft, it was important that the g-load not go above 2.5 g's for extended periods of time. With MGUAS the maximum g-load could potentially be greater which opens up more path opportunities for optimization of energy maintenance. With MGUAS being a new platform option in the field of microgravity research, path optimization has a high possibilities. Along with path planning in between maneuvers, never exceed logic (for both maximum airspeed and safety floor) should eventually be implemented. Most importantly this logic would include a floor for the aircraft to be commanded to pull up should it go bellow a certain altitude. This logic would be very useful for safety in flight testing and should be verified in simulation prior to flight. An "if then" logic could be used to command a safe flight altitude should the aircraft approach floor of safety. Acceleration feedback control should be further investigated however it is not a trivial task. The nature of using accelerations to command pitch actuators reveals high level controls issues that the author does not have experience in. However, the result of a successful controller may lead to a more responsive system to gusts and perturbations away from the zero gravity condition.

7.3.3 HIL

Once the flight controller is achieving microgravity in HIL, it is a good idea to use Xplanes ability to change atmospheric effects. By evaluating the airframe at different conditions, the researcher can produce a recommended test flight envelope in terms of the maximum allowable atmospheric conditions as was done with the MATLAB simulation. The results between the two simulation should be comparable. The first tests will evaluate the UAS's ability to respond to head on constant wind with with increasing strength between runs. Additionally, the wind direction will be changed to produce a side, aft, downdraft and updraft constant wind. It will be more difficult to maintain the desired path when the wind is pushing the aircraft off course. The next conditions to be evaluated are of gusts in deferent directions and magnitude. The last conditions to be evaluated will be increasing magnitudes of wind speed and gusts in all directions.

7.3.4 Flight test

Flight testing is needed to show that the MGUAS prototype works to expectation. To start, the flight test campaigned outlined in chapter 5 should be followed. Separately, a manual flight attempt at producing zero acceleration should be made and followed by a semi-manual done similarly to HIL. From these test, a comparison could be made to quantify how close HIL simulation was to prediction of flight aerodynamics. The flight test champagne should finish with a fully autonomous maneuver. During the fully autonomous maneuver, flight data is recorded from both the flight computer and Arduino accelerometer within the payload bay. This data should be compared during ground checks prior to flight so that both accelerometers have equal offsets. After flight test the data should also be compared to show residual accelerations due to pitch rate and should conclude to be of little effect. Finally, a simple fluids experiment should be mounted into the payload bay with a recording camera. Should the aircraft achieve weightlessness during flight, the experiment would conclude the results.

CHAPTER 8

Appendix

```
******************************  INPUT DATA CARDS  ******************************

 CASEID Penguin-b : Flight Conditions, Body, Wing, and Flaps
  $FLTCON WT=33.0, LOOP=1.0,
  NMACH=1.0, MACH=0.1,
  NALPHA=5.0, ALSCHD(1)=-2.0,0.0,1.0,2.0,4.0,
  NALT=1.0, ALT(1)=0.0$
  $OPTINS BLREF=11.0,SREF=8.5,CBARR=1.0$
  $SYNTHS XW=1.94,ZW=0.31,XH=6.30,ZH=1.1,XCG=2.45,ZCG=0.06,
  ZV=0.2,XV=6.15,ALIW=0.0,ALIH=0.0$
  $BODY NX=20.0, ITYPE=1.0, BNOSE=2.0, BTAIL=2.0,
  X(1)=  0.0,  0.328,  0.655,  0.983,  1.31,
  1.638,  1.965,  2.293,  2.62,  2.948,
  3.275,  3.603,  3.93,  4.258,  4.585,
  4.913,  5.24,  5.5675,  6.9,  7.0,
  R(1)=  0.0,  0.2,  0.35,  0.40,  0.41,
  0.42,  0.40, 0.40,  0.35,  0.30,
  0.15,  0.10,  0.10,  0.10,  0.10,
  0.10,  0.10,  0.10,  0.10,  0.0,
  ZU(1)=  0.0,  0.2,  0.35,  0.40,  0.41,
  0.42,  0.40, 0.40,  0.35,  0.30,
  0.30,  0.30,  0.30,  0.30,  0.30,
 0.30,  0.30,  0.30,  0.30,  0.2,
 ZL(1)=  -0.0,  -0.2,  -0.30,  -0.35,  -0.38,
 -0.39,  -0.40, -0.40,  -0.35,  -0.1,
 0.05,  0.10,  0.10,  0.10,  0.10,
 0.10,  0.10,  0.10,  0.10,  0.2,$
NACA-W-4-2408
 $WGPLNF CHRDTP=0.2,SSPNE=5.2,SSPN=5.4,CHRDR=1.0,SAVSI=5.0,CHSTAT=0.25,
 TWISTA=0.0,SSPNDD=0.0,DHDADI=0.0,DHDADO=0.0,TYPE=1.0$
 $SYMFLP FTYPE=1.0, NTYPE=1.0,
 NDELTA=5.0, DELTA(1)= 0.0, 10.0, 20.0, 30.0, 40.0,
 SPANFI=0.5, SPANFO=1.5, CHRDFI=0.3, CHRDFO=0.3,
 CB=0.452, TC=0.20, PHETE=0.003, PHETEP=0.002$
SAVE
NEXT CASE
DAMP
DERIV RAD
CASEID Penguin-b: Ailerons
 $ASYFLP STYPE=1.0, PHETE=0.05228,
 NDELTA=9.0,
 DELTAL(1)=-25.0,-20.0,-10.0,-5.0, 0.0, 5.0, 10.0, 20.0, 25.0,
 DELTAR(1)= 25.0, 20.0, 10.0, 5.0, 0.0,-5.0,-10.0,-20.0,-25.0,
 SPANFI=2.0, SPANFO=5.0, CHRDFI=0.2, CHRDFO=0.1$
SAVE
NEXT CASE
CASEID Penguin-b: Total
NACA-V-4-0012
 $VTPLNF CHRDR=0.0, CHRDTP=0.0, SAVSI=0.0, SSPN=0.0, SSPNOP=0.0,
 SSPNE=0.0, CHRDBP=0.0, SAVSO=0.0, CHSTAT=0.0, TYPE=0.0,$
NACA-H-4-0012
 $HTPLNF CHRDR=0.5, CHRDTP=0.5, SSPN=1.265, SAVSI=0.0,
 SSPNE=1.25, CHSTAT=0.25, TWISTA=0.0,
 DHDADI=-42.0, TYPE=1.0, DHDADO=0.0$
```

```
  $SYMFLP FTYPE=1.0, NTYPE=1.0,
  NDELTA=9.0, DELTA(1)=-20.0,-15.0,-10.0,-5.0,0.0,5.0,10.0,15.0,20.0,
  SPANFI=0.2, SPANFO=1.2, CHRDFI=0.1, CHRDFO=0.1,
  CB=0.452, TC=0.20, PHETE=0.003, PHETEP=0.002$
 NEXT CASE
1          THE FOLLOWING IS A LIST OF ALL INPUT CARDS FOR THIS CASE.
0
 CASEID Penguin-b : Flight Conditions, Body, Wing, and Flaps
  $FLTCON WT=33.0, LOOP=1.0,
  NMACH=1.0, MACH=0.1,
  NALPHA=5.0, ALSCHD(1)=-2.0,0.0,1.0,2.0,4.0,
  NALT=1.0, ALT(1)=0.0$
  $OPTINS BLREF=11.0,SREF=8.5,CBARR=1.0$
  $SYNTHS XW=1.94,ZW=0.31,XH=6.30,ZH=1.1,XCG=2.45,ZCG=0.06,
  ZV=0.2,XV=6.15,ALIW=0.0,ALIH=0.0$
  $BODY NX=20.0, ITYPE=1.0, BNOSE=2.0, BTAIL=2.0,
  X(1)=  0.0,  0.328,  0.655,  0.983,  1.31,
  1.638,  1.965,  2.293,  2.62,  2.948,
  3.275,  3.603,  3.93,  4.258,  4.585,
  4.913,  5.24,  5.5675,  6.9,  7.0,
  R(1)=  0.0,  0.2,  0.35,  0.40,  0.41,
  0.42,  0.40, 0.40,  0.35,  0.30,
  0.15,  0.10,  0.10,  0.10,  0.10,
  0.10,  0.10,  0.10,  0.10,  0.0,
  ZU(1)=  0.0,  0.2,  0.35,  0.40,  0.41,
  0.42,  0.40, 0.40,  0.35,  0.30,
  0.30,  0.30,  0.30,  0.30,  0.30,
  0.30,  0.30,  0.30,  0.30,  0.2,
  ZL(1)=  -0.0,  -0.2,  -0.30,  -0.35,  -0.38,
  -0.39,  -0.40, -0.40,  -0.35,  -0.1,
  0.05,  0.10,  0.10,  0.10,  0.10,
  0.10,  0.10,  0.10,  0.10,  0.2,$
 NACA-W-4-2408
  $WGPLNF CHRDTP=0.2,SSPNE=5.2,SSPN=5.4,CHRDR=1.0,SAVSI=5.0,CHSTAT=0.25,
  TWISTA=0.0,SSPNDD=0.0,DHDADI=0.0,DHDADO=0.0,TYPE=1.0$
  $SYMFLP FTYPE=1.0, NTYPE=1.0,
  NDELTA=5.0, DELTA(1)= 0.0, 10.0, 20.0, 30.0, 40.0,
  SPANFI=0.5, SPANFO=1.5, CHRDFI=0.3, CHRDFO=0.3,
  CB=0.452, TC=0.20, PHETE=0.003, PHETEP=0.002$
 SAVE
 NEXT CASE
0 INPUT DIMENSIONS ARE IN FT, SCALE FACTOR IS 1.0000

1                             AUTOMATED STABILITY AND CONTROL METHODS PER APRIL 1976 VE
                                                        WING SECTION DEFINITION
0                                 IDEAL ANGLE OF ATTACK =    .25757 DEG.


                              ZERO LIFT ANGLE OF ATTACK =  -1.94052 DEG.


                                 IDEAL LIFT COEFFICIENT =    .25602


                  ZERO LIFT PITCHING MOMENT COEFFICIENT =   -.05165


                             MACH ZERO LIFT-CURVE-SLOPE =    .09924 /DEG.


                                    LEADING EDGE RADIUS =    .00705 FRACTION CHORD


                              MAXIMUM AIRFOIL THICKNESS =    .08000 FRACTION CHORD


                                                DELTA-Y =   2.11265 PERCENT CHORD



0                         MACH=  .1000 LIFT-CURVE-SLOPE =    .09965 /DEG.
XAC =    .25542
```

```
 WARNING*** BODY ALONE DYNAMIC DERIVATIVE METHOD VALID FOR NOSE CYLINDER ONLY
            TAIL EFFECTS IGNORED]
1                               AUTOMATED STABILITY AND CONTROL METHODS PER APRIL 1976
                                         CHARACTERISTICS AT ANGLE OF ATTACK AND IN SIDE
                                                       WING-BODY CONFIGURATION
                                       Penguin-b : Flight Conditions, Body, Wing, and B

 ------------------------ FLIGHT CONDITIONS  ------------------------
--------------  REFERENCE DIMENSIONS  ------------
  MACH    ALTITUDE   VELOCITY    PRESSURE    TEMPERATURE     REYNOLDS
REF.      REFERENCE LENGTH   MOMENT REF. CENTER
 NUMBER                                                       NUMBER
AREA       LONG.     LAT.     HORIZ      VERT
             FT       FT/SEC     LB/FT**2       DEG R         1/FT
FT**2        FT        FT        FT        FT
0  .100        .00     111.63   2.1162E+03     518.670     7.0682E+05
8.500      1.000    11.000     2.450      .060
0                                                               -------------------DERI
0 ALPHA     CD       CL       CM       CN       CA       XCP        CLA
CMA          CYB          CNB          CLB
0
   -2.0     .015    -.007    -.0476   -.008     .015    6.311    7.137E-02
9.236E-03   -4.835E-03   -2.396E-04   -1.409E-04
     .0     .016     .139    -.0298    .139     .016    -.215    7.424E-02
8.550E-03                             -1.516E-04
    1.0     .018     .214    -.0214    .214     .014    -.100    7.557E-02
8.193E-03                             -1.570E-04
    2.0     .020     .290    -.0134    .290     .010    -.046    7.676E-02
7.802E-03                             -1.626E-04
    4.0     .026     .446     .0014    .446    -.005     .003    7.910E-02
6.976E-03                             -1.740E-04
0*** VEHICLE WEIGHT =     33.00 LB.
```

```
0*** LEVEL FLIGHT LIFT COEFFICIENT =  .26208

1                            AUTOMATED STABILITY AND CONTROL METHODS PER APRIL 1976 VER

                                        CHARACTERISTICS OF HIGH LIFT AND CONTROL DEVIC

                                           WING PLAIN TRAILING-EDGE FLAP CONFIGURATION

                                      Penguin-b : Flight Conditions, Body, Wing, and E

 -----------------------  FLIGHT CONDITIONS  ------------------------

--------------  REFERENCE DIMENSIONS  ------------

  MACH    ALTITUDE   VELOCITY    PRESSURE    TEMPERATURE     REYNOLDS

REF.      REFERENCE LENGTH   MOMENT REF. CENTER

 NUMBER                                                       NUMBER

AREA       LONG.     LAT.     HORIZ      VERT

             FT       FT/SEC     LB/FT**2       DEG R          1/FT

FT**2        FT         FT         FT         FT

0  .100        .00      111.63   2.1162E+03     518.670     7.0682E+05

8.500      1.000    11.000     2.450      .060

0            ---------INCREMENTS DUE TO DEFLECTION---------

---DERIVATIVES (PER DEGREE)---

0     DELTA     D(CL)      D(CM)    D(CL MAX)    D(CD MIN)

(CLA)D     (CH)A       (CH)D



         .0      .000      .0000      .000       .00000

NDM       2.249E-02   6.236E-02

       10.0      .111     -.0092      .055       .00426

NDM                   6.236E-02

       20.0      .172     -.0213      .096       .01197

NDM                   6.276E-02

       30.0      .197     -.0334      .127       .02389

NDM                   6.308E-02

       40.0      .233     -.0355      .146       .03918

NDM                   6.320E-02

0  *** NOTE * HINGE MOMENT DERIVATIVES ARE BASED ON TWICE THE AREA-MOMENT OF THE CONTRO
```

```
0            --------- INDUCED DRAG COEFFICIENT INCREMENT , D(CDI) , DUE TO DEFLECTION
0       DELTA =    .0      10.0      20.0      30.0      40.0
   ALPHA
0
    -2.0       -2.80E-08  8.28E-04  2.00E-03  2.66E-03  3.73E-03
      .0        9.43E-07  1.80E-03  3.50E-03  4.39E-03  5.77E-03
     1.0        1.43E-06  2.28E-03  4.26E-03  5.25E-03  6.79E-03
     2.0        1.91E-06  2.77E-03  5.01E-03  6.12E-03  7.82E-03
     4.0        2.88E-06  3.74E-03  6.51E-03  7.85E-03  9.86E-03
0***NDM PRINTED WHEN NO DATCOM METHODS EXIST
1          THE FOLLOWING IS A LIST OF ALL INPUT CARDS FOR THIS CASE.
0
 DAMP
 DERIV RAD
 CASEID Penguin-b: Ailerons
  $ASYFLP STYPE=1.0, PHETE=0.05228,
  NDELTA=9.0,
  DELTAL(1)=-25.0,-20.0,-10.0,-5.0, 0.0, 5.0, 10.0, 20.0, 25.0,
  DELTAR(1)= 25.0, 20.0, 10.0, 5.0, 0.0,-5.0,-10.0,-20.0,-25.0,
  SPANFI=2.0, SPANFO=5.0, CHRDFI=0.2, CHRDFO=0.1$
 SAVE
 NEXT CASE
0 INPUT DIMENSIONS ARE IN FT, SCALE FACTOR IS 1.0000

1                             AUTOMATED STABILITY AND CONTROL METHODS PER APRIL 1976 VE
                                                          WING SECTION DEFINITION
0                                 IDEAL ANGLE OF ATTACK =    .25757 DEG.


                              ZERO LIFT ANGLE OF ATTACK =  -1.94052 DEG.


                                 IDEAL LIFT COEFFICIENT =    .25602
```

```
                  ZERO LIFT PITCHING MOMENT COEFFICIENT =   -.05165

                             MACH ZERO LIFT-CURVE-SLOPE =    .09924 /DEG.

                                    LEADING EDGE RADIUS =    .00705 FRACTION CHORD

                              MAXIMUM AIRFOIL THICKNESS =    .08000 FRACTION CHORD

                                                DELTA-Y =   2.11265 PERCENT CHORD



0                         MACH=  .1000 LIFT-CURVE-SLOPE =    .09965 /DEG.
XAC =    .25542
 WARNING*** BODY ALONE DYNAMIC DERIVATIVE METHOD VALID FOR NOSE CYLINDER ONLY
            TAIL EFFECTS IGNORED]
1                               AUTOMATED STABILITY AND CONTROL METHODS PER APRIL 1976
                                         CHARACTERISTICS AT ANGLE OF ATTACK AND IN SIDE
                                                       WING-BODY CONFIGURATION
                                                        Penguin-b: Ailerons

 -----------------------  FLIGHT CONDITIONS  ------------------------
--------------  REFERENCE DIMENSIONS  ------------
  MACH    ALTITUDE   VELOCITY    PRESSURE    TEMPERATURE     REYNOLDS
REF.      REFERENCE LENGTH   MOMENT REF. CENTER
 NUMBER                                                       NUMBER
AREA       LONG.     LAT.     HORIZ      VERT
             FT       FT/SEC     LB/FT**2       DEG R          1/FT
FT**2        FT         FT         FT         FT
0  .100         .00     111.63   2.1162E+03     518.670     7.0682E+05
8.500      1.000    11.000     2.450      .060
0                                                               -------------------DERI
```

```
0 ALPHA     CD       CL       CM       CN       CA       XCP        CLA
CMA          CYB          CNB          CLB
0
   -2.0     .015    -.007    -.0476   -.008     .015    6.311    4.089E+00
5.292E-01   -2.770E-01   -1.373E-02   -8.073E-03
     .0     .016     .139    -.0298    .139     .016    -.215    4.254E+00
4.899E-01                             -8.684E-03
    1.0     .018     .214    -.0214    .214     .014    -.100    4.330E+00
4.695E-01                             -8.998E-03
    2.0     .020     .290    -.0134    .290     .010    -.046    4.398E+00
4.470E-01                             -9.318E-03
    4.0     .026     .446     .0014    .446    -.005     .003    4.532E+00
3.997E-01                             -9.971E-03
1                               AUTOMATED STABILITY AND CONTROL METHODS PER APRIL 1976
                                                         DYNAMIC DERIVATIVES
                                                       WING-BODY CONFIGURATION
                                                        Penguin-b: Ailerons

 -----------------------  FLIGHT CONDITIONS  ------------------------
--------------  REFERENCE DIMENSIONS  ------------
  MACH    ALTITUDE   VELOCITY    PRESSURE    TEMPERATURE     REYNOLDS
REF.      REFERENCE LENGTH   MOMENT REF. CENTER
 NUMBER                                                       NUMBER
AREA       LONG.     LAT.     HORIZ      VERT
             FT       FT/SEC     LB/FT**2       DEG R          1/FT
FT**2        FT         FT         FT         FT
0  .100        .00     111.63   2.1162E+03     518.670     7.0682E+05
8.500      1.000    11.000     2.450      .060
                                                    DYNAMIC DERIVATIVES (PER RADIAN)
0           -------PITCHING-------    -----ACCELERATION------    --------------ROLLING-
--------YAWING--------
```

```
0   ALPHA       CLQ          CMQ            CLAD          CMAD          CLP
CYP           CNP           CNR           CLR
0
    -2.00    9.870E-01    3.793E-01       NDM           NDM       -3.186E-01
3.859E-04    3.749E-04   -2.541E-03   -8.774E-04
      .00                                                         -3.320E-01
-1.282E-02   -1.235E-02   -2.946E-03    2.924E-02
     1.00                                                         -3.383E-01
-1.959E-02   -1.881E-02   -3.490E-03    4.476E-02
     2.00                                                         -3.438E-01
-2.643E-02   -2.530E-02   -4.277E-03    6.053E-02
     4.00                                                         -3.543E-01
-4.042E-02   -3.854E-02   -6.615E-03    9.274E-02
0*** NDM PRINTED WHEN NO DATCOM METHODS EXIST
0*** VEHICLE WEIGHT =     33.00 LB.
0*** LEVEL FLIGHT LIFT COEFFICIENT =  .26208
1                            AUTOMATED STABILITY AND CONTROL METHODS PER APRIL 1976 VER
                                        CHARACTERISTICS OF HIGH LIFT AND CONTROL DEVIC
                                              WING WITH FLAP SPOILER CONFIGURATION
                                                       Penguin-b: Ailerons
 -----------------------  FLIGHT CONDITIONS  ------------------------
--------------  REFERENCE DIMENSIONS  ------------
  MACH    ALTITUDE   VELOCITY    PRESSURE    TEMPERATURE     REYNOLDS
REF.      REFERENCE LENGTH   MOMENT REF. CENTER
 NUMBER                                                         NUMBER
AREA       LONG.     LAT.     HORIZ      VERT
             FT       FT/SEC     LB/FT**2       DEG R          1/FT
FT**2        FT         FT         FT         FT
0  .100        .00      111.63   2.1162E+03     518.670     7.0682E+05
8.500      1.000    11.000     2.450      .060
0                                    XS/C        HS/C        DS/C        (CL)ROLL
CN
```

```
0
                                    .0000        .0000        .0000      1.9455E-03
5.169E-32
                                    .0000        .0000        .0000      1.9455E-03
5.169E-32
                                    .0000        .0000        .0000      1.9455E-03
5.169E-32
                                    .0000        .0000        .0000      1.9455E-03
5.169E-32
                                    .0000        .0000        .0000      1.9455E-03
5.169E-32
                                    .0000        .0000        .0000      1.9455E-03
5.169E-32
                                    .0000        .0000        .0000      1.9455E-03
5.169E-32
                                    .0000        .0000        .0000      1.9455E-03
5.169E-32
                                    .0000        .0000        .0000      1.9455E-03
5.169E-32
1          THE FOLLOWING IS A LIST OF ALL INPUT CARDS FOR THIS CASE.
0
 CASEID Penguin-b: Total
 NACA-V-4-0012
  $VTPLNF CHRDR=0.0, CHRDTP=0.0, SAVSI=0.0, SSPN=0.0, SSPNOP=0.0,
  SSPNE=0.0, CHRDBP=0.0, SAVSO=0.0, CHSTAT=0.0, TYPE=0.0,$
 NACA-H-4-0012
  $HTPLNF CHRDR=0.5, CHRDTP=0.5, SSPN=1.265, SAVSI=0.0,
  SSPNE=1.25, CHSTAT=0.25, TWISTA=0.0,
  DHDADI=-42.0, TYPE=1.0, DHDADO=0.0$
  $SYMFLP FTYPE=1.0, NTYPE=1.0,
  NDELTA=9.0, DELTA(1)=-20.0,-15.0,-10.0,-5.0,0.0,5.0,10.0,15.0,20.0,
  SPANFI=0.2, SPANFO=1.2, CHRDFI=0.1, CHRDFO=0.1,
  CB=0.452, TC=0.20, PHETE=0.003, PHETEP=0.002$
 NEXT CASE
0 INPUT DIMENSIONS ARE IN FT, SCALE FACTOR IS 1.0000


1                             AUTOMATED STABILITY AND CONTROL METHODS PER APRIL 1976 VE
                                                        WING SECTION DEFINITION
0                                 IDEAL ANGLE OF ATTACK =    .25757 DEG.


                              ZERO LIFT ANGLE OF ATTACK =  -1.94052 DEG.


                                 IDEAL LIFT COEFFICIENT =    .25602


                  ZERO LIFT PITCHING MOMENT COEFFICIENT =   -.05165


                             MACH ZERO LIFT-CURVE-SLOPE =    .09924 /DEG.


                                    LEADING EDGE RADIUS =    .00705 FRACTION CHORD


                              MAXIMUM AIRFOIL THICKNESS =    .08000 FRACTION CHORD


                                                DELTA-Y =   2.11265 PERCENT CHORD



0                         MACH=  .1000 LIFT-CURVE-SLOPE =    .09965 /DEG.
XAC =    .25542
1                             AUTOMATED STABILITY AND CONTROL METHODS PER APRIL 1976 VE
                                                   HORIZONTAL TAIL SECTION DEFINITION
0                                 IDEAL ANGLE OF ATTACK =    .00000 DEG.


                              ZERO LIFT ANGLE OF ATTACK =    .00000 DEG.


                                 IDEAL LIFT COEFFICIENT =    .00000
                  ZERO LIFT PITCHING MOMENT COEFFICIENT =    .00000


                             MACH ZERO LIFT-CURVE-SLOPE =    .09596 /DEG.


                                    LEADING EDGE RADIUS =    .01587 FRACTION CHORD


                              MAXIMUM AIRFOIL THICKNESS =    .12000 FRACTION CHORD


                                                DELTA-Y =   3.16898 PERCENT CHORD



0                         MACH=  .1000 LIFT-CURVE-SLOPE =    .09636 /DEG.
XAC =    .25852
0*** WARNING *** V.T. NOT STRAIGHT TAPERED. UNIFORM SECTION ASSUMED.
1                             AUTOMATED STABILITY AND CONTROL METHODS PER APRIL 1976 VE
                                                   VERTICAL TAIL SECTION DEFINITION
0                                 IDEAL ANGLE OF ATTACK =    .00000 DEG.


                              ZERO LIFT ANGLE OF ATTACK =    .00000 DEG.


                                 IDEAL LIFT COEFFICIENT =    .00000


                  ZERO LIFT PITCHING MOMENT COEFFICIENT =    .00000


                             MACH ZERO LIFT-CURVE-SLOPE =    .09596 /DEG.


                                    LEADING EDGE RADIUS =    .01587 FRACTION CHORD


                              MAXIMUM AIRFOIL THICKNESS =    .12000 FRACTION CHORD


                                                DELTA-Y =   3.16898 PERCENT CHORD
```

```
0                         MACH=  .1000 LIFT-CURVE-SLOPE =    .09636 /DEG.
XAC =    .25852
 WARNING - DUPLICATE X VALUES AT X =  7.5000000E-01 IN TBFUNX, CALLED FROM SUBLAT
FOR FIGURE 5.3.1.1-22D
 WARNING*** BODY ALONE DYNAMIC DERIVATIVE METHOD VALID FOR NOSE CYLINDER ONLY
            TAIL EFFECTS IGNORED]
1                               AUTOMATED STABILITY AND CONTROL METHODS PER APRIL 1976
                                         CHARACTERISTICS AT ANGLE OF ATTACK AND IN SIDE
                                        WING-BODY-VERTICAL TAIL-HORIZONTAL TAIL CONFIGU
                                                         Penguin-b: Total

 -----------------------  FLIGHT CONDITIONS  ------------------------
--------------  REFERENCE DIMENSIONS  ------------
  MACH    ALTITUDE   VELOCITY    PRESSURE    TEMPERATURE     REYNOLDS
REF.      REFERENCE LENGTH   MOMENT REF. CENTER
 NUMBER                                                     NUMBER
AREA       LONG.     LAT.     HORIZ      VERT
             FT       FT/SEC     LB/FT**2       DEG R         1/FT
FT**2        FT         FT        FT         FT
0  .100        .00     111.63   2.1162E+03     518.670     7.0682E+05
8.500      1.000    11.000     2.450      .060
0                                                                  --------------------DERI
0 ALPHA     CD        CL        CM        CN        CA        XCP        CLA
CMA          CYB          CNB          CLB
0
   -2.0   -1.#QO    -.028     .0383  -1.#QO   -1.#QO   -1.#QO    4.578E+00
-1.357E+00   **********   -1.#QOE+00   **********
     .0   -1.#QO     .134    -.0107  -1.#QO   -1.#QO   -1.#QO    4.732E+00
-1.418E+00                            **********
```

```
    1.0   -1.#QO     .218    -.0356  -1.#QO   -1.#QO   -1.#QO    4.804E+00
-1.433E+00                             **********
    2.0   -1.#QO     .302    -.0608  -1.#QO   -1.#QO   -1.#QO    4.877E+00
-1.483E+00                             **********
    4.0   -1.#QO     .475    -.1154  -1.#QO   -1.#QO   -1.#QO    5.036E+00
-1.648E+00                             **********
0                                    ALPHA     Q/QINF    EPSLON  D(EPSLON)/D(ALPHA)
0
                                     -2.0      1.000      -.012         .207
                                       .0      1.000       .401         .211
                                      1.0      1.000       .614         .215
                                      2.0      1.000       .830         .218
                                      4.0      1.000      1.273         .221
0*** VEHICLE WEIGHT =     33.00 LB.
0*** LEVEL FLIGHT LIFT COEFFICIENT =  .26208
1                            AUTOMATED STABILITY AND CONTROL METHODS PER APRIL 1976 VER
                                         CHARACTERISTICS OF HIGH LIFT AND CONTROL DEVIC
                                            TAIL PLAIN TRAILING-EDGE FLAP CONFIGURATION
                                                        Penguin-b: Total
 -----------------------  FLIGHT CONDITIONS  ------------------------
--------------  REFERENCE DIMENSIONS  ------------
  MACH    ALTITUDE   VELOCITY    PRESSURE    TEMPERATURE     REYNOLDS
REF.      REFERENCE LENGTH   MOMENT REF. CENTER
 NUMBER                                                       NUMBER
AREA       LONG.     LAT.     HORIZ      VERT
             FT       FT/SEC     LB/FT**2       DEG R         1/FT
FT**2        FT         FT         FT         FT
0  .100        .00     111.63   2.1162E+03     518.670     7.0682E+05
8.500      1.000    11.000     2.450      .060
0            ---------INCREMENTS DUE TO DEFLECTION---------
---DERIVATIVES (PER DEGREE)---
```

```
0     DELTA     D(CL)     D(CM)    D(CL MAX)    D(CD MIN)
(CLA)D     (CH)A       (CH)D



      -20.0     -.080      .2922      .052       .00268
NDM       5.131E-02   1.766E-01
      -15.0     -.068      .2466      .042       .00165
NDM                   1.747E-01
      -10.0     -.046      .1682      .030       .00059
NDM                   1.743E-01
       -5.0     -.023      .0841      .015       .00026
NDM                   1.743E-01
         .0      .000     -.0002      .000       .00000
NDM                   1.743E-01
        5.0      .023     -.0841      .015       .00026
NDM                   1.743E-01
       10.0      .046     -.1682      .030       .00059
NDM                   1.743E-01
       15.0      .068     -.2466      .042       .00165
NDM                   1.747E-01
       20.0      .080     -.2934      .052       .00268
NDM                   1.766E-01
0  *** NOTE * HINGE MOMENT DERIVATIVES ARE BASED ON TWICE THE AREA-MOMENT OF THE CONTRO

0            --------- INDUCED DRAG COEFFICIENT INCREMENT , D(CDI) , DUE TO DEFLECTION
0       DELTA = -20.0     -15.0     -10.0      -5.0        .0       5.0
10.0      15.0      20.0
   ALPHA
0
    -2.0        2.56E-03  1.83E-03  8.53E-04  2.18E-04 -1.65E-08  2.00E-04
8.19E-04  1.78E-03  2.50E-03
```

```
      .0        1.55E-03  9.75E-04  2.73E-04 -7.23E-05  5.63E-07  4.90E-04
1.40E-03  2.63E-03  3.51E-03
     1.0        1.05E-03  5.53E-04 -1.44E-05 -2.16E-04  8.51E-07  6.34E-04
1.69E-03  3.05E-03  4.01E-03
     2.0        5.53E-04  1.33E-04 -3.01E-04 -3.59E-04  1.14E-06  7.77E-04
1.97E-03  3.47E-03  4.51E-03
     4.0       -4.37E-04 -7.03E-04 -8.70E-04 -6.44E-04  1.71E-06  1.06E-03
2.54E-03  4.30E-03  5.50E-03
0***NDM PRINTED WHEN NO DATCOM METHODS EXIST
1          THE FOLLOWING IS A LIST OF ALL INPUT CARDS FOR THIS CASE.
0
1 END OF JOB.


0******************************  INPUT DATA CARDS  ******************************


 CASEID Anaconda : Flight Conditions, Body, Wing, and Flaps
  $FLTCON WT=9.0, LOOP=1.0,
  NMACH=1.0, MACH=0.05,
  NALPHA=5.0, ALSCHD(1)=-2.0,0.0,1.0,2.0,4.0,
  NALT=1.0, ALT(1)=500.0$
  $OPTINS BLREF=6.7,SREF=5.27,CBARR=0.85$
  $SYNTHS XW=1.60,ZW=0.21,XH=4.2,ZH=0.82,XCG=1.8,ZCG=0.0,
  ZV=0.1,XV=4.12,ALIW=0.0,ALIH=0.0$
  $BODY NX=20.0, ITYPE=1.0, BNOSE=2.0, BTAIL=2.0,
  X(1)=  0.0,  0.15,  0.3,  0.6,  0.92,
  1.15,  1.38,  1.65,  1.84,  2.08,
  2.3,  2.53,  2.7,  2.9,  3.45,
  3.68,  3.91,  4.14,  4.37,  4.6,
  R(1)=  0.0,  0.15,  0.25,  0.31,  0.32,
  0.31,  0.29, 0.27,  0.24,  0.23,
  0.22,  0.21,  0.18,  0.12,  0.08,
  0.08,  0.08,  0.08,  0.08,  0.0,
  ZU(1)=  0.0,  0.15,  0.20,  0.26,  0.27,
  0.265,  0.26, 0.255,  0.25,  0.25,
  0.25,  0.25,  0.25,  0.25,  0.25,
  0.25,  0.25,  0.25,  0.25,  0.2,
  ZL(1)=  -0.0,  -0.15,  -0.22,  -0.25,  -0.255,
  -0.24,  -0.23, -0.21,  -0.21,  -0.2,
  -0.18,  -0.10,  0.0,  0.05,  0.08,
  0.08,  0.08,  0.08,  0.08,  0.2,$
 NACA-W-4-2410
  $WGPLNF CHRDR=0.83, CHRDTP=0.7, CHRDBP=0.85, SSPN=3.38,
  DHDADI=0.0, DHDADO=0.0, CHSTAT=0.25, TWISTA=0.0, TYPE=1.0,
  SSPNE=3.38, SAVSI=-0.40,$
  $SYMFLP FTYPE=1.0, NTYPE=1.0,
  NDELTA=5.0, DELTA(1)= 0.0, 10.0, 20.0, 30.0, 40.0,
  SPANFI=0.3, SPANFO=1.0, CHRDFI=0.2, CHRDFO=0.18,
  CB=0.452, TC=0.20, PHETE=0.003, PHETEP=0.002$
 SAVE
 NEXT CASE
 DAMP
 DERIV RAD
 CASEID Anaconda: Ailerons
  $ASYFLP STYPE=1.0, PHETE=0.05228,
  NDELTA=9.0,
  DELTAL(1)=-25.0,-20.0,-10.0,-5.0, 0.0, 5.0, 10.0, 20.0, 25.0,
  DELTAR(1)= 25.0, 20.0, 10.0, 5.0, 0.0,-5.0,-10.0,-20.0,-25.0,
  SPANFI=1.5, SPANFO=3.38, CHRDFI=0.2, CHRDFO=0.2$
 SAVE
 NEXT CASE
 CASEID Anaconda: Total
 NACA-V-4-0012
  $VTPLNF CHRDR=0.0, CHRDTP=0.0, SAVSI=.0, SSPN=0.0,
  SSPNE=0.0, CHRDBP=0.0, SAVSO=0.0, CHSTAT=0.0, TYPE=1.0,$
 NACA-H-4-0012
  $HTPLNF CHRDR=0.5, CHRDTP=0.5, SSPN=0.8, SAVSI=0.0,
  SSPNE=1.27, CHSTAT=0.25, TWISTA=0.0,
  DHDADI=-41.0, TYPE=1.0, DHDADO=0.0$
  $SYMFLP FTYPE=1.0, NTYPE=1.0,
  NDELTA=9.0, DELTA(1)=-20.0,-15.0,-10.0,-5.0,0.0,5.0,10.0,15.0,20.0,
  SPANFI=0.1, SPANFO=0.8, CHRDFI=0.1, CHRDFO=0.1,
  CB=0.452, TC=0.20, PHETE=0.003, PHETEP=0.002$
 NEXT CASE
1          THE FOLLOWING IS A LIST OF ALL INPUT CARDS FOR THIS CASE.
0
 CASEID Anaconda : Flight Conditions, Body, Wing, and Flaps
  $FLTCON WT=9.0, LOOP=1.0,
  NMACH=1.0, MACH=0.05,
  NALPHA=5.0, ALSCHD(1)=-2.0,0.0,1.0,2.0,4.0,
  NALT=1.0, ALT(1)=500.0$
  $OPTINS BLREF=6.7,SREF=5.27,CBARR=0.85$
  $SYNTHS XW=1.60,ZW=0.21,XH=4.2,ZH=0.82,XCG=1.8,ZCG=0.0,
  ZV=0.1,XV=4.12,ALIW=0.0,ALIH=0.0$
  $BODY NX=20.0, ITYPE=1.0, BNOSE=2.0, BTAIL=2.0,
  X(1)=  0.0,  0.15,  0.3,  0.6,  0.92,
  1.15,  1.38,  1.65,  1.84,  2.08,
  2.3,  2.53,  2.7,  2.9,  3.45,
  3.68,  3.91,  4.14,  4.37,  4.6,
  R(1)=  0.0,  0.15,  0.25,  0.31,  0.32,
  0.31,  0.29, 0.27,  0.24,  0.23,
  0.22,  0.21,  0.18,  0.12,  0.08,
  0.08,  0.08,  0.08,  0.08,  0.0,
  ZU(1)=  0.0,  0.15,  0.20,  0.26,  0.27,
  0.265,  0.26, 0.255,  0.25,  0.25,
  0.25,  0.25,  0.25,  0.25,  0.25,
  0.25,  0.25,  0.25,  0.25,  0.2,
  ZL(1)=  -0.0,  -0.15,  -0.22,  -0.25,  -0.255,
  -0.24,  -0.23, -0.21,  -0.21,  -0.2,
  -0.18,  -0.10,  0.0,  0.05,  0.08,
  0.08,  0.08,  0.08,  0.08,  0.2,$
 NACA-W-4-2410
  $WGPLNF CHRDR=0.83, CHRDTP=0.7, CHRDBP=0.85, SSPN=3.38,
  DHDADI=0.0, DHDADO=0.0, CHSTAT=0.25, TWISTA=0.0, TYPE=1.0,
  SSPNE=3.38, SAVSI=-0.40,$
  $SYMFLP FTYPE=1.0, NTYPE=1.0,
  NDELTA=5.0, DELTA(1)= 0.0, 10.0, 20.0, 30.0, 40.0,
  SPANFI=0.3, SPANFO=1.0, CHRDFI=0.2, CHRDFO=0.18,
  CB=0.452, TC=0.20, PHETE=0.003, PHETEP=0.002$
 SAVE
 NEXT CASE
0 INPUT DIMENSIONS ARE IN FT, SCALE FACTOR IS 1.0000

1                             AUTOMATED STABILITY AND CONTROL METHODS PER APRIL 1976 VE
                                                        WING SECTION DEFINITION
0                                 IDEAL ANGLE OF ATTACK =    .25757 DEG.

                              ZERO LIFT ANGLE OF ATTACK =  -1.90954 DEG.

                                 IDEAL LIFT COEFFICIENT =    .25602

                  ZERO LIFT PITCHING MOMENT COEFFICIENT =   -.05127

                             MACH ZERO LIFT-CURVE-SLOPE =    .09777 /DEG.

                                    LEADING EDGE RADIUS =    .01102 FRACTION CHORD

                              MAXIMUM AIRFOIL THICKNESS =    .10000 FRACTION CHORD
```

```
                                                DELTA-Y =   2.64081 PERCENT CHORD



0                          MACH=  .0500 LIFT-CURVE-SLOPE =    .09786 /DEG.
XAC =    .25656
 WARNING*** BODY ALONE DYNAMIC DERIVATIVE METHOD VALID FOR NOSE CYLINDER ONLY
            TAIL EFFECTS IGNORED]
1                                AUTOMATED STABILITY AND CONTROL METHODS PER APRIL 1976
                                          CHARACTERISTICS AT ANGLE OF ATTACK AND IN SIDE
                                                        WING-BODY CONFIGURATION
                                         Anaconda : Flight Conditions, Body, Wing, and F

 -----------------------  FLIGHT CONDITIONS  ------------------------
--------------  REFERENCE DIMENSIONS  ------------
  MACH    ALTITUDE   VELOCITY    PRESSURE    TEMPERATURE     REYNOLDS
REF.      REFERENCE LENGTH   MOMENT REF. CENTER
 NUMBER                                                          NUMBER
AREA       LONG.     LAT.     HORIZ      VERT
             FT       FT/SEC     LB/FT**2       DEG R          1/FT
FT**2        FT         FT         FT         FT
0  .050     500.00      55.72   2.0783E+03     516.887     3.4860E+05
5.270       .850     6.700     1.800      .000
0                                                                  --------------------DERI
0 ALPHA     CD        CL        CM        CN        CA        XCP         CLA
CMA           CYB          CNB          CLB
0
   -2.0     .021    -.012    -.0529   -.013     .021    4.211    8.032E-02
4.121E-03   -1.#IOE+00   -2.171E-04    7.694E-06
     .0     .022     .153    -.0458    .153     .022    -.299    8.495E-02
2.982E-03                             -9.963E-05
```

```
    1.0     .023     .240    -.0431    .240     .019    -.180    8.714E-02
2.398E-03                             -1.555E-04
    2.0     .025     .328    -.0410    .328     .014    -.125    8.916E-02
1.788E-03                             -2.128E-04
    4.0     .031     .510    -.0387    .511    -.005    -.076    9.310E-02
5.498E-04                             -3.311E-04
0*** VEHICLE WEIGHT =      9.00 LB.
0*** LEVEL FLIGHT LIFT COEFFICIENT =  .46956
1                            AUTOMATED STABILITY AND CONTROL METHODS PER APRIL 1976 VER
                                        CHARACTERISTICS OF HIGH LIFT AND CONTROL DEVIC
                                           WING PLAIN TRAILING-EDGE FLAP CONFIGURATION
                                       Anaconda : Flight Conditions, Body, Wing, and F
 -----------------------  FLIGHT CONDITIONS  ------------------------
--------------  REFERENCE DIMENSIONS  ------------
  MACH    ALTITUDE   VELOCITY    PRESSURE    TEMPERATURE     REYNOLDS
REF.      REFERENCE LENGTH   MOMENT REF. CENTER
 NUMBER                                                       NUMBER
AREA       LONG.     LAT.     HORIZ      VERT
             FT       FT/SEC     LB/FT**2       DEG R         1/FT
FT**2        FT         FT         FT         FT
0  .050     500.00      55.72   2.0783E+03     516.887     3.4860E+05
5.270       .850     6.700     1.800      .000
0            ---------INCREMENTS DUE TO DEFLECTION---------
---DERIVATIVES (PER DEGREE)---
0     DELTA     D(CL)      D(CM)    D(CL MAX)    D(CD MIN)
(CLA)D     (CH)A       (CH)D



         .0      .000      .0000      .000       .00000
NDM       3.118E-02   9.610E-02
       10.0      .117     -.0358      .052       .00354
NDM                   9.610E-02
```

```
       20.0      .201     -.0643      .090       .01215
NDM                   9.670E-02
       30.0      .230     -.0806      .121       .02108
NDM                   9.754E-02
       40.0      .271     -.0887      .138       .03337
NDM                   9.785E-02
0  *** NOTE * HINGE MOMENT DERIVATIVES ARE BASED ON TWICE THE AREA-MOMENT OF THE CONTRO

0            --------- INDUCED DRAG COEFFICIENT INCREMENT , D(CDI) , DUE TO DEFLECTION
0       DELTA =    .0      10.0      20.0      30.0      40.0
   ALPHA
0
    -2.0       -5.32E-08  6.85E-04  2.07E-03  2.72E-03  3.80E-03
      .0        1.14E-06  1.88E-03  4.11E-03  5.06E-03  6.55E-03
     1.0        1.74E-06  2.48E-03  5.14E-03  6.22E-03  7.93E-03
     2.0        2.33E-06  3.07E-03  6.16E-03  7.39E-03  9.30E-03
     4.0        3.53E-06  4.27E-03  8.20E-03  9.73E-03  1.21E-02
0***NDM PRINTED WHEN NO DATCOM METHODS EXIST
1          THE FOLLOWING IS A LIST OF ALL INPUT CARDS FOR THIS CASE.
0
 DAMP
 DERIV RAD
 CASEID Anaconda: Ailerons
  $ASYFLP STYPE=1.0, PHETE=0.05228,
  NDELTA=9.0,
  DELTAL(1)=-25.0,-20.0,-10.0,-5.0, 0.0, 5.0, 10.0, 20.0, 25.0,
  DELTAR(1)= 25.0, 20.0, 10.0, 5.0, 0.0,-5.0,-10.0,-20.0,-25.0,
  SPANFI=1.5, SPANFO=3.38, CHRDFI=0.2, CHRDFO=0.2$
 SAVE
 NEXT CASE
0 INPUT DIMENSIONS ARE IN FT, SCALE FACTOR IS 1.0000
```

```
1                             AUTOMATED STABILITY AND CONTROL METHODS PER APRIL 1976 VE
                                                        WING SECTION DEFINITION
0                                 IDEAL ANGLE OF ATTACK =    .25757 DEG.

                              ZERO LIFT ANGLE OF ATTACK =  -1.90954 DEG.

                                 IDEAL LIFT COEFFICIENT =    .25602

                  ZERO LIFT PITCHING MOMENT COEFFICIENT =   -.05127

                             MACH ZERO LIFT-CURVE-SLOPE =    .09777 /DEG.

                                    LEADING EDGE RADIUS =    .01102 FRACTION CHORD

                              MAXIMUM AIRFOIL THICKNESS =    .10000 FRACTION CHORD

                                                DELTA-Y =   2.64081 PERCENT CHORD


0                         MACH=  .0500 LIFT-CURVE-SLOPE =    .09786 /DEG.
XAC =    .25656
 WARNING*** BODY ALONE DYNAMIC DERIVATIVE METHOD VALID FOR NOSE CYLINDER ONLY
           TAIL EFFECTS IGNORED]
1                               AUTOMATED STABILITY AND CONTROL METHODS PER APRIL 1976
                                         CHARACTERISTICS AT ANGLE OF ATTACK AND IN SIDE
                                                       WING-BODY CONFIGURATION
                                                        Anaconda: Ailerons

 -----------------------  FLIGHT CONDITIONS  ------------------------
--------------  REFERENCE DIMENSIONS  ------------
  MACH    ALTITUDE   VELOCITY    PRESSURE    TEMPERATURE     REYNOLDS
REF.      REFERENCE LENGTH   MOMENT REF. CENTER
```

```
 NUMBER                                                         NUMBER
AREA       LONG.     LAT.     HORIZ      VERT
             FT       FT/SEC     LB/FT**2       DEG R         1/FT
FT**2        FT         FT         FT         FT
0  .050     500.00      55.72   2.0783E+03     516.887     3.4860E+05
5.270       .850     6.700     1.800      .000
0                                                                 ------------------DERI
0 ALPHA     CD        CL        CM        CN        CA        XCP         CLA
CMA           CYB           CNB           CLB
0
   -2.0     .021    -.012    -.0529   -.013     .021    4.211    4.602E+00
2.361E-01   -1.#IOE+00   -1.244E-02    4.408E-04
     .0     .022     .153    -.0458    .153     .022    -.299    4.867E+00
1.709E-01                            -5.708E-03
    1.0     .023     .240    -.0431    .240     .019    -.180    4.993E+00
1.374E-01                            -8.912E-03
    2.0     .025     .328    -.0410    .328     .014    -.125    5.108E+00
1.025E-01                            -1.219E-02
    4.0     .031     .510    -.0387    .511    -.005    -.076    5.334E+00
3.150E-02                            -1.897E-02
1                                AUTOMATED STABILITY AND CONTROL METHODS PER APRIL 1976
                                                         DYNAMIC DERIVATIVES
                                                       WING-BODY CONFIGURATION
                                                        Anaconda: Ailerons

 -----------------------  FLIGHT CONDITIONS  ------------------------
--------------  REFERENCE DIMENSIONS  ------------
  MACH    ALTITUDE   VELOCITY    PRESSURE    TEMPERATURE     REYNOLDS
REF.      REFERENCE LENGTH   MOMENT REF. CENTER
 NUMBER                                                         NUMBER
AREA       LONG.     LAT.     HORIZ      VERT
```

```
             FT       FT/SEC     LB/FT**2       DEG R         1/FT

FT**2        FT         FT         FT         FT

0  .050     500.00      55.72   2.0783E+03     516.887     3.4860E+05

5.270       .850     6.700     1.800      .000

                                                       DYNAMIC DERIVATIVES (PER RADIAN)

0           -------PITCHING-------    -----ACCELERATION------    --------------ROLLING-

--------YAWING--------

0   ALPHA       CLQ          CMQ           CLAD         CMAD          CLP

CYP          CNP          CNR          CLR

0

    -2.00    2.102E+00    5.033E-02       NDM          NDM       -5.004E-01

-2.653E-05    8.076E-04   -4.058E-03      NDM

      .00                                                        -5.299E-01

5.758E-04   -1.751E-02   -4.462E-03      NDM

     1.00                                                        -5.439E-01

8.896E-04   -2.704E-02   -5.023E-03      NDM

     2.00                                                        -5.565E-01

1.211E-03   -3.679E-02   -5.848E-03      NDM

     4.00                                                        -5.802E-01

1.874E-03   -5.690E-02   -8.347E-03      NDM

0*** NDM PRINTED WHEN NO DATCOM METHODS EXIST

0*** VEHICLE WEIGHT =      9.00 LB.

0*** LEVEL FLIGHT LIFT COEFFICIENT =  .46956

1                            AUTOMATED STABILITY AND CONTROL METHODS PER APRIL 1976 VER

                                        CHARACTERISTICS OF HIGH LIFT AND CONTROL DEVIC

                                              WING WITH FLAP SPOILER CONFIGURATION

                                                     Anaconda: Ailerons

 -----------------------  FLIGHT CONDITIONS  ------------------------

--------------  REFERENCE DIMENSIONS  ------------

  MACH    ALTITUDE   VELOCITY    PRESSURE    TEMPERATURE     REYNOLDS

REF.      REFERENCE LENGTH   MOMENT REF. CENTER
```

```
 NUMBER                                                             NUMBER
AREA       LONG.     LAT.     HORIZ      VERT
             FT       FT/SEC     LB/FT**2       DEG R         1/FT
FT**2        FT         FT         FT         FT
0  .050     500.00      55.72   2.0783E+03     516.887     3.4860E+05
5.270       .850     6.700     1.800      .000
0                                    XS/C         HS/C         DS/C         (CL)ROLL
CN
0
                                     .0000        .0000        .0000      3.2373E-03
1.355E-31
                                     .0000        .0000        .0000      3.2373E-03
1.355E-31
                                     .0000        .0000        .0000      3.2373E-03
1.355E-31
                                     .0000        .0000        .0000      3.2373E-03
1.355E-31
                                     .0000        .0000        .0000      3.2373E-03
1.355E-31
                                     .0000        .0000        .0000      3.2373E-03
1.355E-31
                                     .0000        .0000        .0000      3.2373E-03
1.355E-31
                                     .0000        .0000        .0000      3.2373E-03
1.355E-31
                                     .0000        .0000        .0000      3.2373E-03
1.355E-31
1          THE FOLLOWING IS A LIST OF ALL INPUT CARDS FOR THIS CASE.
0
 CASEID Anaconda: Total
 NACA-V-4-0012
  $VTPLNF CHRDR=0.0, CHRDTP=0.0, SAVSI=.0, SSPN=0.0,
  SSPNE=0.0, CHRDBP=0.0, SAVSO=0.0, CHSTAT=0.0, TYPE=1.0,$
 NACA-H-4-0012
  $HTPLNF CHRDR=0.5, CHRDTP=0.5, SSPN=0.8, SAVSI=0.0,
  SSPNE=1.27, CHSTAT=0.25, TWISTA=0.0,
  DHDADI=-41.0, TYPE=1.0, DHDADO=0.0$
  $SYMFLP FTYPE=1.0, NTYPE=1.0,
  NDELTA=9.0, DELTA(1)=-20.0,-15.0,-10.0,-5.0,0.0,5.0,10.0,15.0,20.0,
  SPANFI=0.1, SPANFO=0.8, CHRDFI=0.1, CHRDFO=0.1,
  CB=0.452, TC=0.20, PHETE=0.003, PHETEP=0.002$
 NEXT CASE
0 INPUT DIMENSIONS ARE IN FT, SCALE FACTOR IS 1.0000

1                             AUTOMATED STABILITY AND CONTROL METHODS PER APRIL 1976 VE
                                                        WING SECTION DEFINITION
0                                 IDEAL ANGLE OF ATTACK =    .25757 DEG.


                              ZERO LIFT ANGLE OF ATTACK =  -1.90954 DEG.


                                 IDEAL LIFT COEFFICIENT =    .25602


                  ZERO LIFT PITCHING MOMENT COEFFICIENT =   -.05127


                             MACH ZERO LIFT-CURVE-SLOPE =    .09777 /DEG.


                                    LEADING EDGE RADIUS =    .01102 FRACTION CHORD


                              MAXIMUM AIRFOIL THICKNESS =    .10000 FRACTION CHORD


                                                DELTA-Y =   2.64081 PERCENT CHORD
```

```
0                         MACH=  .0500 LIFT-CURVE-SLOPE =    .09786 /DEG.

XAC =    .25656

1                             AUTOMATED STABILITY AND CONTROL METHODS PER APRIL 1976 VE

                                                   HORIZONTAL TAIL SECTION DEFINITION

0                                 IDEAL ANGLE OF ATTACK =    .00000 DEG.


                              ZERO LIFT ANGLE OF ATTACK =    .00000 DEG.


                                 IDEAL LIFT COEFFICIENT =    .00000


                  ZERO LIFT PITCHING MOMENT COEFFICIENT =    .00000


                             MACH ZERO LIFT-CURVE-SLOPE =    .09596 /DEG.


                                    LEADING EDGE RADIUS =    .01587 FRACTION CHORD


                              MAXIMUM AIRFOIL THICKNESS =    .12000 FRACTION CHORD


                                                DELTA-Y =   3.16898 PERCENT CHORD



0                         MACH=  .0500 LIFT-CURVE-SLOPE =    .09606 /DEG.

XAC =    .25845

1                             AUTOMATED STABILITY AND CONTROL METHODS PER APRIL 1976 VE

                                                    VERTICAL TAIL SECTION DEFINITION

0                                 IDEAL ANGLE OF ATTACK =    .00000 DEG.


                              ZERO LIFT ANGLE OF ATTACK =    .00000 DEG.


                                 IDEAL LIFT COEFFICIENT =    .00000


                  ZERO LIFT PITCHING MOMENT COEFFICIENT =    .00000
```

```
                              MACH ZERO LIFT-CURVE-SLOPE =    .09596 /DEG.

                                     LEADING EDGE RADIUS =    .01587 FRACTION CHORD

                               MAXIMUM AIRFOIL THICKNESS =    .12000 FRACTION CHORD

                                                 DELTA-Y =   3.16898 PERCENT CHORD



0                        MACH=  .0500 LIFT-CURVE-SLOPE =    .09606 /DEG.
XAC =    .25845
 WARNING*** BODY ALONE DYNAMIC DERIVATIVE METHOD VALID FOR NOSE CYLINDER ONLY
           TAIL EFFECTS IGNORED]
1                             AUTOMATED STABILITY AND CONTROL METHODS PER APRIL 1976
                                       CHARACTERISTICS AT ANGLE OF ATTACK AND IN SIDE
                                     WING-BODY-VERTICAL TAIL-HORIZONTAL TAIL CONFIGU
                                                      Anaconda: Total

 -----------------------  FLIGHT CONDITIONS  ------------------------
--------------  REFERENCE DIMENSIONS  ------------
  MACH    ALTITUDE   VELOCITY    PRESSURE    TEMPERATURE     REYNOLDS
REF.      REFERENCE LENGTH   MOMENT REF. CENTER
 NUMBER                                                       NUMBER
AREA       LONG.     LAT.     HORIZ      VERT
             FT       FT/SEC     LB/FT**2       DEG R         1/FT
FT**2        FT         FT         FT         FT
0  .050     500.00      55.72   2.0783E+03     516.887     3.4860E+05
5.270       .850     6.700     1.800      .000
0                                                               -------------------DERI
0 ALPHA     CD        CL        CM        CN        CA        XCP         CLA
CMA          CYB          CNB          CLB
```

```
0
   -2.0   -1.#QO    -.045     .0501  -1.#QO   -1.#QO   -1.#QO    5.232E+00
-1.572E+00   **********   -1.#QOE+00   **********
     .0   -1.#QO     .142    -.0071  -1.#QO   -1.#QO   -1.#QO    5.482E+00
-1.660E+00                             **********
    1.0   -1.#QO     .238    -.0363  -1.#QO   -1.#QO   -1.#QO    5.595E+00
-1.666E+00                             **********
    2.0   -1.#QO     .337    -.0653  -1.#QO   -1.#QO   -1.#QO    5.702E+00
-1.685E+00                             **********
    4.0   -1.#QO     .540    -.1258  -1.#QO   -1.#QO   -1.#QO    5.930E+00
-1.780E+00                             **********
0                                    ALPHA     Q/QINF    EPSLON  D(EPSLON)/D(ALPHA)
0
                                     -2.0      1.000      -.032         .362
                                       .0      1.000       .693         .371
                                      1.0      1.000      1.068         .380
                                      2.0      1.000      1.452         .387
                                      4.0      1.000      2.240         .394
0*** VEHICLE WEIGHT =      9.00 LB.
0*** LEVEL FLIGHT LIFT COEFFICIENT =  .46956
1                            AUTOMATED STABILITY AND CONTROL METHODS PER APRIL 1976 VER
                                        CHARACTERISTICS OF HIGH LIFT AND CONTROL DEVIC
                                           TAIL PLAIN TRAILING-EDGE FLAP CONFIGURATION
                                                         Anaconda: Total
 -----------------------  FLIGHT CONDITIONS  ------------------------
--------------  REFERENCE DIMENSIONS  ------------
  MACH    ALTITUDE   VELOCITY    PRESSURE    TEMPERATURE     REYNOLDS
REF.      REFERENCE LENGTH   MOMENT REF. CENTER
 NUMBER                                                       NUMBER
AREA       LONG.     LAT.     HORIZ      VERT
             FT       FT/SEC     LB/FT**2       DEG R         1/FT
FT**2        FT        FT         FT         FT
```

```
0  .050     500.00      55.72   2.0783E+03     516.887     3.4860E+05
5.270       .850     6.700     1.800      .000
0            ---------INCREMENTS DUE TO DEFLECTION---------
---DERIVATIVES (PER DEGREE)---
0     DELTA     D(CL)     D(CM)    D(CL MAX)    D(CD MIN)
(CLA)D     (CH)A       (CH)D



      -20.0     -.143      .3832      .058       .00444
NDM       3.863E-02   1.714E-01
      -15.0     -.121      .3221      .047       .00271
NDM                   1.686E-01
      -10.0     -.082      .2197      .034       .00094
NDM                   1.680E-01
       -5.0     -.041      .1098      .017       .00044
NDM                   1.680E-01
         .0      .000     -.0002      .000       .00000
NDM                   1.680E-01
        5.0      .041     -.1098      .017       .00044
NDM                   1.680E-01
       10.0      .082     -.2197      .034       .00094
NDM                   1.680E-01
       15.0      .121     -.3221      .047       .00271
NDM                   1.686E-01
       20.0      .143     -.3838      .058       .00444
NDM                   1.714E-01
0  *** NOTE * HINGE MOMENT DERIVATIVES ARE BASED ON TWICE THE AREA-MOMENT OF THE CONTRO

0            --------- INDUCED DRAG COEFFICIENT INCREMENT , D(CDI) , DUE TO DEFLECTION
0       DELTA = -20.0     -15.0     -10.0      -5.0        .0       5.0
10.0      15.0      20.0
   ALPHA
```

```
0
    -2.0        4.43E-03  3.16E-03  1.48E-03  3.78E-04 -3.48E-08  3.42E-04
1.41E-03  3.05E-03  4.30E-03
      .0        3.05E-03  1.99E-03  6.85E-04 -1.80E-05  7.58E-07  7.39E-04
2.20E-03  4.22E-03  5.68E-03
     1.0        2.37E-03  1.42E-03  2.96E-04 -2.12E-04  1.15E-06  9.33E-04
2.59E-03  4.79E-03  6.36E-03
     2.0        1.70E-03  8.62E-04 -8.69E-05 -4.04E-04  1.53E-06  1.12E-03
2.97E-03  5.35E-03  7.02E-03
     4.0        3.94E-04 -2.44E-04 -8.40E-04 -7.81E-04  2.28E-06  1.50E-03
3.72E-03  6.45E-03  8.33E-03
0***NDM PRINTED WHEN NO DATCOM METHODS EXIST
1           THE FOLLOWING IS A LIST OF ALL INPUT CARDS FOR THIS CASE.
0
1 END OF JOB.
```

```
% main simulation body
% Jacob Hathaway 2-1-2016
% simple 3-DOF sim for microgravity flight

clear all; close all;

%% Setup sim
sim.dt = .05;
sim.end_time = 20; %s

%% Setup truth
tru.r0 = [600 0]; % meters
tru.v0 = [40 40];  % m/s
tru.theta = 1; % deg (angle rel to horizontal)
tru.theta_dot = 0;
tru.mass = 6.0; % kg

tru.grav = 9.81; % m/s2

Mars.grav=tru.grav/3;

Lunar.grav=tru.grav/6;

%% Start simulation


t = 0:sim.dt:sim.end_time;

x(:,1) = [tru.r0'; tru.v0'];

alpha(1) = 0;thrust(1) = 8;

alpha_gain(1)=1;

gamma_des(1)=atan2(x(3,1),x(4,1));

gamma_err_int(1) = 0;

thrust_des(1)=8;

thrust_err_int(1)= 0;

thrust_err_int(2)= 0;


% this is for simulating response time of the aircraft to pitch and

% throttle

        zeta = 0.7;

        wn = 5*2*pi;

        num = wn^2;

        den = [1 2*zeta*wn wn^2];

        dt = sim.dt; %s

        D = c2d(tf(num,den),dt);


for i = 2:numel(t)


    %% flight computer


time(i)=i*sim.dt;


% Vy_true=x(3,1);
% Vx_true=x(4,1);
%
% Vy_des(i)=Vy_true-tru.grav*time(i);
% Vx_des(i)=Vx_true;
% Alt_des(i)=Vy_true*time(i)-1/2*true.grav*(time(i))^2+x(1,1);
% gamma_des(i)=atan2(Vy_des(i),Vx_des(i));


    %Projectile motion calcs for path command (earth frame)
         Vy_des(1)=x(3,1);
         Vx_des(1)=x(4,1);
         Vy_des(i)=x(3,1)-tru.grav*time(i);
         Vx_des(i)=x(4,1); %x velocity shouldnt change
         Vmag_des(i)=sqrt(Vx_des(i)^2+Vy_des(i)^2);
         Alt_des(1)=x(1,1);
         Alt_des(i)=x(3,1)*time(i)-1/2*tru.grav*(time(i))^2+x(1,1);
         gamma_des(i)=atan2(Vy_des(i),Vx_des(i));  %flight path angle
         %        alpha(i)=theta(i)-gamma(i); %flight path to AOA

    alpha_Kp(i)=.4;
    alpha_Ki(i)=.25;
    alpha_Kd(i)=.01;
%     gamma_des(i)=0;
    gamma(1)=atan2(x(3,1),x(4,1));
    gamma(i)=atan2(x(3,i-1),x(4,i-1));
    gamma_err(i)=gamma_des(i)-gamma(i);

    gamma_err_int(i) = gamma_err_int(i-1) + gamma_err(i)*sim.dt;
    gamma_err_der(i) = (gamma_err(i)-gamma_err(i-1))/sim.dt;
    alpha_des(i)=gamma_err(i)*alpha_Kp(i) + gamma_err_int(i)*alpha_Ki(i)+gamma_err_der(
    alpha(1:i)=filter(D.num{1},D.den{1},alpha_des(1:i));
    %% throttle controller
    if i==2
         thrust(i)= 8;
    else

        thrust_des(i)=drag(i-1);
        throttle_cmd(i)=ThrottlefromThrust(thrust_des(i));
        %commanding throttle to achieve T=D
       throttle_actual(1:i)=filter(D.num{1},D.den{1},throttle_cmd(1:i));
          %for delayed response in throttle to thrust
%         throttle_actual(i) = filter(D.num{1}, D.den{1},throttle_cmd(i));
        thrust(i)=Thrustfromthrottle(throttle_actual(i));
                 %this is a throtle function based off estimated thrust values
    end

    %     alpha(i) = .5*pi/180; %if kept constant
    %     thrust(i) = 9.7;

    % in theory you can add the reverse of "get_aero"
    % 1) aoa_des = get_reverse_aero(lift_desired)
    % 2) lookup drag based on aoa_desired
    % 3) compute thrust based on expected drag



    %% Integrate truth dynamics
    [dxdt(:,i) lift(i) drag(i) Fx(i) Fy(i)] = eom(x(:,i-1),thrust(i), alpha(i), tru);
    % super simple euler method (maybe step this up to RK4 (below)
    x(:,i) = x(:,i-1) + dxdt(:,i)*sim.dt;

%     k1 = dt*eom(t(i-1),x(:,i-1));
%     k2 = dt*eom(t(i-1)+dt/2, x(:,i-1)+k1/2);
%     k3 = dt*eom(t(i-1)+dt/2, x(:,i-1)+k2/2);
%     k4 = dt*eom(t(i-1)+dt, x(:,i-1)+k3);
%     x(:,i) = x(:,i-1) + (k1+2*k2+2*k3+k4)/6;

end
Acc=(sqrt(dxdt(3,:).^2+dxdt(4,:).^2)-9.81)/9.81;
figure;
plot(t,gamma_des(:)*180/pi,t,gamma(:)*180/pi);grid on;
xlabel('Time (s)');ylabel('Flight path angle (deg)')

figure;
plot(t,gamma_err(:)*180/pi);grid on;
xlabel('Time (s)');ylabel('Gamma error')

figure;
plot(t,alpha(:)*180/pi,t,alpha_des(:)*180/pi);grid on;
xlabel('Time (s)');ylabel('Alpha(deg)')

figure;
plot(t,sqrt(x(3,:).^2+x(4,:).^2));grid on;
xlabel('Time (s)');ylabel('Velocity magnitude(m/s)')

figure;hold all;
plot(t,lift);grid on;
plot(t,drag);
xlabel('Time (s)');ylabel('Lift and Drag (N)')

figure;
plot(t,gamma_des);grid on;
xlabel('Time (s)');ylabel('Gamma [rad]');

figure;
plot(t,Alt_des(:),t,x(1,:));grid on;
```

```
xlabel('Time (s)');ylabel('Altitude[m]');

figure;plot(t,sqrt(dxdt(3,:).^2+dxdt(4,:).^2)-9.81);
xlabel('Time (s)');ylabel('Acceleration [m/s]');

figure;
plot(t,thrust_des(:),t,thrust(:));grid on;
xlabel('Time (s)');ylabel('Thrust[N]')



% alpha - angle of attack (rad)
% r - position (m)
% v - vel (m/s)
function [lift drag] = get_aero(alpha, r, v)
alt = sqrt(r(1)^2 + r(2)^2);
vmag = sqrt(v(1)^2 + v(2)^2);

% stdatm1976
atm = [ ...
         0  2.88150000e+002  1.01325000e+005  1.22499916e+000  3.40294108e+002
      1000  2.81661248e+002  8.98762852e+004  1.11161863e+000  3.36440808e+002
      2000  2.75172496e+002  7.95014246e+004  1.00648589e+000  3.32542861e+002
      3000  2.68683744e+002  7.01211622e+004  9.09170878e-001  3.28598679e+002
      4000  2.62194991e+002  6.16604441e+004  8.19256806e-001  3.24606576e+002
      5000  2.55706239e+002  5.40482861e+004  7.36340017e-001  3.20564761e+002
      6000  2.49217487e+002  4.72176425e+004  6.60029866e-001  3.16471331e+002
      7000  2.42728735e+002  4.11052757e+004  5.89948599e-001  3.12324256e+002
      8000  2.36239983e+002  3.56516283e+004  5.25731221e-001  3.08121369e+002
      9000  2.29751231e+002  3.08006953e+004  4.67025371e-001  3.03860355e+002
     10000  2.23262479e+002  2.64998981e+004  4.13491193e-001  2.99538733e+002];

stdatm.alt  = atm(:,1);    % Altitude [m]
stdatm.T    = atm(:,2);    % Temperature [K]
stdatm.P    = atm(:,3);    % Pressure [Pa]
stdatm.rho  = atm(:,4);    % Density [kg/m3]
stdatm.a    = atm(:,5);    % Speed of sound, m/s (held constant above 86 km)

rho = interp1(stdatm.alt,stdatm.rho,alt);
rho=limit_var(1.2250:0.4135,rho);

Q = 0.5*rho*vmag^2;


% simplistic aerodynamic data (from penguin-b datcom at 111.25 ft/s)
% only at 1 mach and not accounting for any deflection
%        AoA (deg)    CD      CL
data = [...
          -4.0    0.022   -0.209
           -2.0    0.015   -0.007
            0.0    0.016    0.139
            0.1    0.018    0.214
            2.0    0.020    0.290
            4.0    0.026    0.446
            6.0    0.049    0.663
            8.0    0.068    0.851
           10.0    0.089    1.011
           12.0    0.111    1.150
           14.0    0.132    1.260   ];
aero.aoa = data(:,1);
aero.cd = data(:,2);
aero.cl = data(:,3);
ft2m = .3048;
Sref = 8.5*ft2m^2; % m^2
```

```
cl = interp1(aero.aoa,aero.cl,alpha*180/pi);
cd = interp1(aero.aoa,aero.cd,alpha*180/pi);
cl=limit_var(-.209:1.26,cl);
cd=limit_var(.022:.132,cd);


% compute normalized lift and drag
lift = Q*cl*Sref;
drag = Q*cd*Sref;
end



% 3DOF equations of motion
function [dxdt lift drag Fx Fy] = eom(x,thrust,alpha,tru)

r = x(1:2)';
v = x(3:4)';
% could later add in theta and theta dot (need to compute
% MOI and compute the aero CM about the CG)
% theta = x(5);
% theta_dot = x(6);

% flight path angle and pitch angle
gamma = atan2(v(1),v(2)); % rad
theta = alpha + gamma; % rad

[lift drag] = get_aero(alpha, r, v);
Fx = -tru.mass*tru.grav + sin(theta)*thrust - sin(gamma)*drag + cos(gamma)*lift;
Fy = cos(theta)*thrust - cos(gamma)*drag - sin(gamma)*lift;

dxdt(1:2,1) = v;
dxdt(3,1) = Fx/tru.mass;
dxdt(4,1) = Fy/tru.mass;
```

BIBLIOGRAPHY

[1] J. Lekan, “Microgravity Research in NASA Ground-Basted Facilities,” *AIAA Aerospace Sciences Meeting*, vol. 27, pp. 1–2, January 1989.

[2] National Aeronautics and Space Administration, “NASA Website.” https://www.nasa.gov/, 2016.

[3] NASA Glenn Research Center, “Zero Gravity Research Facility.” http://facilities.grc.nasa.gov/documents/TOPS/TopZERO.pdf, 2016.

[4] Zero G company, “The Weightless Experience.” https://www.gozerog.com/, 2016.

[5] J. Gundlach, *Designing Unmanned Aircraft Systems: A Comprehensive Approach.* American Institute of Aeronautics and Astronautics Inc., first ed., 2013.

[6] NASA Johnson Space Center, “Unmanned Micrograviy Flight program.” http://research.jsc.nasa.gov/BiennialResearchReport/2011/197-2011-Biennial.pdf, 2016.

[7] S.-I. Higashino and S. Kozai, “Automatic Microgravity Flight System and Flight Testing Using a Small Unmanned Aerial Vehicle,” *International Journal of Microgravity Science and Application*, vol. 27, no. 1, pp. 1–20, 2010.

[8] P. G. Hofmeister and J. Blum, “Parabolic Flights @ Home,” *Microgravity Sci. Technolgy*, vol. 23, pp. 1–5, November 2010.

[9] J. A. Castagnetta and R. S. Larson, “Aerodynamic Evaluation of the NASA Microgravity Unmanned Aerial Vehicle,” *AIAA SciTech*, vol. 54, pp. 1–5, January 2016.

[10] R. C. Nelson, *Flight Stability and Automatic Control*. Tom Casson, second ed., 1998.

[11] R. A. Serway, *Physics for Scientist and Engineers*. Mary Finch, eighth ed., 2010.

[12] B. L. Stevens and F. L. Lewis, *Aircraft Control and Simulation*. John Wiley and Sons Inc, second edition ed., 2003.

[13] F. Karmali and M. Shelhamer, “The dynamics of parabolic flight: flight characteristics and passenger percepts,” Manuscript 63, National Institute of Health, Baltimore, MD, September 2009.

[14] D. J. Diston, *Computational Modeling and Simulation of Aircraft and the Environment*, vol. One: Platform Kinematics and Synthetic Environment. John Wiley and Sons Inc., 2009.

[15] *The USAF Stability and Control DATCOM User Manual*.

[16] *Datcom+ Pro User Manual*.

[17] M.-L. Roy and S. M. Sliwa, “A Computer Program For Obtaining Airplane Configuration Plots from Digital Datcom Input Data,” NASA Technical Memorandum 84639, National Aeronautics and Space Administration, Hampton, Virginia, March 1983.

[18] *Plane Maker manual for X-Plane 10*.

[19] *Airfoil Maker manual for X-Plane 10*.

[20] Laminar Research, “How X-Plane works.” http://www.x-plane.com/desktop/how-x-plane-works/, 2016.

[21] MathWorks, “MathWorks website for MATLAB.” http://www.mathworks.com/products/matlab/, 2016.

[22] MathWorks, “MathWorks Website for MATLAB.” http://www.mathworks.com/products/simulink/, 2016.

[23] tech. rep.

[24] J. Hanson and B. Beard, “Applying Monte Carlo Simulation to Launch Vechicle Design and Requirements Analysis,” NASA Technical Publication 216447, National Aeronautics and Space Administration, Huntsville, AL, September 2010.

[25] P. H. Zipfel, *Modeling and Simulation of Aerospace Vehicle Dynamics.* American Institute of Aeronautics and Astronautics, Inc., second ed., 2007.

[26] Ready Made Radio Controlled, “Anaconda airframe.” http://www.readymaderc.com/store/index/, 2016.

[27] *RFD900 Data Sheet.*

[28] QGroundControl, “Overview.” http://qgroundcontrol.org/about, 2016.

[29] *Futaba R6303SB user Manual.*

[30] *VN-200 User Manual.*

VITA

Jacob Hathaway

Candidate for the Degree of

Master of Science

Thesis: DEVELOPMENT OF A MICROGRAVITY UAS TEST BED

Major Field: Mechanical and Aerospace Engineering

Biographical:

Personal Data: Born in Tulsa, Oklahoma on March 16th 1990

Education:

Received the B.S. degree from Oklahoma State University, Stillwater, OK, USA, 2014, in Aerospace Engineering

Completed the requirements for the degree of Bachelors of Science with a major in Mechanical and Aerospace Engineering at Oklahoma State University, Stillwater, Oklahoma in May 2014.